NASA

Technical Memorandum 81983

THE CHARACTERISTICS AND LIMITATIONS OF THE MPS/MMS BATTERY CHARGING SYSTEM

Floyd E. Ford, Charles F. Palandati, John F. Davis and C. Michael Tasevoli

NOVEMBER 1980

National Aeronautics and Space Administration

Goddard Space Flight Center
Greenbelt, Maryland 20771

TM-81983

THE CHARACTERISTICS AND LIMITATIONS OF THE MPS MMS BATTERY CHARGING SYSTEM

Floyd F. Ford
Charles F. Palane, Jr.
John F. Davis
C. Michael Fasevoli
Space Power Applications Branch
Spacecraft Technology Division
Goddard Space Flight Center
Greenbelt, Maryland

November 1980

GODDARD SPACE FLIGHT CENTER
Greenbelt, Maryland

THE CHARACTERISTICS AND LIMITATIONS OF THE MPS/MMS BATTERY CHARGING SYSTEM

by
Floyd F. Ford
Charles F. Palandati
John F. Davis
C. Michael Tasevoli
Space Power Applications Branch
Spacecraft Technology Division
Goddard Space Flight Center
Greenbelt, Maryland

ABSTRACT

In conjunction with the development of the Modular Power System (MPS) for the Multi-mission Modular Spacecraft (MMS), a program was initiated to evaluate the engineering limitations of parallel battery operation both under normal and abnormal orbital conditions. Using the multiple voltage versus temperature levels designed into the MPS, a series of tests were conducted on two 12-ampere hour nickel-cadmium batteries under a simulated cycle regime. These tests included, battery recharge as a function of voltage control level; temperature imbalance between two parallel batteries; a shorted or partially shorted cell in one of the two parallel batteries; impedance imbalance of one of the parallel battery circuits; and disabling and enabling one of the batteries from the bus at various charge and discharge states.

The results demonstrate that the eight commandable voltage versus temperature levels designed into the MPS provide a very flexible system that not only can accommodate a wide range of normal power system operation, but also provides a high degree of flexibility in responding to abnormal operating conditions. For a normal 25 percent depth-of-discharge (DOD) on each battery, voltage level five provided for optimum battery recharge over the temperature range of 0 degrees to 20 degrees Centigrade. Operating one battery at 10 degrees Centigrade resulted in divergence in both depth-of-discharge and ampere hour recharge ratio. The recharge ratio ranged from adequate to substantial overcharge, depending on the voltage level selected for charge control. Increasing the resistance in one parallel path from .077 to .177 ohms resulted in a decrease in depth-of-discharge from 25 percent to 22 percent. The other battery (resistance at .077 ohms) increased from 25 percent depth-of-discharge to 28 percent. The ampere recharge ratio remained essentially independent of impedance. Simulation of one shorted cell in one battery resulted in severe overcharge (recharge ratio exceeded 2.0) and high cell pressure for the battery with the shorted cell. Lowering the charge voltage from level five to level three provided for stable operation with a recharge ratio of 1.2 on the battery with the shorted cell and approximately 1.0 on the 22-cell battery. Disabling and enabling on battery from the charge bus resulted in a peak current of 57.0 amperes when one battery was fully charged and the other battery discharged to 100 percent rated capacity (12 ampere hour). The current peaks measured at re-enabling of the battery were determined to be dependent on the difference in voltage between the batteries and the impedance in each parallel battery circuit. For larger capacity batteries where the battery internal impedance is less than the 12 ampere hour batteries used in this test, peaks substantially greater than 57 amperes would be expected.

Page Intentionally Left Blank

CONTENTS

ILLUSTRATIONS

ILLUSTRATIONS (continued)

TABLES

THE CHARACTERISTICS AND LIMITATIONS OF THE MPS/MMS BATTERY CHARGING SYSTEM

Introduction

The feasibility of operating high capacity nickel-cadmium batteries in parallel was demonstrated during development testing of the power system for the Orbiting Astronomical Observatory (OAO) in 1967. OAO-2 spacecraft which was launched in December 1968 contained three twenty ampere-hour 21 cell nickel-cadmium batteries that were charged in parallel from a power regulator unit (PRU) using eight commandable temperature compensated voltage levels. The batteries and power system performed flawlessly for five years at which time the spacecraft was deactivated. OAO-4 was launched in August 1972 with identical power system with the exception that the battery charge levels had been modified[2] based on experience gained on OAO-2 and life cycle test results. To date a eight year life has been obtained on the OAO-4 spacecraft with flawless power system performance[3]. Between the two spacecraft a total of 11 years of operational life has been demonstrated on parallel charging and discharging of high capacity Ni-Cd batteries. Because of the extensive life and excellent reliability demonstrated by this OAO power system design the Module Power System (MPS) for the Multi-Mission Spacecraft (MMS) was a natural outgrowth of the already proven concept. During the early studies for the MPS/MMS concept, it became apparent that while extensive experience with parallel battery operations had been gained on the OAO program, there were a number of unanswered questions concerning the limitations of nickel cadmium batteries in a parallel configuration. Consequently, a program was undertaken to define these limitations and to understand the interaction of batteries operated in parallel. This paper summarizes the results and presents conclusions derived from the program.

Background

The Multimission Modular Spacecraft (MMS) is an assemblage of modules providing the housekeeping functions of communications and data handling, propulsion, attitude control, and power conditioning and energy storage for an attached payload. One module of the MMS, the Modular

Power Subsystem (MPS) conditions power from a mission-unique solar array for distribution to other MMS modules and payloads, and recharging of storage batteries which satisfy load requirements during eclipse. The MPS contains a Standard Power Regulator Unit (SPRU) which operates as a peak power tracker on the solar array when the combined demand of the external load and batteries exceed the power available from the solar array. Parallel battery charging is also controlled by the SPRU with the aid of eight temperature-compensated voltage-levels as shown in Figure 1. The MPS also provides a battery temperature environment of 10°C ± 10°C under normal conditions.

Objectives

The objectives of the entire test program is to understand the limitations of parallel charging and discharging of Ni-Cd batteries under several simulations of normal and abnormal flight conditions. The test was organized with several operating constraints. The orbital regime is 100 minutes long with 36 minutes of shadow and 64 minutes of sunlight. The maximum constant current charge and discharge currents for the parallel batteries was $\frac{C}{2}$ and $\frac{C}{2.2}$ rates respectively and based on the nameplate battery capacity. The battery temperature environment was set at 10°C, the nomial baseline temperature of the batteries in the MPS. The charger voltage limits which permit the battery current to taper towards the end of charge are identical with those in the MPS.
In order to monitor changes between parallel batteries during each of the test conditions, several battery parameters such as voltage, currents, temperatures, cell voltages, and cell pressures were measured and recorded. The battery columetric efficiency defined as the charge-to-discharge ampere-hour ratio X 100% was determined by using an electronic ampere-hour integrator.

A more detailed description of the battery and cell design and the test set-up has been included in Appendix A&B.

Specific objectives of the test program were the following:

- Determine battery charge response in the range of voltage-temperature levels designed

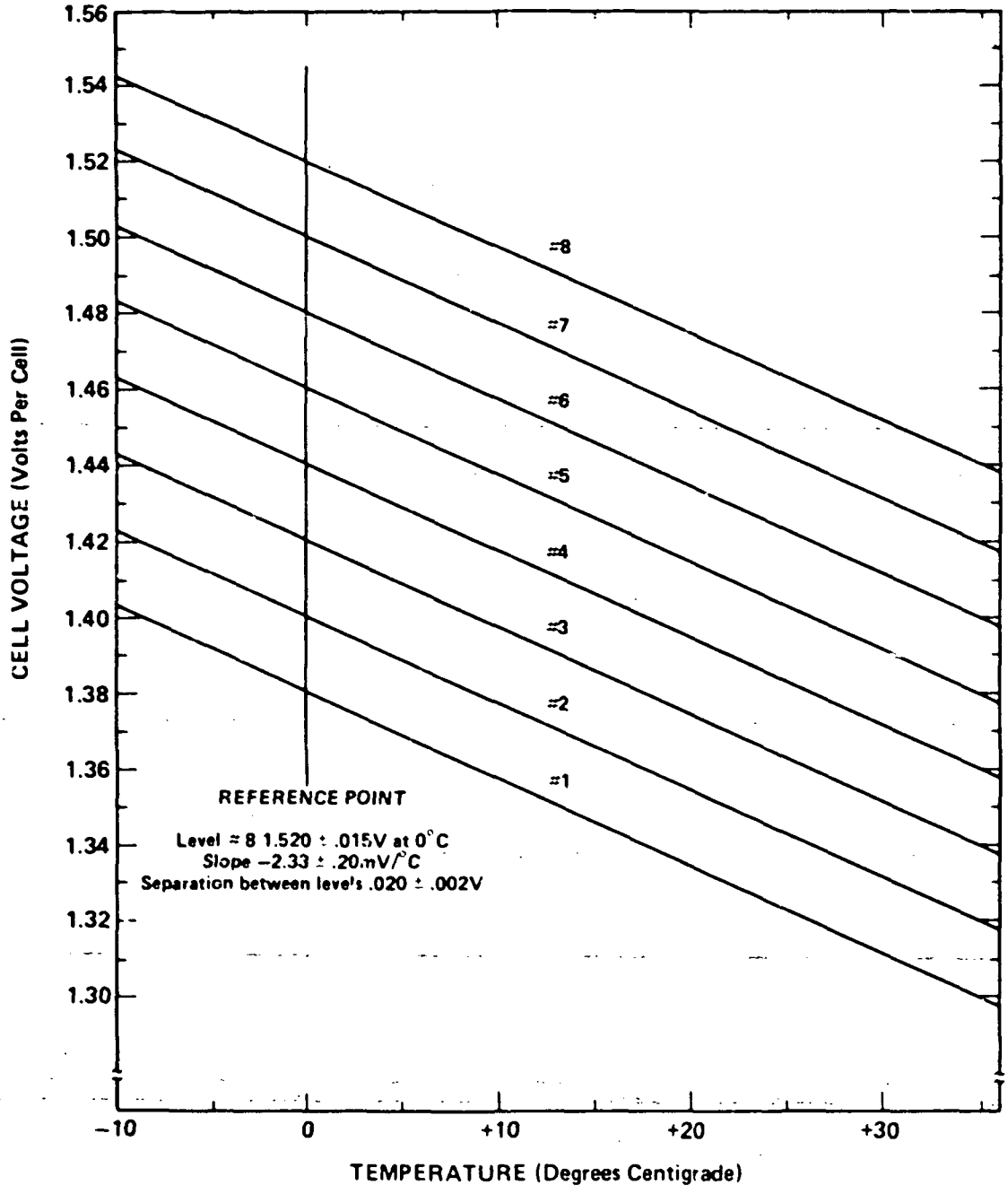

Figure 1. Voltage/Temperature Characteristics for Multilevel Nickel Cadmium Battery Charging

into the MPS. This test was performed at 25% depth-of-discharge (DOD) and voltage levels 3, 5, 6, and 7 over the design temperature range of 0°C to 20°C.

- Effects of temperature imbalance on parallel battery operation. This simulation was accomplished by maintaining the ambient temperature of one battery at 10°C while varying the temperature of the other battery from 0°C to 20°C in 5°C increments at voltage levels 3, 5, 6 and 7. The charger voltage limit at each level was determined by the battery at the higher ambient temperature. The ampere-hour charge-discharge ratios used in determining the overall effect of the temperature imbalance.
- Influence of harness resistance mismatch on battery load sharing and energy balance. Harness mismatches were obtained by introducing precision shunts in one battery circuit of the parallel connection.
- Determine parallel battery operating characteristics with one battery containing a shorted cell. This evaluation determined the following:
  1. The effect of a partially shorted cell in one battery on parallel battery characteristics. The shorted cell was simulated by placing a 1 ohm resistive load across the designated cell while allowing the batteries to continue to cycle.
  2. The optimum charger level for short term stability when one battery develops a hard cell short.
- Determine battery current transients during an abnormal flight condition where one battery may have to be disabled and remain off line for several orbits before being enabled to the charger bus.
- Effect of life cycling on battery characteristics. Battery charge response, shorted cell and harness mismatch tests were repeated and compared with previous results. Battery discharge voltage profile was determined to characterize any battery degradation which may have occurred during the program.

1. Test Results and Discussion

1.1 Evaluation of battery charge response at various voltage levels and temperature.

Table 1 summarizes the battery operating parameters and orbital regime used for charger voltage level evaluation.

Table 1
Operating Parameters for Parallel Batteries During the Battery Charge Response Evaluation

ORBIT REGIME	100 MINUTE (36 MINUTE SHADOW)
DEPTH-OF-DISCHARGE	25%
CHARGE CURRENT	12 AMPERES (maximum)
DISCHARGE CURRENT	10 AMPERES
CHARGER VOLTAGE LEVELS	3, 5, 6 AND 7
AMBIENT TEMPERATURES	0°C TO 20°C IN 5°C INCREMENTS

The final test results given in Figure 3 are plotted only at 0°C, 10°C, and 20°C due to the small variation in battery ampere-hour charge-to-discharge ratio (C/D) at the 5°C increment step. Notice that the trend towards higher charge-to-discharge ratios was evident both at higher ambient tem-

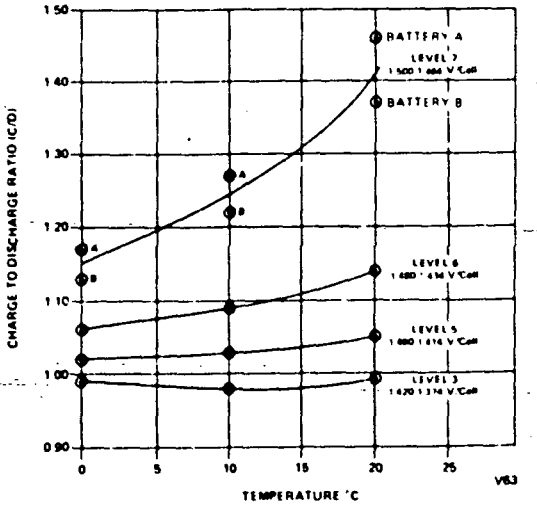

Figure 3. C/D Ratio vs Temperature and Charger Levels

peratures and higher charger levels. At charger level 3 the charge-to-discharge ratio (C/D) was below 1.0 throughout the entire temperature range while at level 5 the ratios measured between 1.02 and 1.05. At the higher charger levels 6 and 7, the average C/D ratios were substantially higher varying from 1.06 to 1.14 at level 6 and 1.13 to 1.47 at level 7.

Figures 4 thru 11 represent comparson plots of battery characteristics at each charger voltage level at various ambient temperatures.

At charger level 3 there is no significant difference in battery parameters during the entire temperature range. The battery C/D ratio stablized below 1.0 indicating that the batteries were experiencing iess than 100% recharge and running down in state-of-charge (SOC).

At level 5 there is also no significant difference in battery parameters. However, the C/D ratios varied between 1.01 and 1.04 while cell temperatures remained at the ambient as cell pressures stablized below 14 psia.

In definite contrast to the lower charger levels, at level 7 both batteries experienced high C/D ratios between 1.13 and 1.47 with cell pressures between 25 and 40 psia and slightly increasing end of charge currents throughout the entire temperature range. Additionally, cell temperatures measured on the top of interior cells in battery A were greater than in battery B. See Table 2.

Table 2
Cell and Battery Temperatures at Level 7 During Battery Charge Response Evaluation

CHARGER LEVEL	BATTERY	C/D RATIO	AMBIENT TEMPERATURE (°C)	THERMAL COOLING PLATE TEMPERATURE (°C)	CELL TOP TEMPERATURE (°C)
7	A	1.17	−0.8	−1.2	2.2
	B	1.13	−0.4	−0.9	−1.7
7	A	1.18	9.8	10.0	12.7
	B	1.15	9.5	9.6	9.0
7	A	1.46	20.6	20.1	26.1
	B	1.37	20.5	19.9	20.9

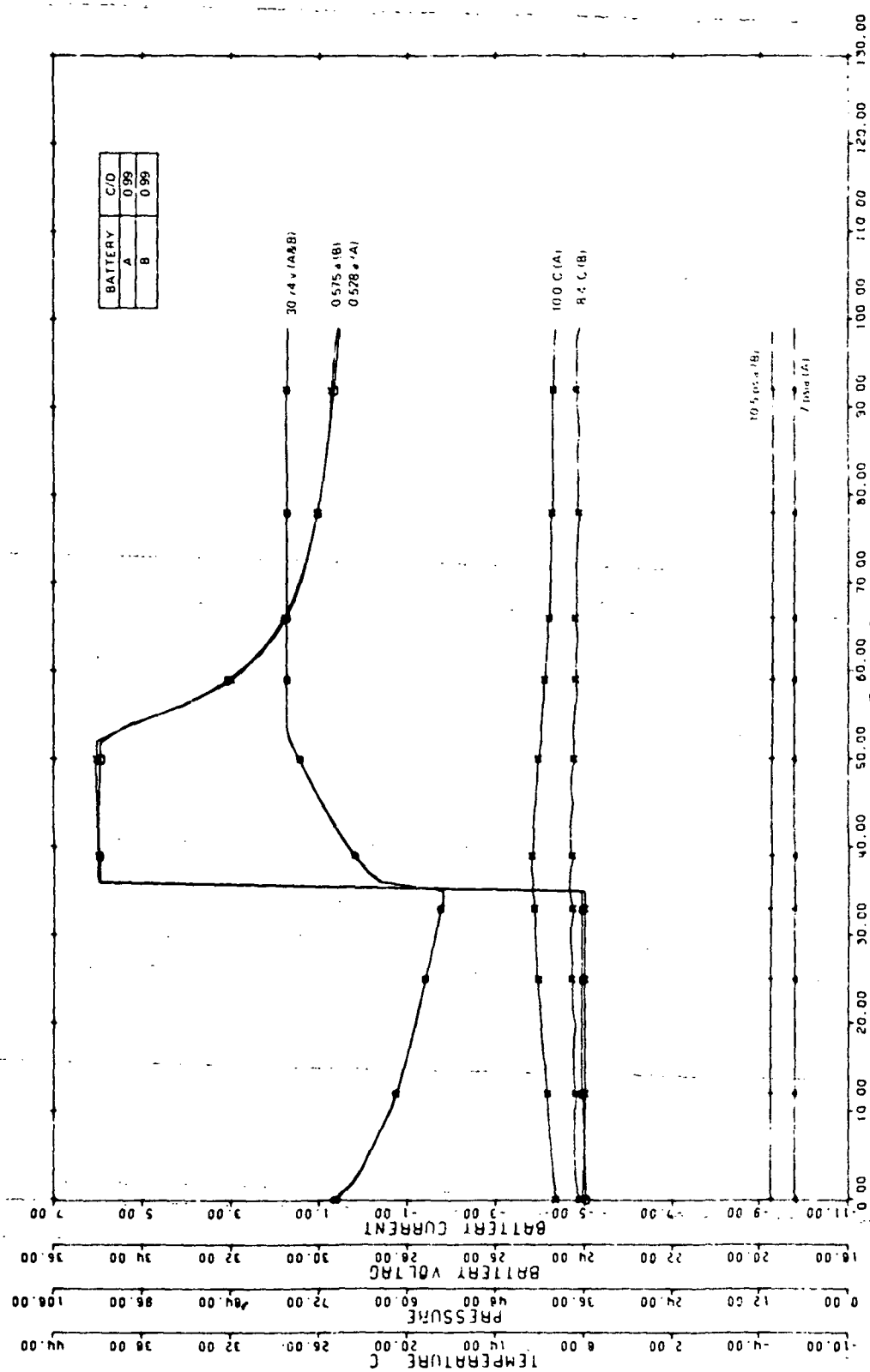

Figure 4. Battery Charge Response at Level 3 and 10°C

This curve and others that follow were plotted using computer data and were identified by different data symbols for convenience.

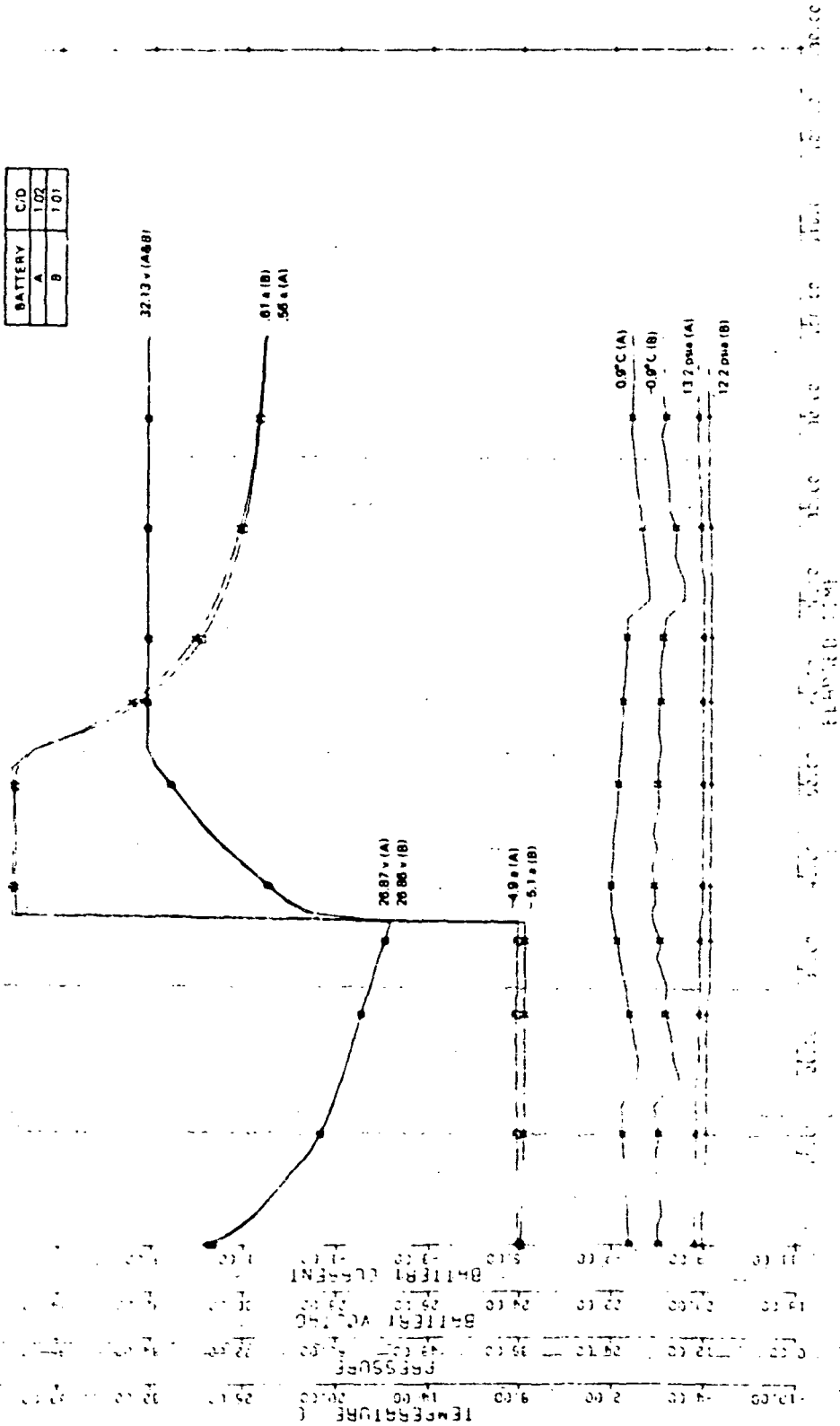

Figure 5. Battery Charge Response at Level 5 and 0°C

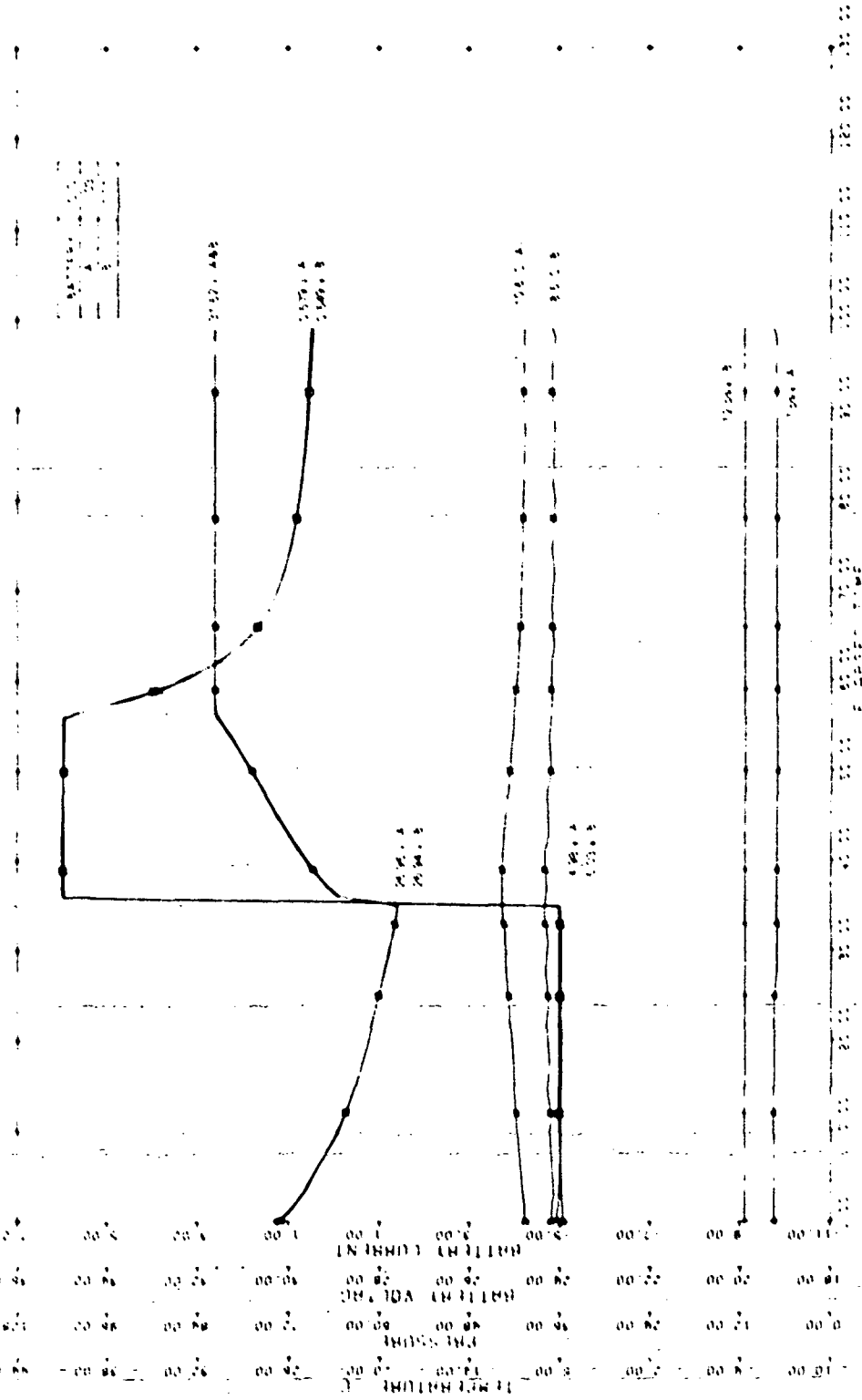

Figure 6. Battery Charge Response at Level 5 and 10°C

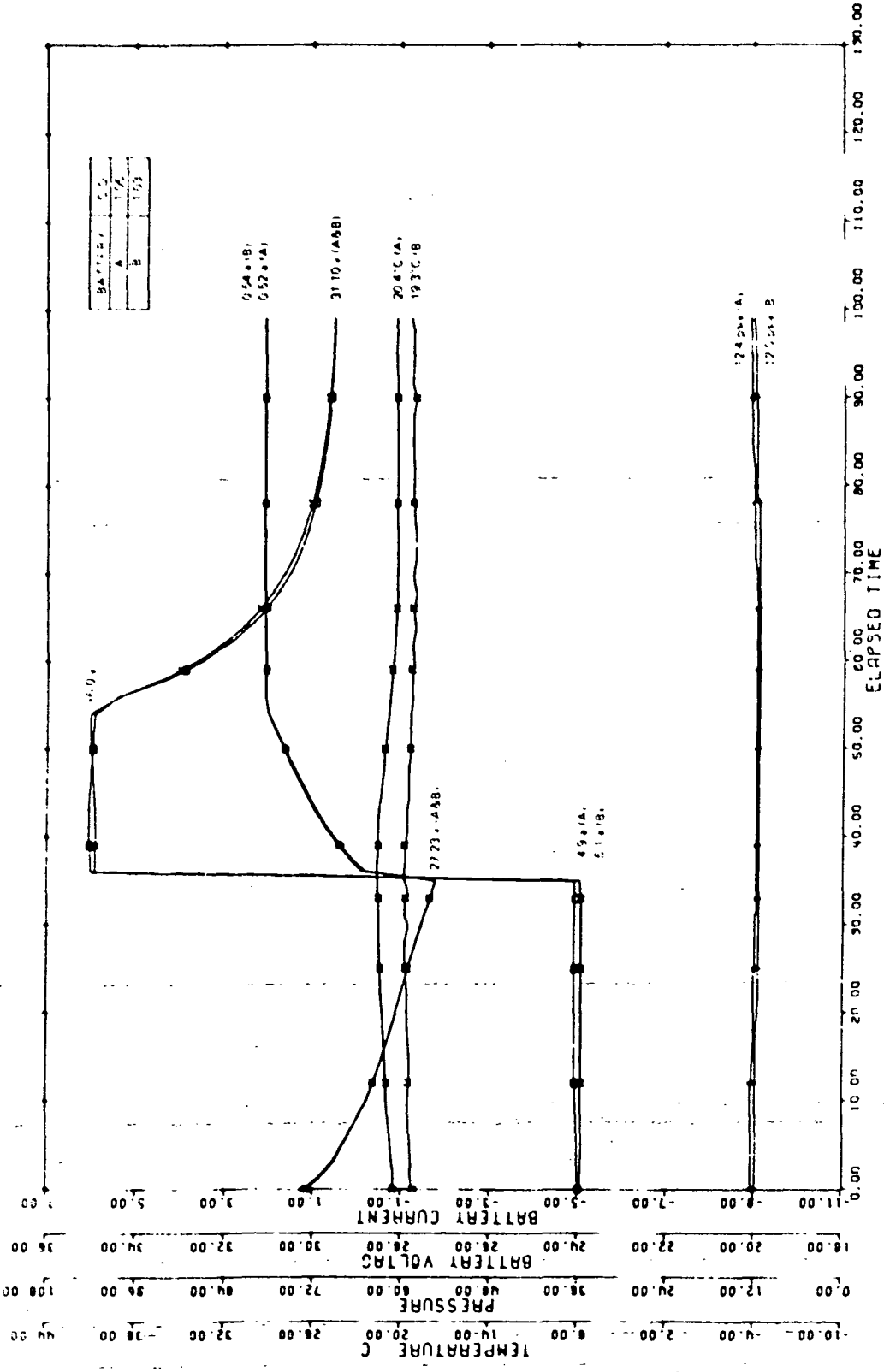

Figure 7. Battery Charge Response at Level 5 and 20°C

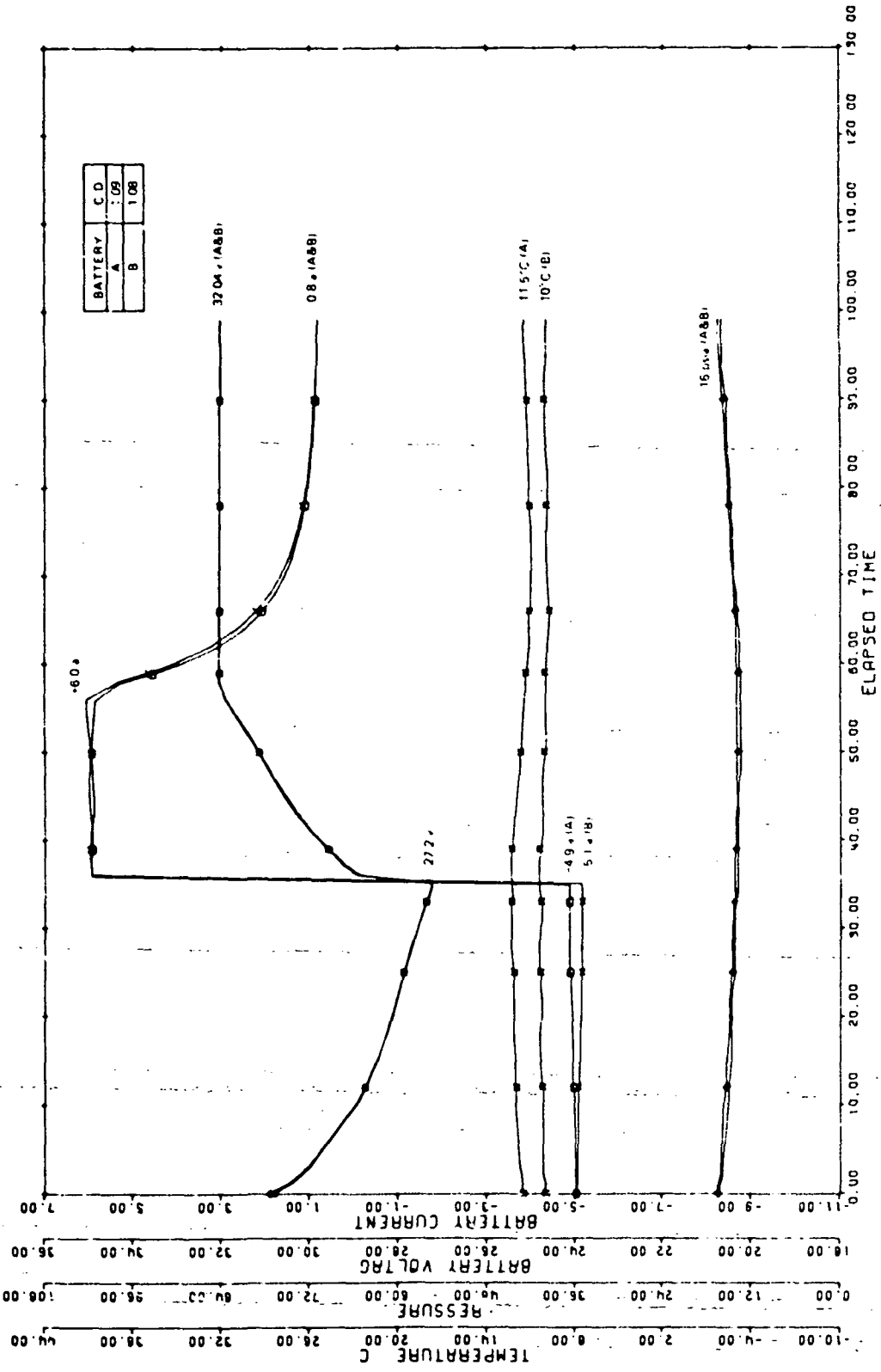

Figure 8. Battery Charge Response at Level 6 and 10°C

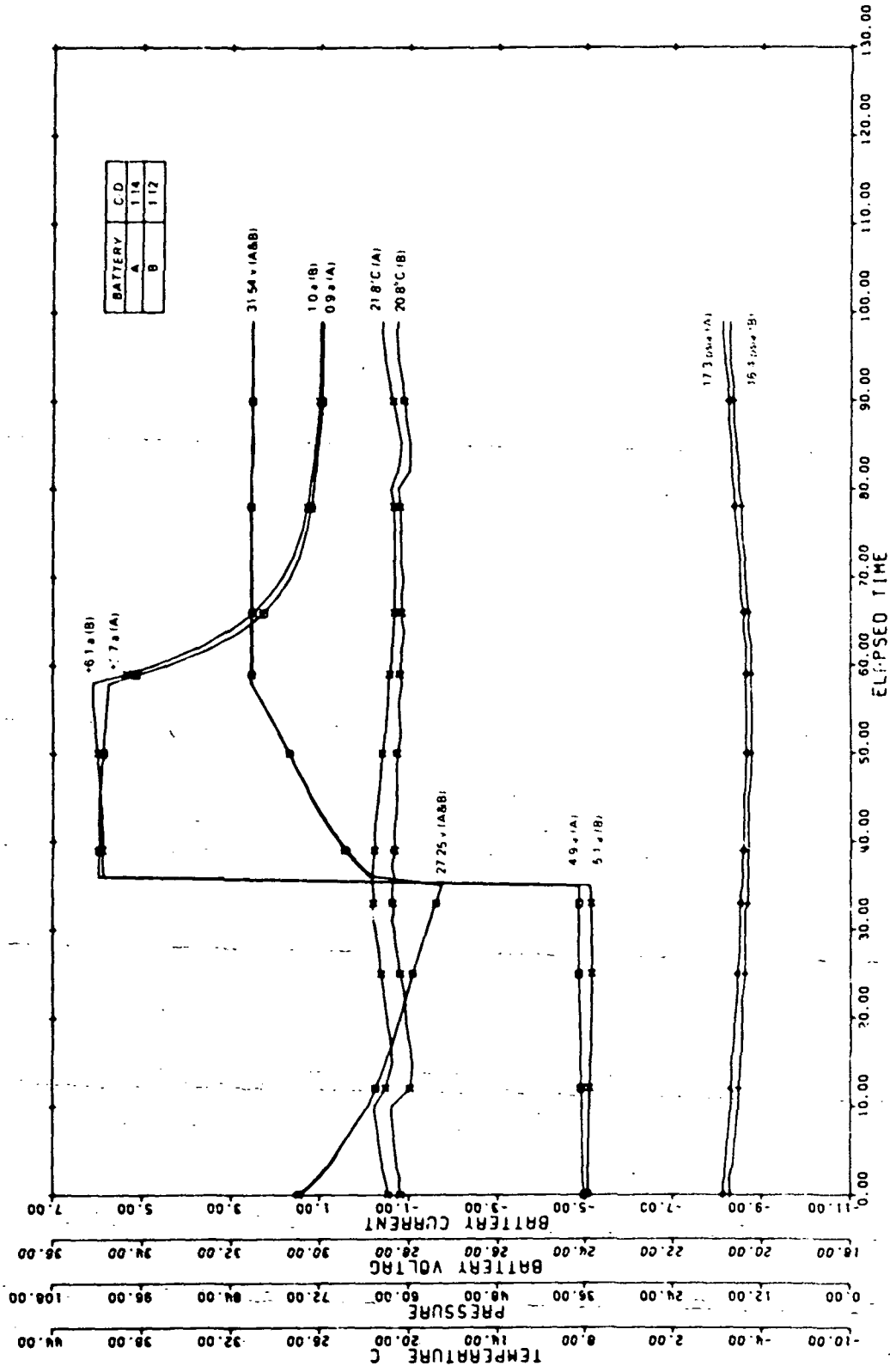

Figure 9. Battery Charge Response at Level 6 and 20°C

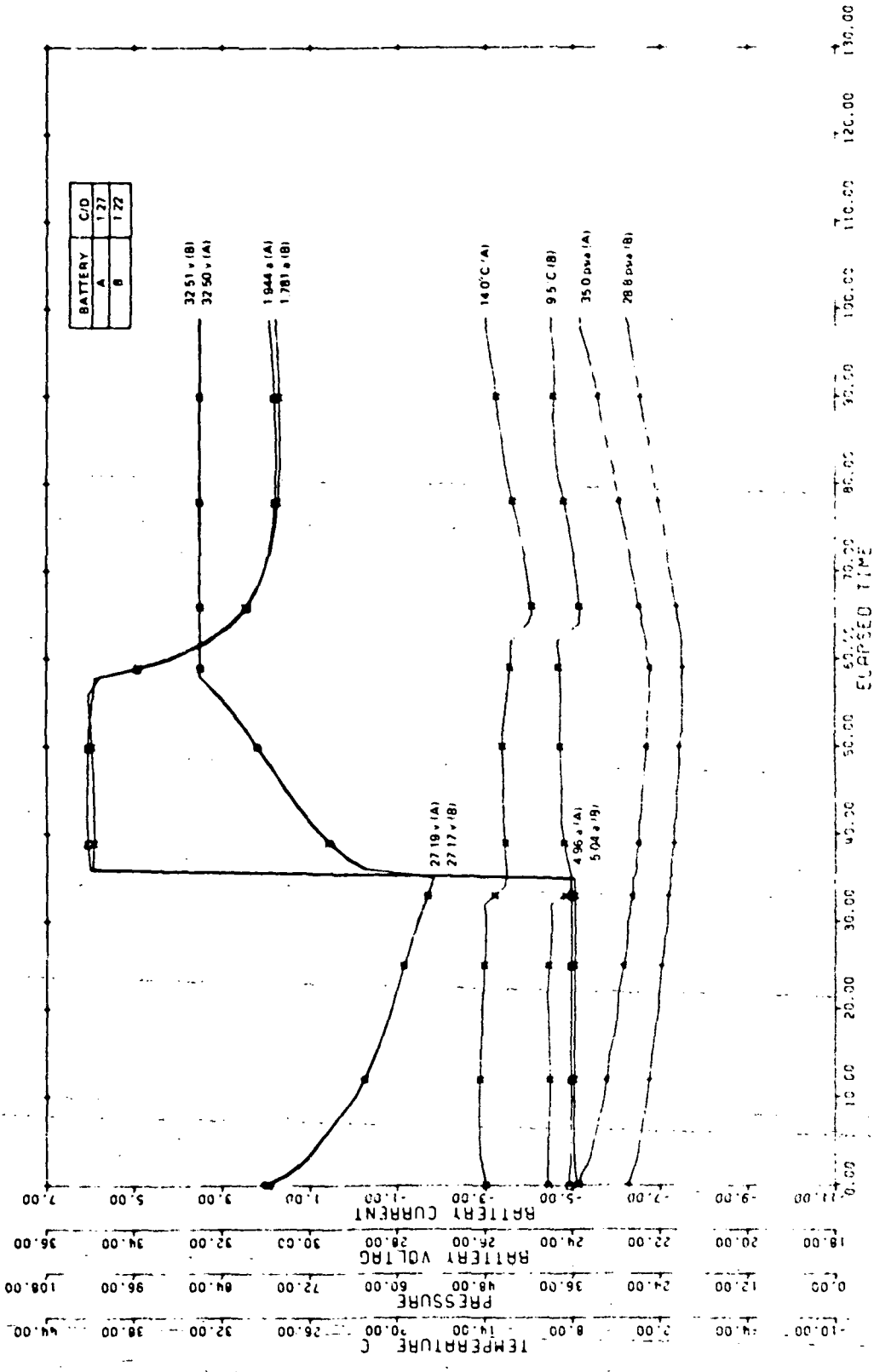

Figure 10. Battery Charge Response at Level 7 and 10°C

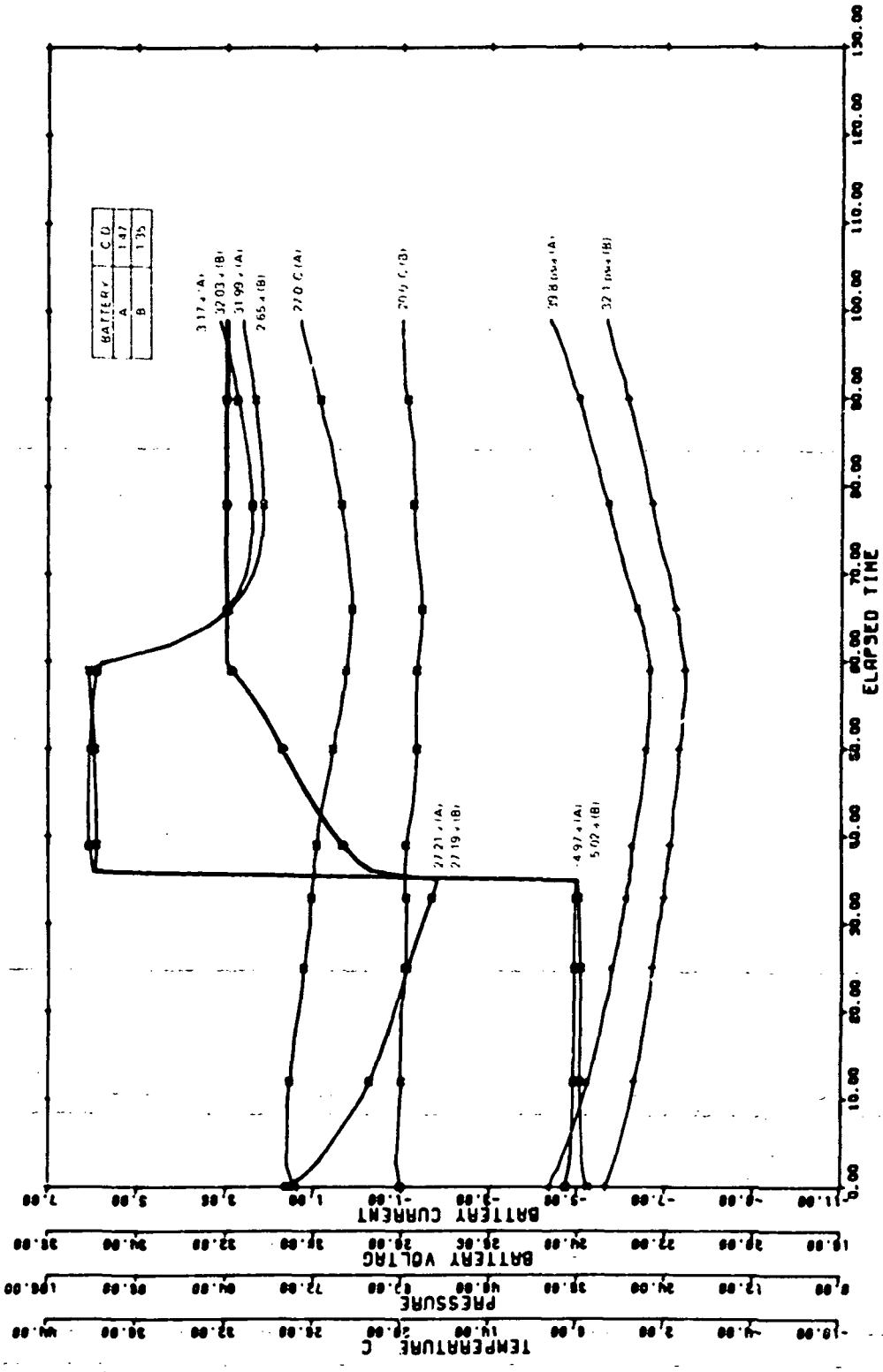

Figure 11. Battery Charge Response at Level 7 and 20°C

These temperature differences which were not observed at level 6 and below are the result of the higher C/D ratio of battery A and the dissimilar thermal environment between batteries caused by different air circulating patterns within each chamber.

1.2 Effect of temperature imbalance on parallel battery performance

Table 3 tabulates the final results. The effect of increasing the temperature imbalance between batteries resulted in the divergence of the battery C/D ratio and depth-of-discharge (DOD). The battery which was maintained at the higher ambient temperature experienced the greater percent recharge and depth-of-discharge. From Figures 12 and 13, the imbalance in percent recharge became more pronounced at higher charger levels while the imbalance in the depth-of-discharge became less significant. At levels 3 and 5, the difference in percent recharge was typically less than 4% at maximum temperature imbalance.

Referring to Figures 14 thru 19, both batteries experienced a C/D ratio between 1.00 to 1.03 at level 5. Cell pressures were less than 15 psia and no significant temperature gradients were observed. These results were similar to the battery charge response over the design temperature range of 0° to 20°C. At level 6 battery C/D ratios were typically 1.00 to 1.10. Cell pressures did not exceed 18 psia. However, at level 7 the battery maintained at the higher temperature experienced a significantly higher C/D ratio typically between 1.26 to 1.33 as the end of charge currents increased and cell pressures measured less than 30 psia. In contrast the battery maintained at the lower ambient temperature experienced a moderate C/D ratio of 1.05 and 1.10 and nominal cell pressures.

No significant cell temperature gradients were observed prior to charger level 7. At the maximum temperature imbalance with battery B at 0°C and battery A at 10°C, battery A experienced a C/D ratio of 1.26 and a vertical cell temperature gradient of + 4°C with respect to the ambient and cooling plate. In contrast, at the other temperature extreme with battery B at 20°C and battery A at 10°C, battery B experienced a C/D ratio of 1.33 and a vertical cell temperature gradient of 1.2°C.

Table 3
C/D Ratio and % DOD vs Temperature Imbalance

BATTERY A			BATTERY B		
TEMP (°C)	C/D RATIO	DOD (%)	DOD (%)	C/D RATIO	TEMP (°C)
		LEVEL 3 (1.397 V/CELL)			
	0.98	23.1	27.2	0.98	20
	0.99	24.8	27.1	0.98	15
	0.98	24.6	25.0	0.98	10
	0.98	26.0	24.7	0.97	5
	0.99	27.0	23.0	0.98	0
		LEVEL 5 (1.437 V/CELL)			
	1.00	23.3	27.0	1.03	20
	1.01	23.3	27.0	1.01	15
	1.00	25.0	25.0	1.00	10
	1.01	25.6	24.6	1.00	5
10°C	1.02	26.3	23.7	1.00	0
		LEVEL 6 (1.467 V/CELL)			
	1.03	23.6	26.6	1.10	20
	1.05	24.1	26.1	1.09	15
	1.09	24.7	25.5	1.08	10
	1.07	25.5	24.6	1.02	5
	1.07	26.8	23.5	1.00	0
		LEVEL 7 (1.477 V/CELL)			
	1.10	24.1	26.3	1.33	20
	1.16	23.8	26.7	1.24	15
	1.18	25.0	25.3	1.15	10
	1.23	25.2	24.4	1.10	5
	1.26	26.1	23.9	1.05	0

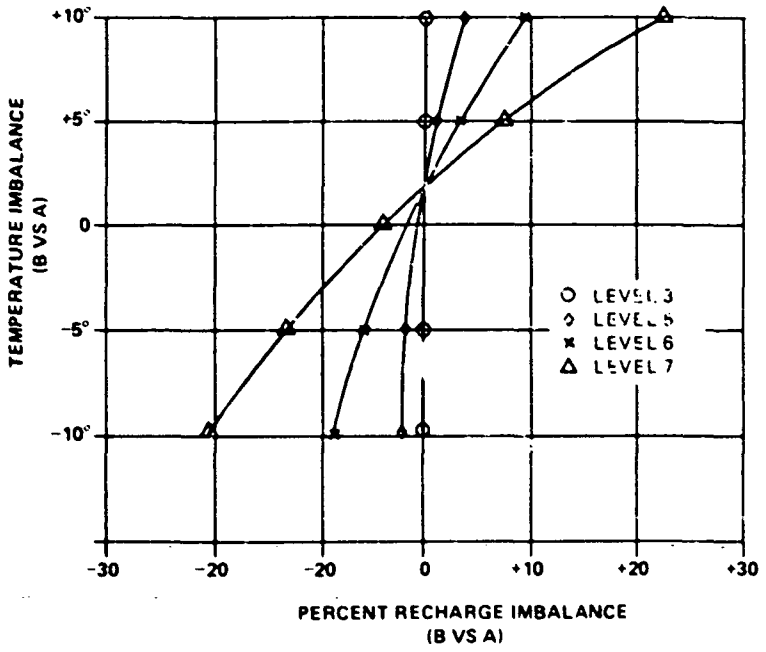

Figure 12. Divergence in Percent Recharge vs Temperature Imbalance

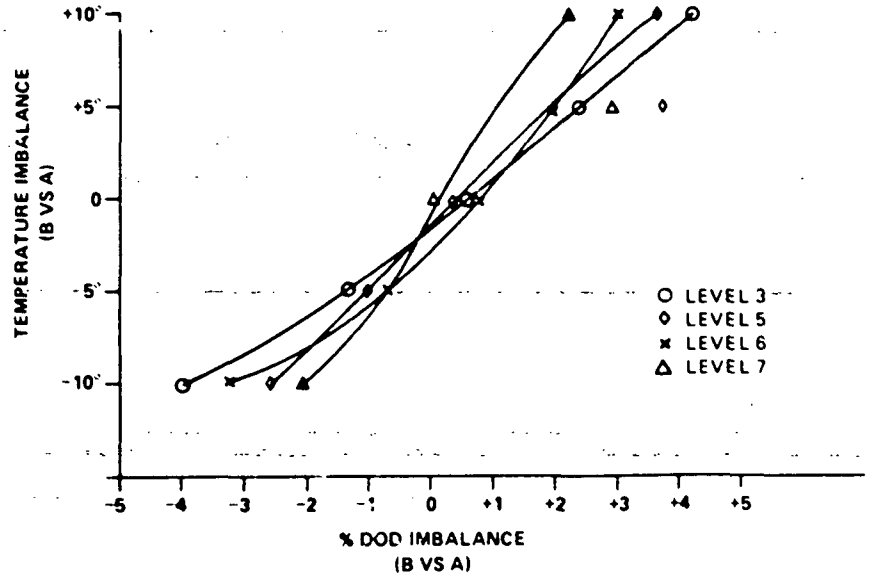

Figure 13. Divergence in Depth-of-Discharge vs Temperature Imbalance

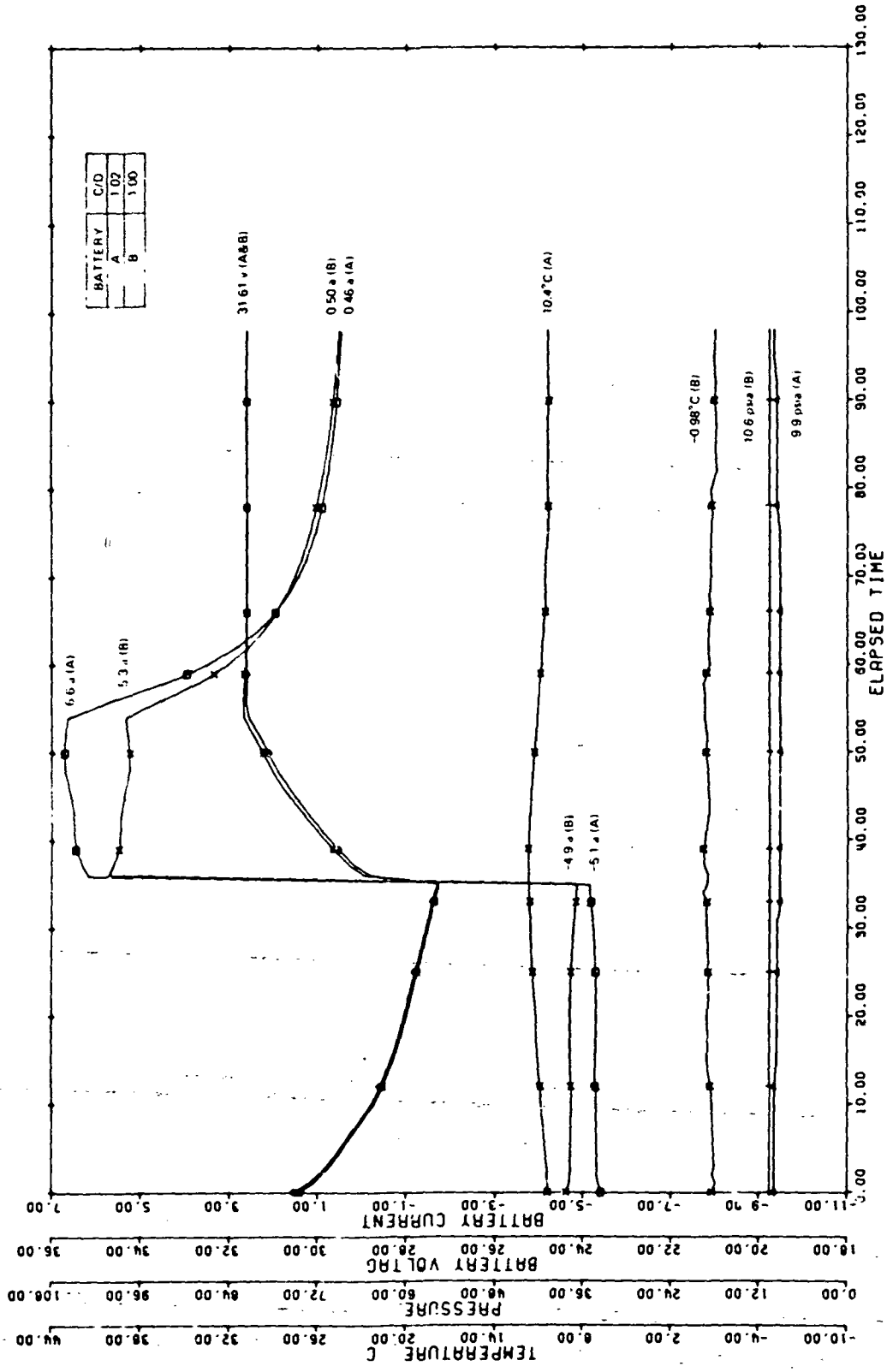

Figure 14. Battery Temperature Imbalance – Battery A Temperature 10°C, Battery B Temperature 0°C at Level 5

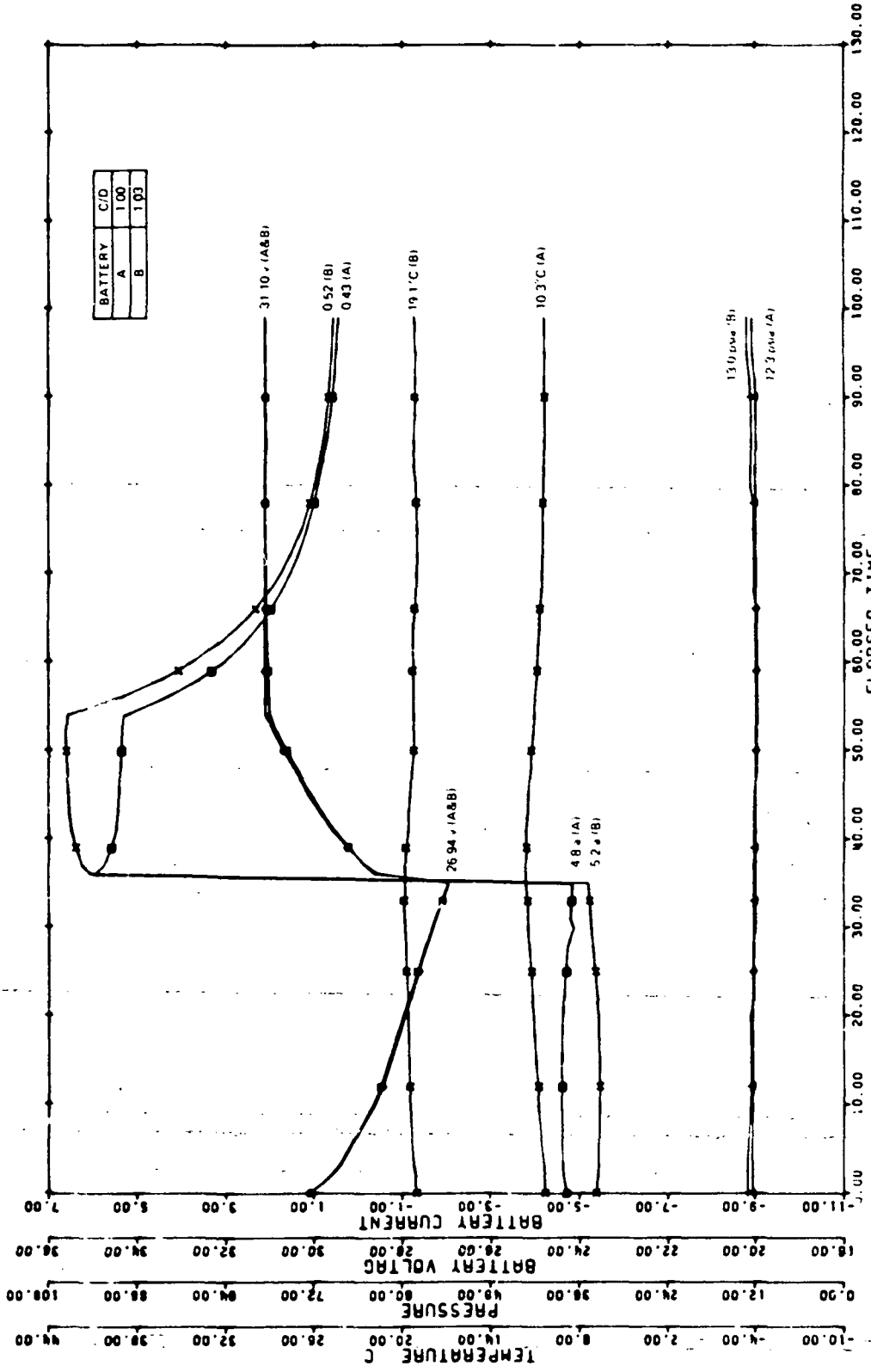

Figure 15. Battery Temperature Imbalance – Battery A Temperature 10°C, Battery B Temperature 20°C at Level 5

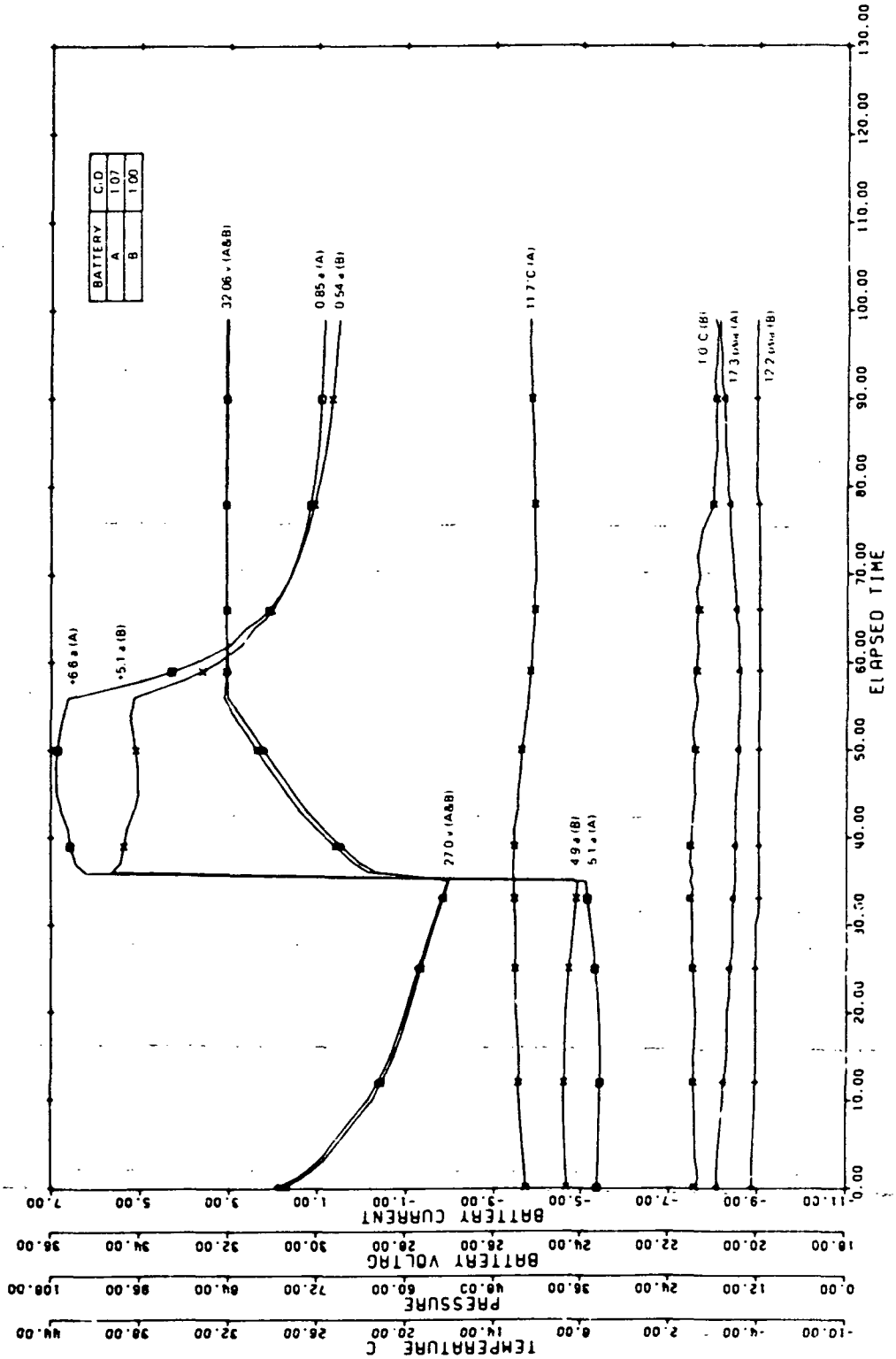

Figure 16. Battery Temperature Imbalance – Battery A Temperature 10°C, Battery B Temperature 0°C at Level 6

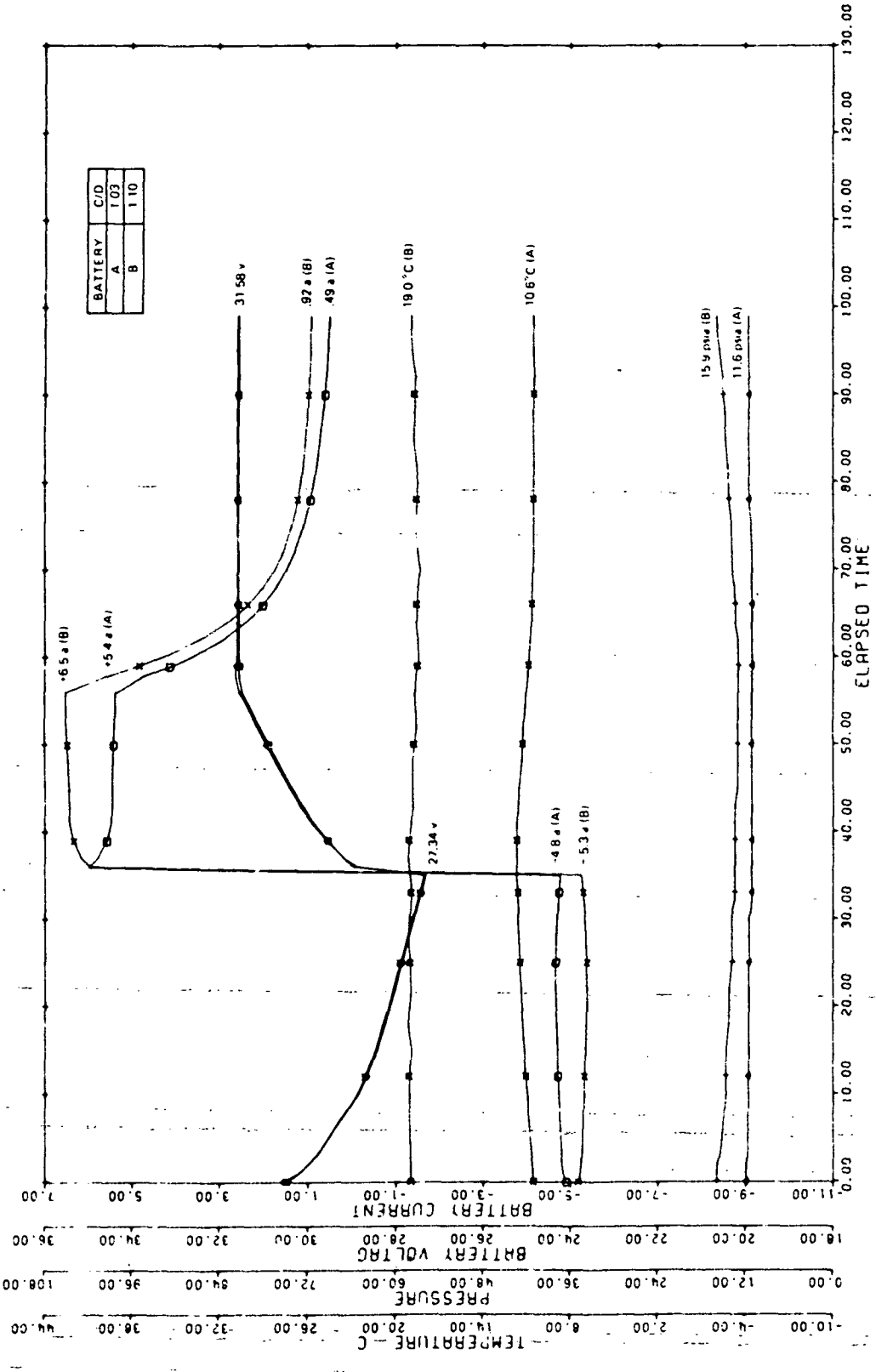

Figure 17. Battery Temperature Inbalance – Battery A Temperature 10°C, Battery B Temperature 20°C at Level 6

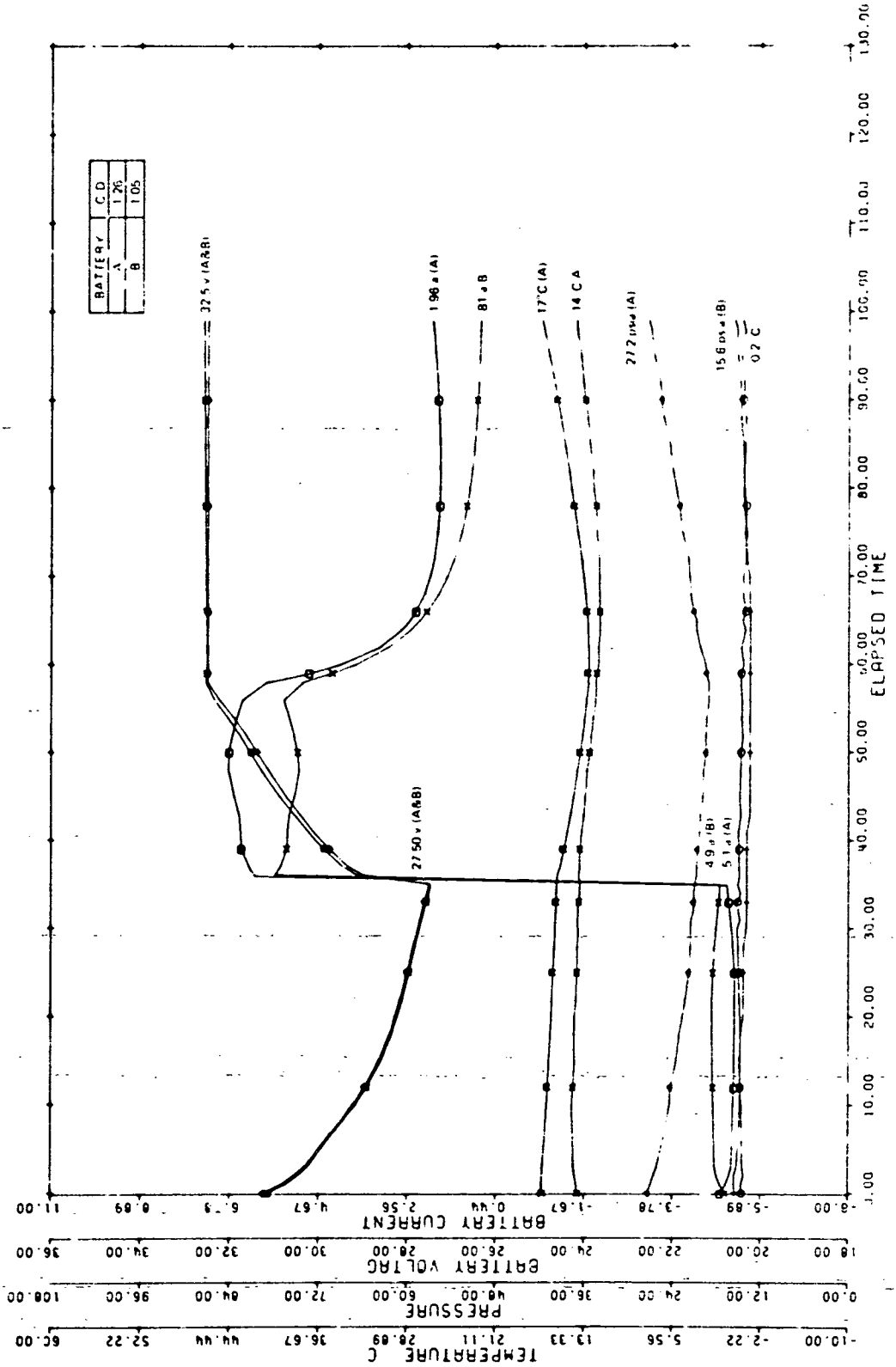

Figure 18. Battery Temperature Imbalance – Battery A Temperature 10°C, Battery B Temperature 0°C at Level 7

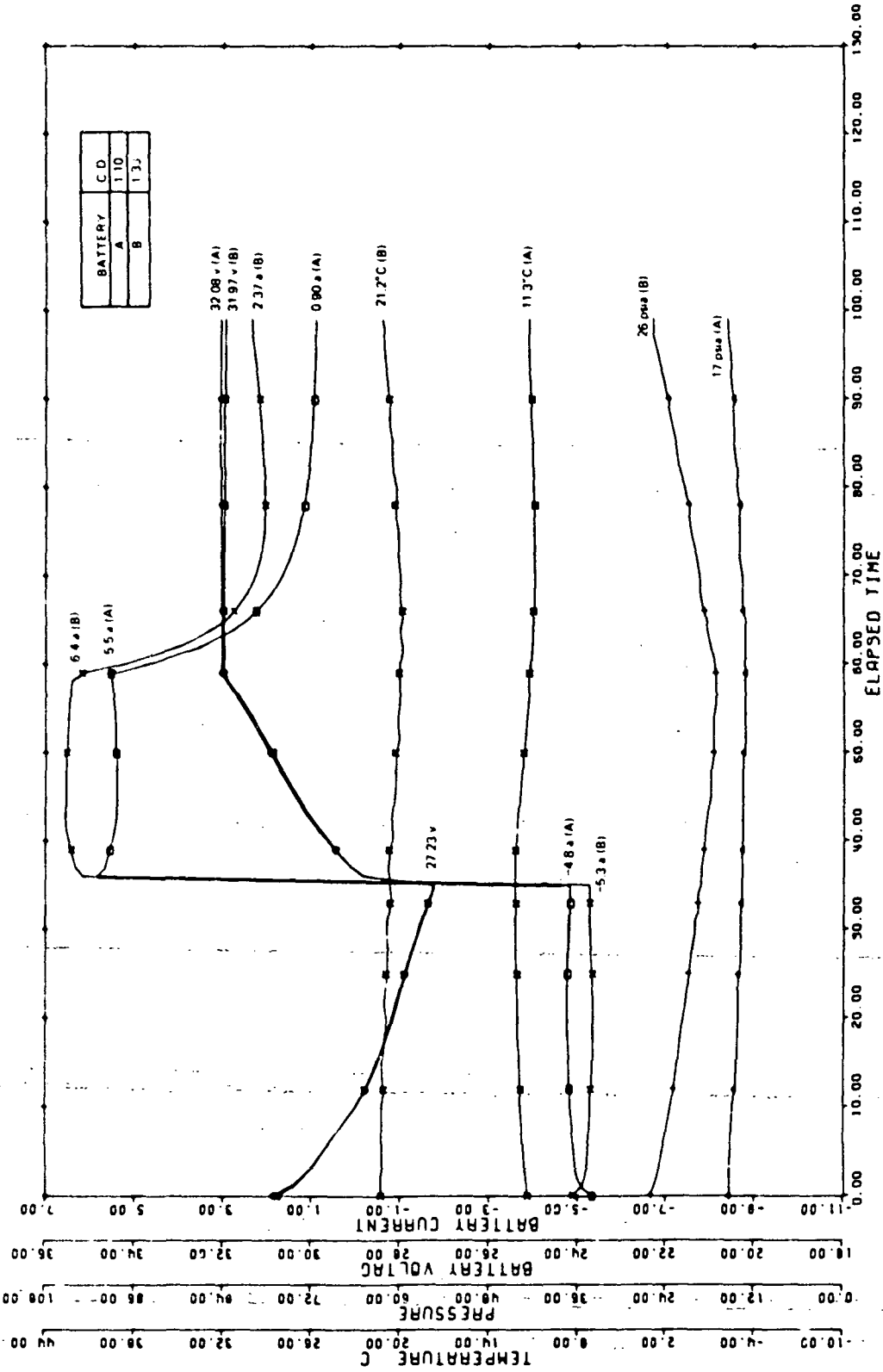

Figure 19. Battery Temperature Imbalance – Battery A Temperature 10°C, Battery B Temperature 20°C at Level 7

This difference in vertical cell gradient was attributed to the physical difference in the thermal environment as explained on page 15.

1.3 Effect of harness resistance mismatch on battery load sharing and energy balance

In the initial test set-up every effort was undertaken to minimize the resistance mismatch between battery power cables. The resistance of battery and power supply cables shown in Figure 20 were determined by applying a known current through each cable and measuring the voltage drop. The internal impedance of each battery was determined by estimating 3 milliohm impedance per cell and by calculating 9 milliohms for all intercell connections. Battery impedance was estimated at approximately 75 milliohms. At 0% cable mismatch, the cable resistance between battery A and the parallel junction measured 76 milliohms while battery B cable resistance to the same point measured 77 milliohms. Cable mismatches of 14.5, 27.6, 40.8, 53.9, 67.1 and 132.9% were attained by introducing precision shunts in 10.0 milliohm steps between battery B and the parallel connection. The batteries were cycled at the normal operating mode of 25% DOD at level 5 and 10°C temperature.

The effect of battery cable mismatch resulted in the divergence in the depth-of-discharge as the battery with the highest cable resistance supported less of the load on discharge. Referring to Table 4, a cable imbalance of 54% resulted in a decrease in the depth-of-discharge of battery B from 25.3% to 24% as battery A increased from 24.8% to 26.2%. In contrast, the ratio of ampere hour charge-to-discharge ratio for either battery remained essentially the same, regardless of the degree of mismatch. Additionally, changing the voltage level from five to six produced identical results. Now, the C/D ratios were higher only to correspond to the higher voltage limit.

After 10,000 cycles, the test was repeated again with lower power cable resistances as specified in Figure 21. The battery cable resistances were lowered by approximately 87% to 10 milliohms for battery B and 9.5 milliohms for battery A. The power supply cable resistance was also lowered from 20 to 8 milliohm.

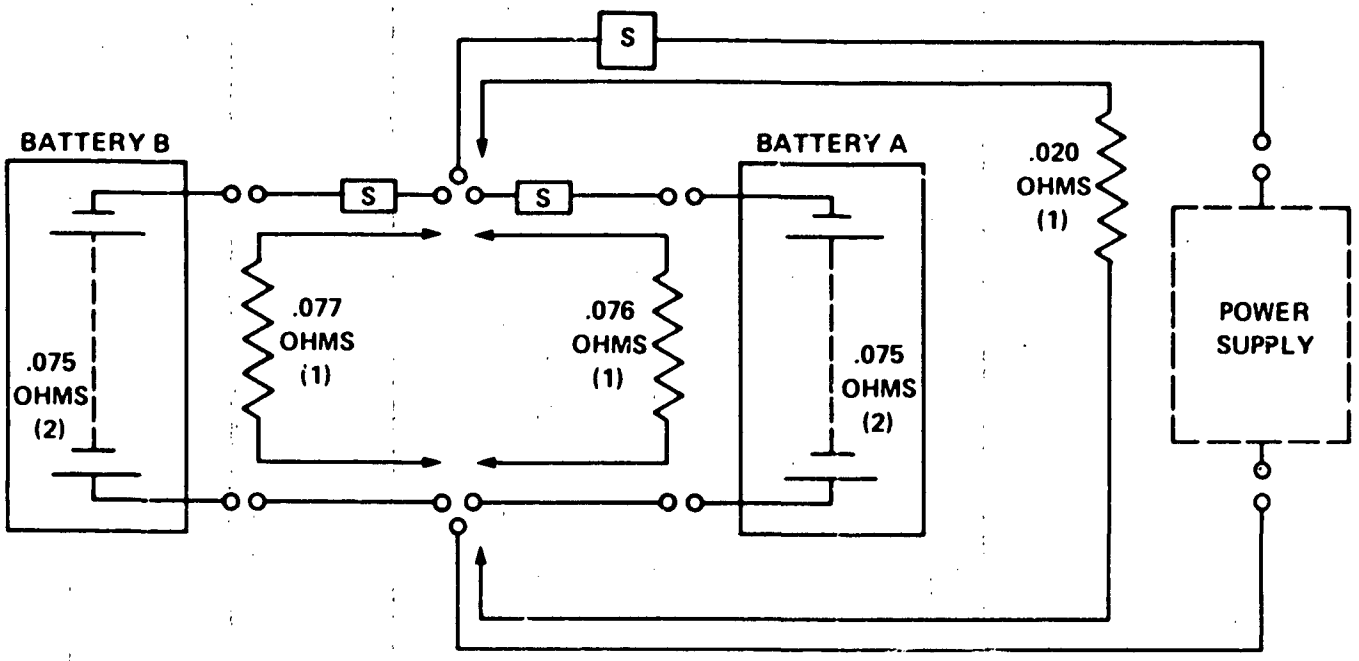

(1) MEASURED VALUES
(2) CALCULATED VALUES BASED ON 3 MΩ/CELL AND 9 MΩ FOR INTERCELL CONNECTIONS

Figure 20. Block Diagram of Power Cable Resistances

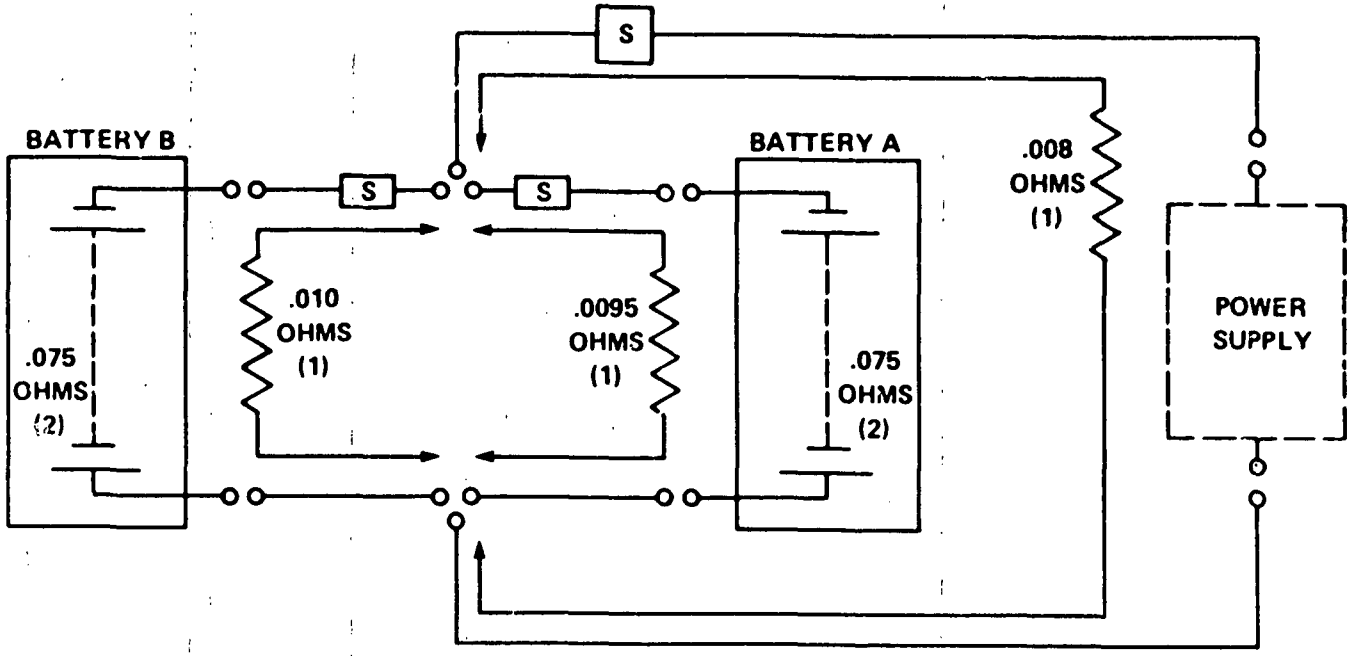

(1) MEASURED VALUES
(2) CALCULATED VALUES BASED ON 3 MΩ/CELL AND 9 MΩ FOR INTERCELL CONNECTIONS

Figure 21. Block Diagram of Modified Power Cable Resistances

Table 4
Effect of Cable Mismatch on Load Sharing and C/D Ratio at V.L. 5

% MISMATCH	BATTERY A		BATTERY B	
	C/D	DEPTH OF DISCHARGE (%)	DEPTH OF DISCHARGE (%)	C/D
0	1.04	24.8	25.3	1.02
14.5	1.04	25.2	25.0	1.03
27.6	1.05	25.5	24.7	1.02
40.8	1.05	25.8	24.3	1.03
53.9	1.04	26.2	24.0	1.03
67.1	1.04	26.6	23.6	1.02
132.8	1.04	28.2	21.9	1.02

Although the test was performed at 57.9 and 105.3% mismatch, the results referring to Table 5 indicate that both batteries experienced similar depths-of-discharge and ampere hour recharge ratio regardless of the mismatch.

In the first evaluation, where the battery cable resistance was nearly identical to the internal battery impedance, small changes in the cable resistance substantially altered the total resistance in the circuit leg comprising both battery impedance and cable resistance. As the cable resistance becomes a smaller faction of the total resistance, the effect of subsequent power cable mismatch becomes less significant.

Referring to Figures 22 to 27, the trend of unequal load currents and battery voltage increased with higher cable mismatches. However, cell pressures and temperatures remained nominal since the C/D ratios were not effected by the mismatches.

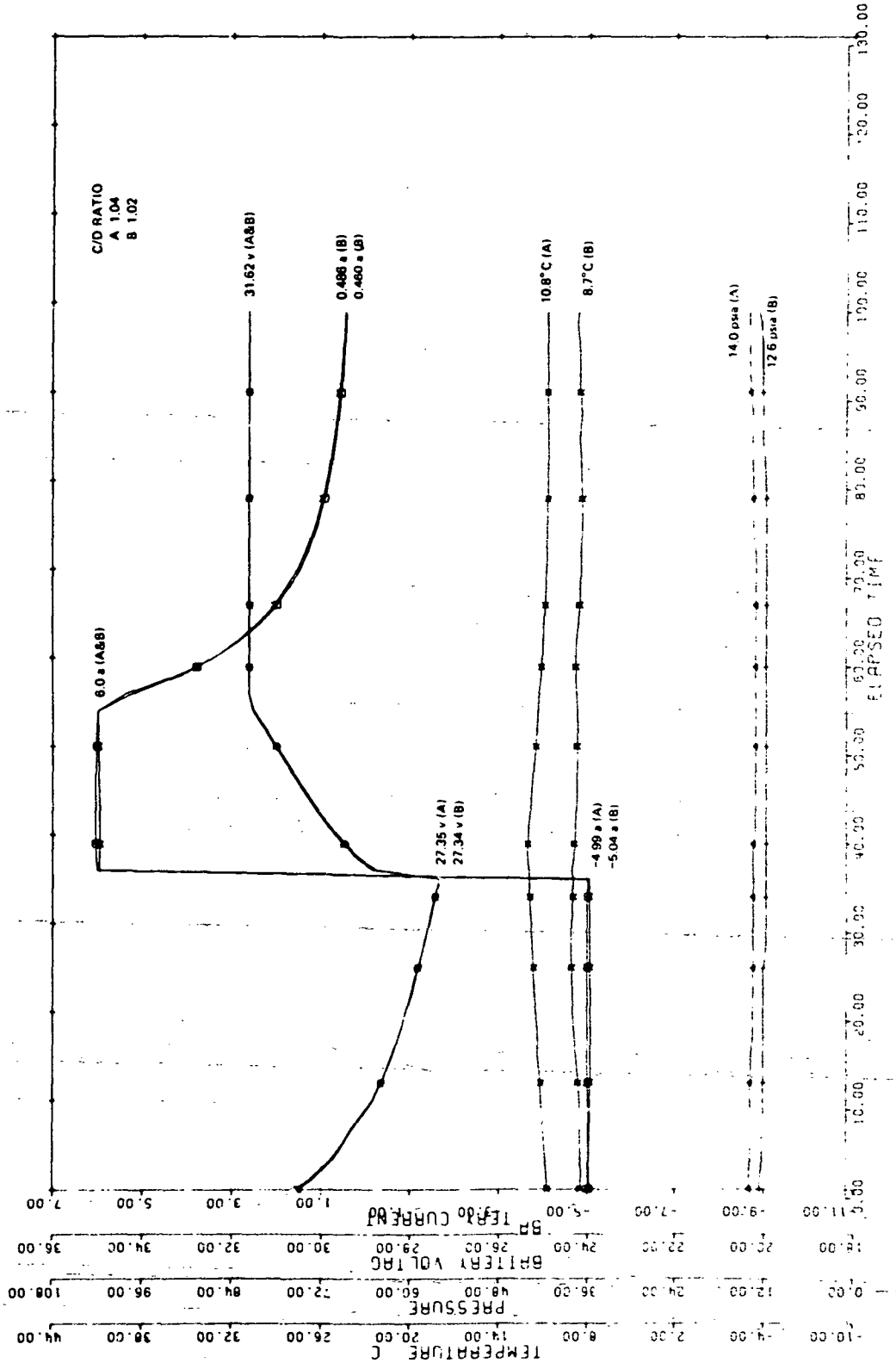

Figure 22. 0% Cable Resistance Mismatch with 77 Milliohm Cables at VL5

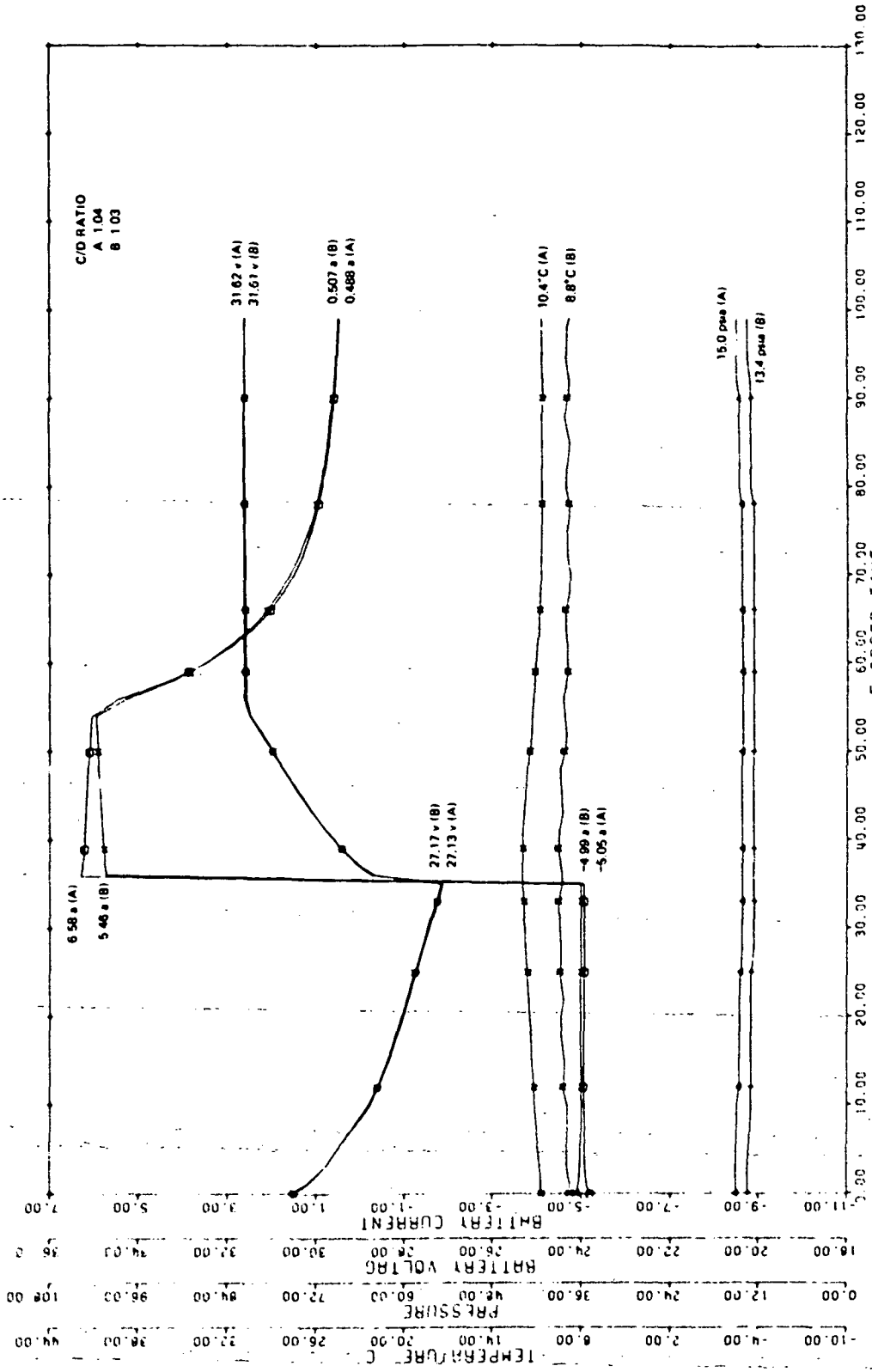

Figure 23. 14.5% Cable Resistance Mismatch with 77 Milliohm Cables at VL5

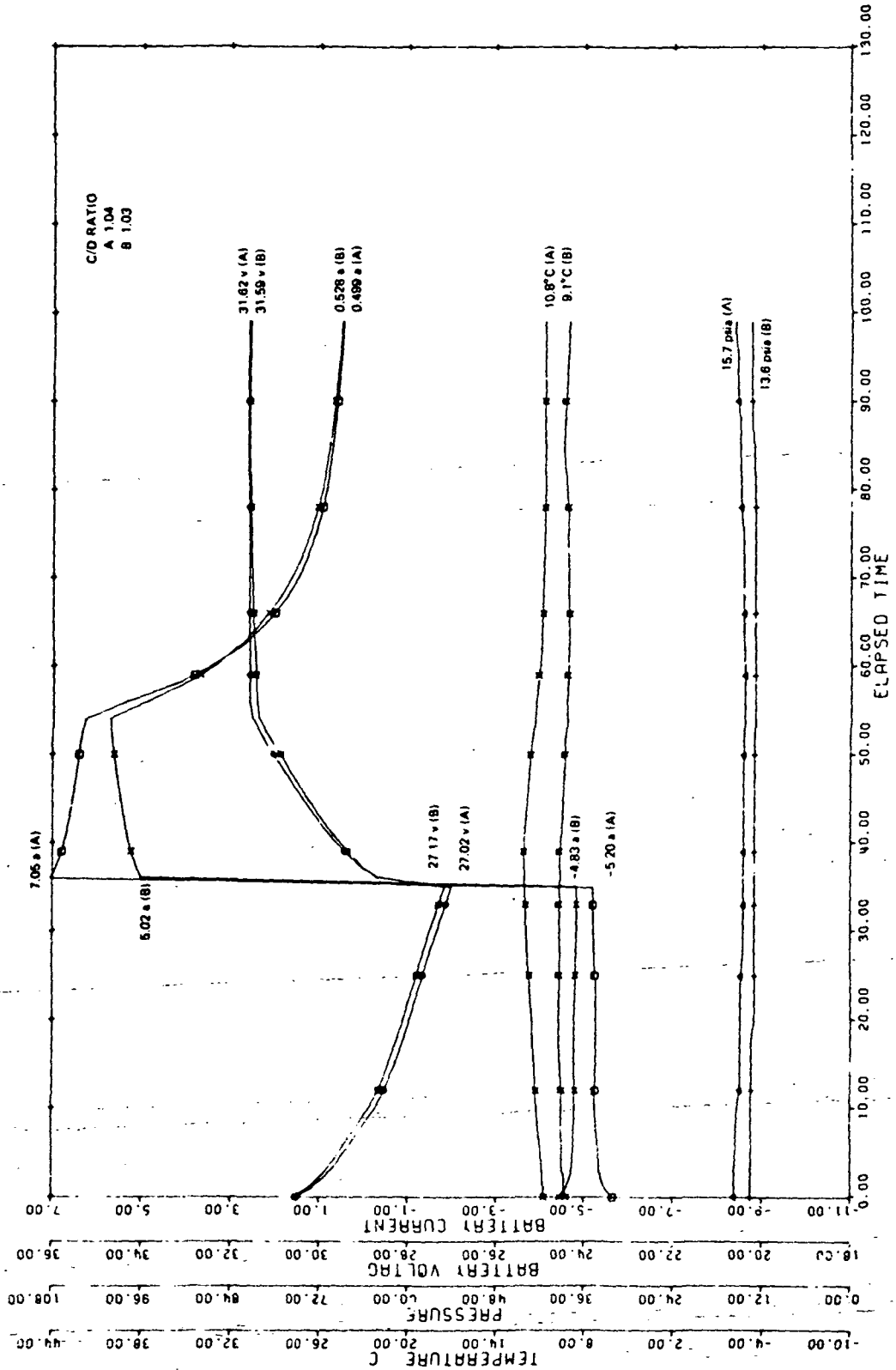

Figure 24. 53.9% Cable Resistance Mismatch with 77 Milliohm Cables at VLS

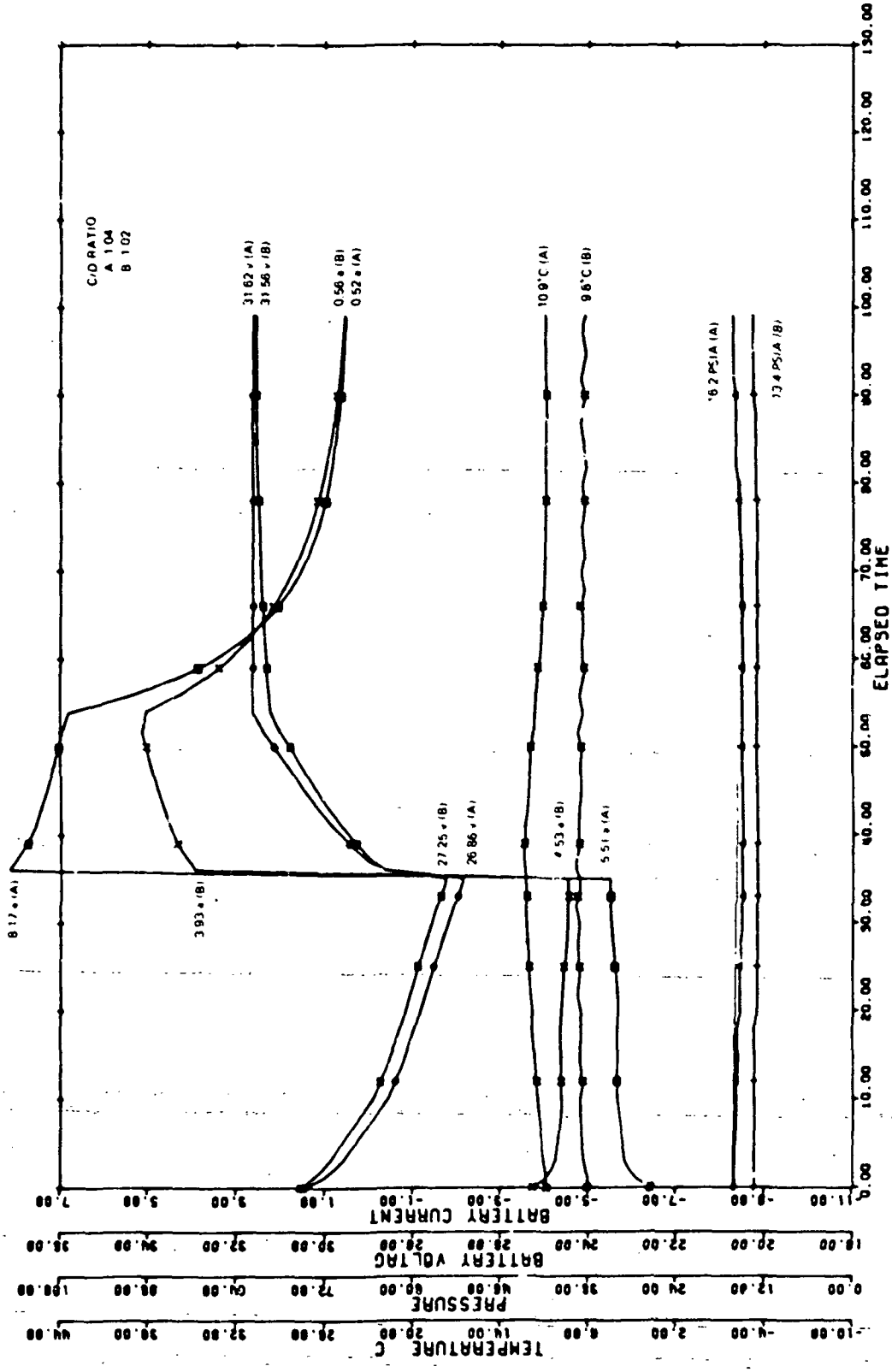

Figure 2... 132.8% Cable Resistance Mismatch with 77 Milliohm Cables at VL5

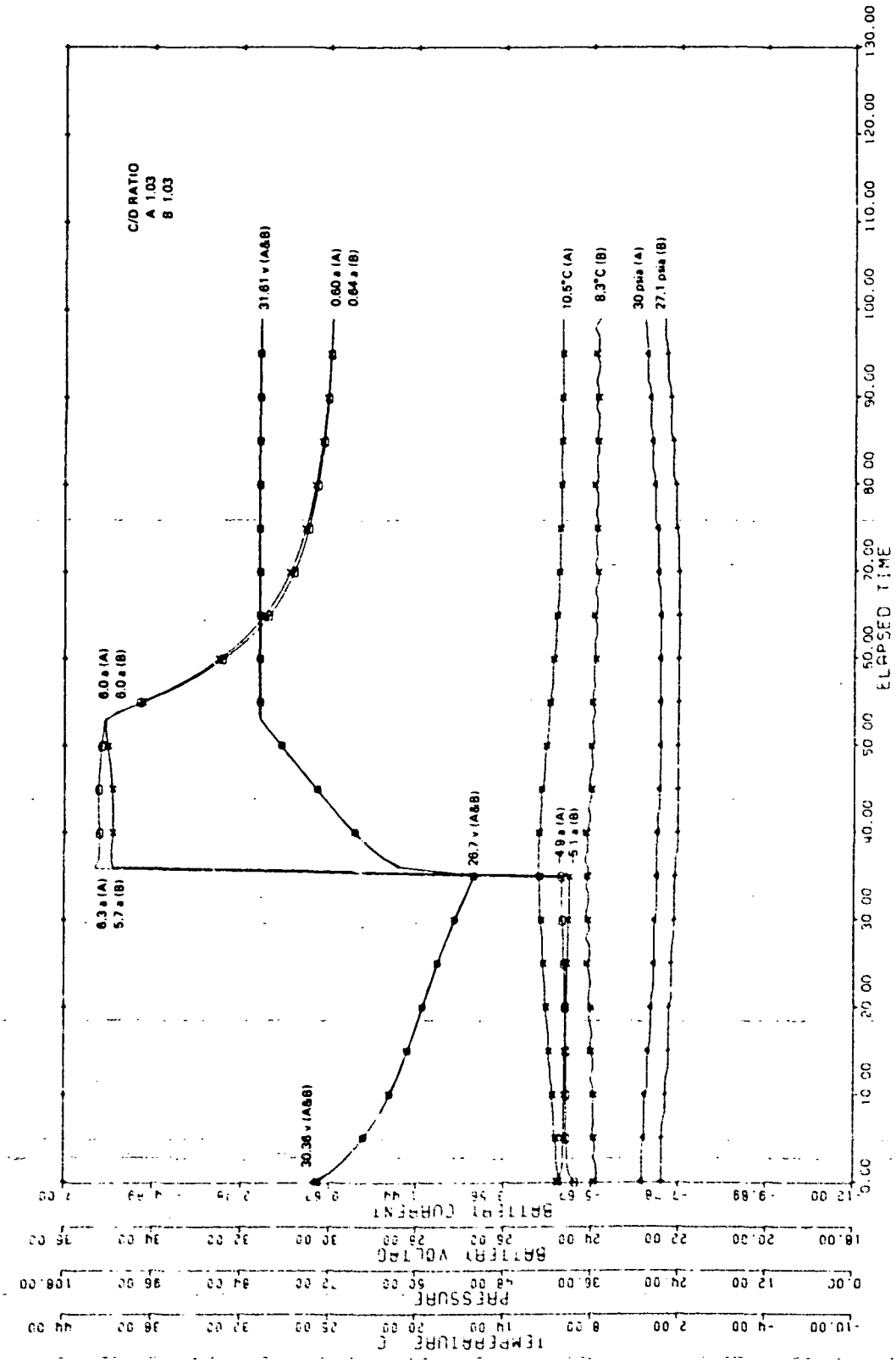

Figure 26. 57.9% Cable Resistance Mismatch with 10 Milliohm Cables at VLS

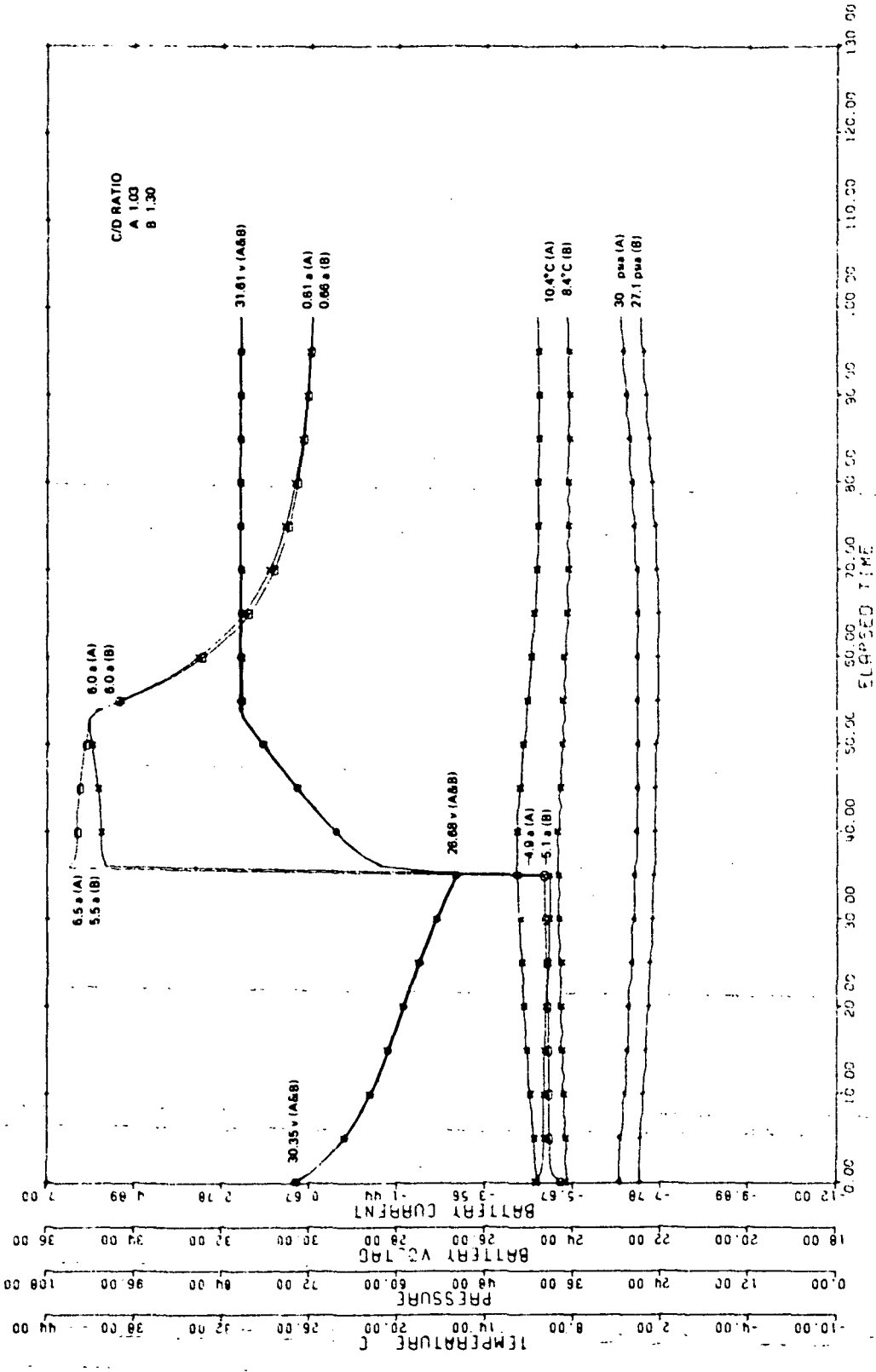

Figure 27. 105.3% Cable Resistance Mismatch with 10 Milliohm Cables at VLS

Table 5
Comparison of Cable Mismatch vs Battery Cable Resistance at V.L. 5

% MISMATCH	BATTERY A POWER CABLE RESISTANCES	BATTERY B POWER CABLE RESISTANCES	BATTERY A C/D	BATTERY A DOD (%)	BATTERY B DOD (%)	BATTERY B C/D
0.	76	77	1.04	24.8	25.3	1.02
53.9		117	1.04	26.2	24.0	1.03
132.9		177	1.04	28.2	21.9	1.02
0	9.5	10	1.03	25.0	25.3	1.03
57.9		15	1.03	25.1	25.2	1.03
105.3		20	1.03	25.3	25.0	1.03

1.4 Effect of one shorted cell battery on parallel battery performance

Prior to the shorted cell simulation, parallel batteries were cycled in the normal orbital regime at the baseline charger level 5 at 25% DOD and 10°C ambient temperature.

The partially shorted cell was simulated by connecting a 1.0 ohm resistive load across one cell in battery B. As the test proceeded, the current through the resistor, which was continuously monitored, was used to determine the current through the shorted cell and the lost cell capacity with each cycle. During this period the partially shorted cell was discharging at 1 ampere greater than the battery and that the end of charge current of the battery had tapered to +0.5 amperes in comparison to −0.5 amperes for the shorted cell, as shown in Figure 28. This cell experienced a cummulative capacity loss of 14.43 ampere hours over eight cycles as the cell voltage decayed to 0.35 volts. From Table 6, note that prior to the last cycle the partially shorted cell supported a substantial charge voltage (1.27 to 1.32 volts) and discharge voltage (1.21 to 1.03) volts in comparison to a typical cell in battery B which consistently measured 1.45 volts on charge and 1.23 volts on discharge.

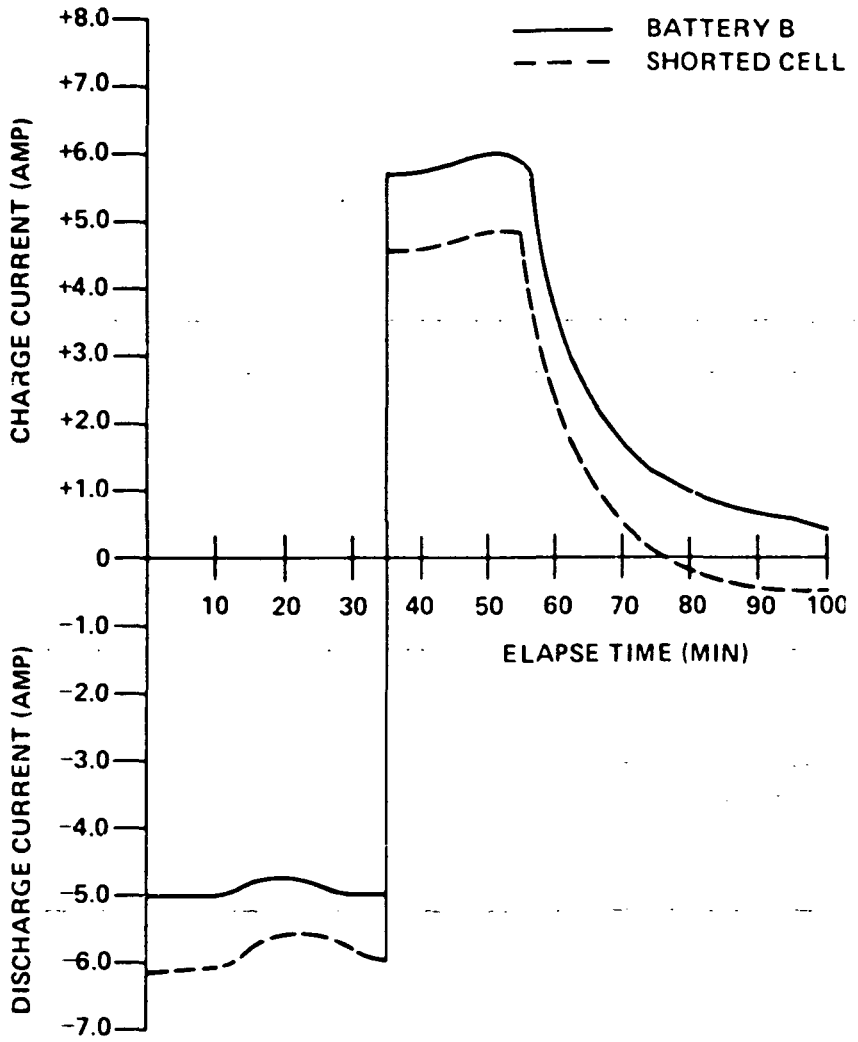

Figure 28. Current Profile of Battery B and the Partially Shorted Cell in Battery B

Table 6
Partially Shorted Cell Characteristics During Decay Period at V.L. 5

CYCLE	LOST CAPACITY (AH)	END OF DISCHARGE VOLTAGE	END OF CHARGE VOLTAGE
1	−1.55	1.21	1.32
2	−1.66	1.20	1.30
3	−1.72	1.19	1.29
4	−1.76	1.18	1.29
5	−1.75	1.15	1.28
6	−1.71	1.06	1.28
7	−1.68	1.03	1.27
8	−2.60	0.35	–

Monitoring battery parameters during the shorted cell decay period revealed no change in C/D ratio and load currents. Data presented in Table 7 indicated that battery voltages were identical and only a slight difference in the end of charge and discharge currents were measured. A comparison of battery parameters prior to complete cell decay depicted in Figure 29 illustrates no significant change in cell pressure and temperature.

Once the discharge voltage of the partially shorted cell dropped to 0.35 volts, the resistive load was replaced with a hard short. The batteries were allowed to remain cycling at level 5. Table 8 itemizes battery parameters for those first three cycles. Initially, the C/D ratio of battery B increased dramatically from 1.04 during the partially shorted cell period to 2.59 in the first cycle. At the end of three cycles battery B was experiencing a 2.22 C/D ratio with steadily increasing end of charge currents which reached a maximum of 5.67 amperes. The end of charge cell pressures

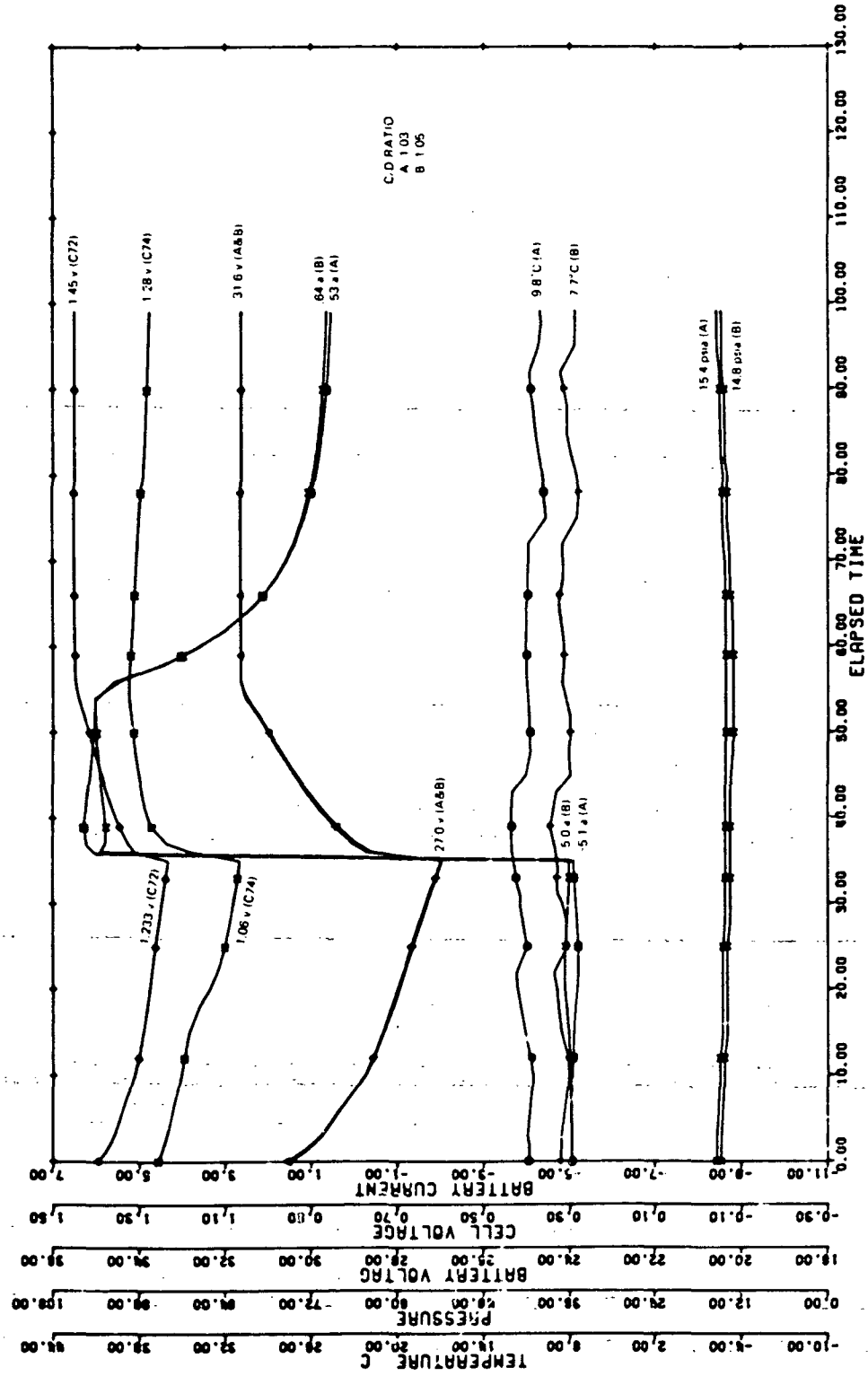

Figure 29. Battery Comparsion Characteristics During Partially Shorted Cell Period at VL5

Table 7
Battery Comparison Characteristics During Cell Decay Period

CYCLE	BATTERY A				BATTERY B			
	END OF DISCHARGE VOLTAGE	END OF DISCHARGE CURRENT	C/D	END OF CHARGE CURRENT	END OF DISCHARGE VOLTAGE	END OF DISCHARGE CURRENT	C/D	END OF CHARGE CURRENT
1	27.02	-5.01	1.03	0.53	27.01	-5.06	1.05	0.62
2	27.04	-4.95	1.03	0.53	27.03	-5.13	1.04	0.63
3	27.03	-4.95	1.03	0.53	27.03	-5.14	1.04	0.64
4	27.03	-4.95	1.05	0.53	27.02	-5.13	1.04	0.64
5	27.02	-5.01	1.03	0.53	27.01	-5.07	1.04	0.64
6	26.98	-5.08	1.03	0.53	26.96	-4.98	1.04	0.64
7	26.96	-5.06	1.03	0.53	26.94	-5.0	1.04	0.64
8	26.96	0.0			26.85	-3.6		

increased significantly, rising from 60 psia to 98 psia with the greatest increase from 17 psia to 60 psia occuring during the first cycle. Cell temperatures measured at the top cell surfaces were 2°C to 3°C higher than the ambient while temperatures on the broad face of interior cells were typically

Table 8
Battery Comparison Characteristics During Hard Cell Short Period at V.L.=5

CYCLE	BATTERY A					BATTERY B				
	END OF DISCH CURRENT (AMP)	Ahr OUT	C/D	END OF CHARGE CURRENT (AMP)	END OF CHARGE PRESSURE (PSIA)	END OF DISCH CURRENT (AMP)	Ahr OUT	C/D	END OF CHARGE CURRENT (AMP)	END OF CHARGE PRESSURE (PSIA)
1	-5.9	3.22	0.95	0.53	15	-4.1	1.77	2.59	4.98	60
2	-5.5	3.64	1.01	0.61	15	-4.5	2.42	2.14	5.49	77
3	-5.5	3.67	1.02	0.63	15	-4.5	2.39	2.22	5.67	90

9°C higher than ambient. In contrast battery A was experiencing a more typical 104% recharge while sharing approximately 60% of the discharge load as cell pressures and temperatures remain nominal. In Figure 30 an examination of battery characteristics on the third cycle and prior to lowering the charger level indicate, that due to the shorted cell in battery B, the average end of charge cell voltage in battery B is 1.51 volts compared to 1.44 volts in battery A.

Because of the unstable condition of battery B the charger level was lowered to level 3 which represents a voltage limit of 30.73 volts or an average cell voltage of 1.397 volts for battery A and 1.463 for battery B with the shorted cell. This resulted in reducing the C/D ratio of battery B from 2.22 at level 5 to 1.19 as cell pressures stablized to less than 25 psia. However, the C/D ratio of battery A dropped from 1.04 at level 5 to 0.99 at level 3 as battery A continued to support approximately 60% of the load. A comparsion of battery characteristics after 29 cycles, Figure 31, revealed a slight difference between battery discharge voltages as charge and discharge currents differ greatly.

1.5 Effect of battery enabling/disabling from the charger bus

Initially, parallel batteries were cycled at the baseline voltage level 5, 25% DOD and 10°C temperature. Battery A remained enabled during the entire test sequence while battery B was disabled and enabled from the charger bus. Referring to Figure 32 the power exerciser consists of a diode in series with each battery which prevents current flow to each battery from the charger (charger disabled), but permits each battery to supply power to the load during discharge. In the spacecraft power system, the normal operating mode exists with these series diodes shorted allowing current to flow into each battery during charge (charger enabled).

The final test results appear in Tables 9 and 10 for battery cable resistances of approximately 77 milliohms and 10 milliohms rspectively. Comparsions of battery characteristics are illustrated in Figures 33 thru 38.

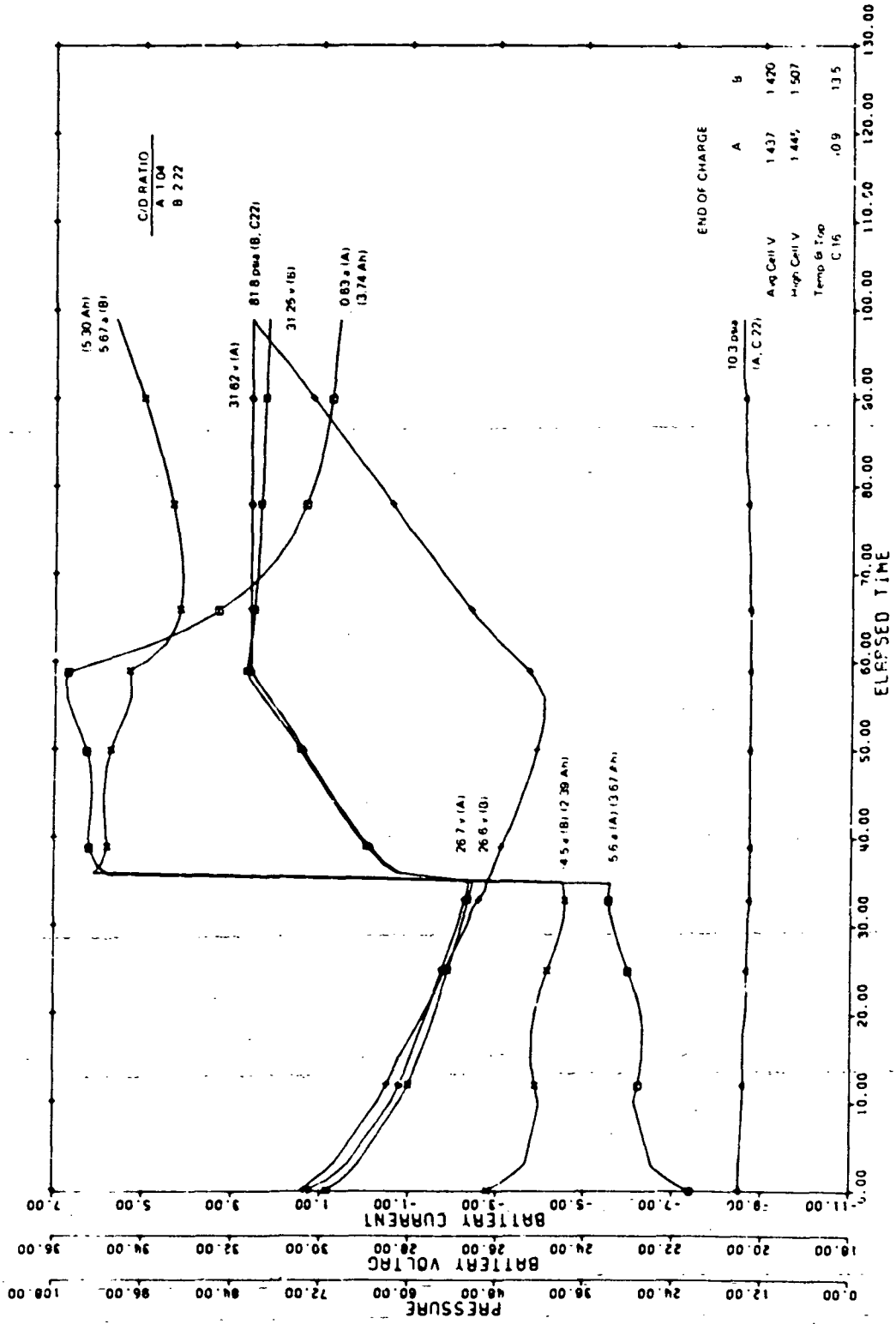

Figure 30. Battery Comparsion Characteristics During Hard Cell Short at VL5

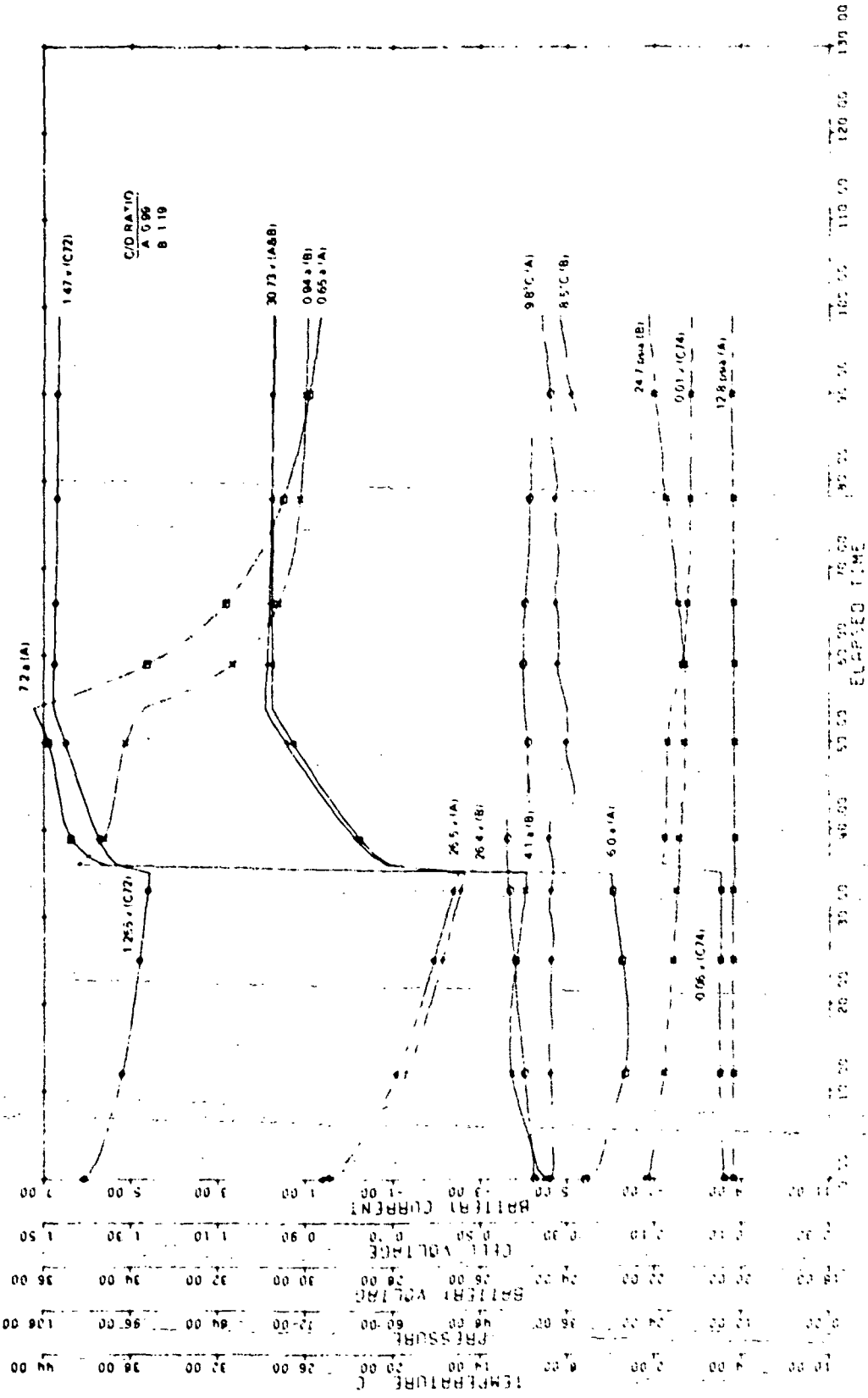

Figure 31. Battery Comparsion Characteristics with Hard Cell Short at VL3

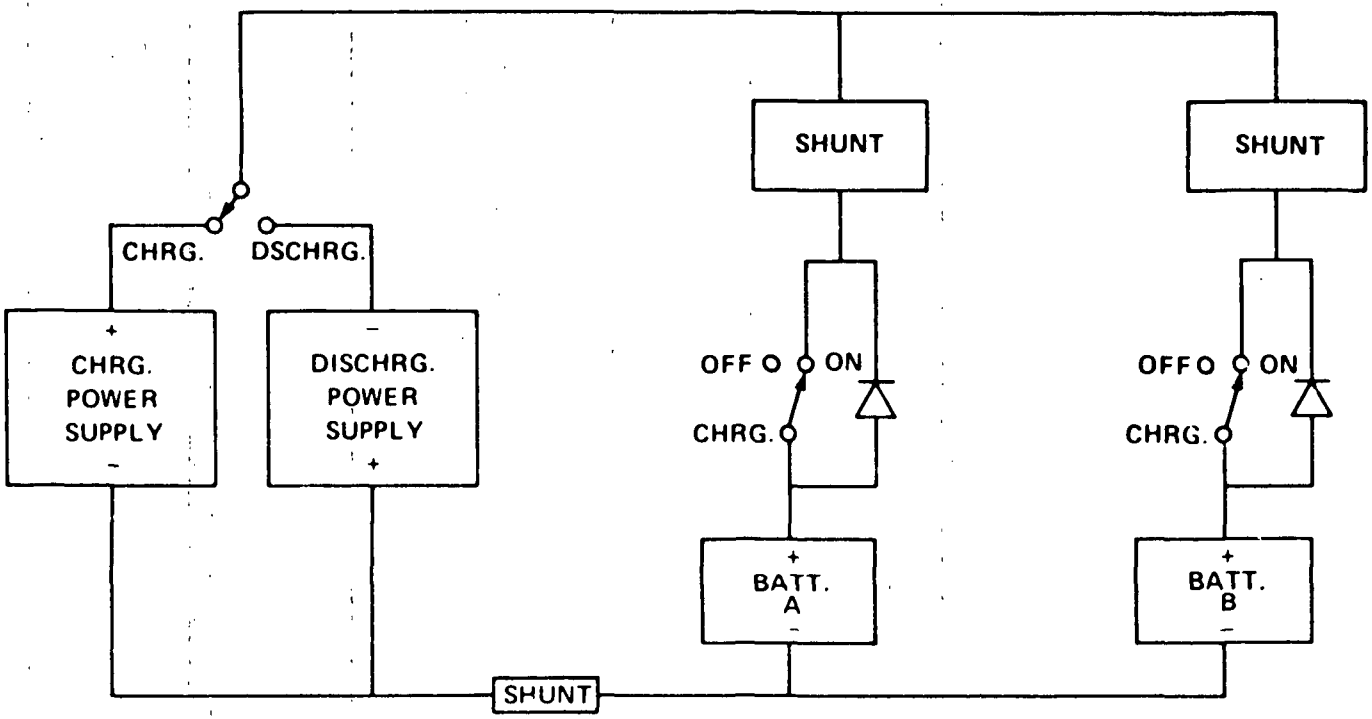

Figure 32. Simplified Block Diagram of Power System Exerciser

Table 9
Disable/Enable Test Summary Cable Resistance 77 Milliohms

PERIOD BATTERY B ENABLED	BATTERY STATUS PRIOR TO ENABLING						BATTERY B CURRENT TRANSIENT (AMP)
	BATTERY A			BATTERY B			
	CURRENT (AMP)	VOLTAGE	AH STATUS	CURRENT (AMP)	VOLTAGE	AH STATUS	
START OF DISCHARGE	10.0	28.1	>12.0	0.0	27.7	5.41	-1.6
END OF DISCHARGE	-7.5	25.5	5.0	-2.7	26.0	5.31	6.5
START OF CHARGE	12.0	29.1	5.37	0.0	26.7	5.34	+23.0
END OF CHARGE	0.75	31.6	>12.0	0.0	27.3	-5.34	+32.0

Table 10
Disable/Enable Test Summary Cable Resistance 10 Milliohms

PERIOD BATTERY B ENABLED	BATTERY STATUS PRIOR TO ENABLING						BATTERY B CURRENT TRANSIENT (AMP)
	BATTERY A			BATTERY B			
	CURRENT (AMP)	VOLTAGE	AH STATUS	CURRENT (AMP)	VOLTAGE	AH STATUS	
START OF DISCHARGE	-10.0	28.7	>12.0	-0.0	28.4	3.5	-6.0
END OF DISCHARGE	8.5	26.1	5.6	1.5	26.8	-4.1	9.0
START OF CHARGE	12.0	29.2	5.2	0.0	27.4	3.7	+25.0
END OF CHARGE	0.8	31.6	>12.0	0.0	28.0	3.8	+49.0
COMPLETE CAPACITY IMBALANCE	0.6	31.6	>12.0	0.0	27.4	12.0	+57.5

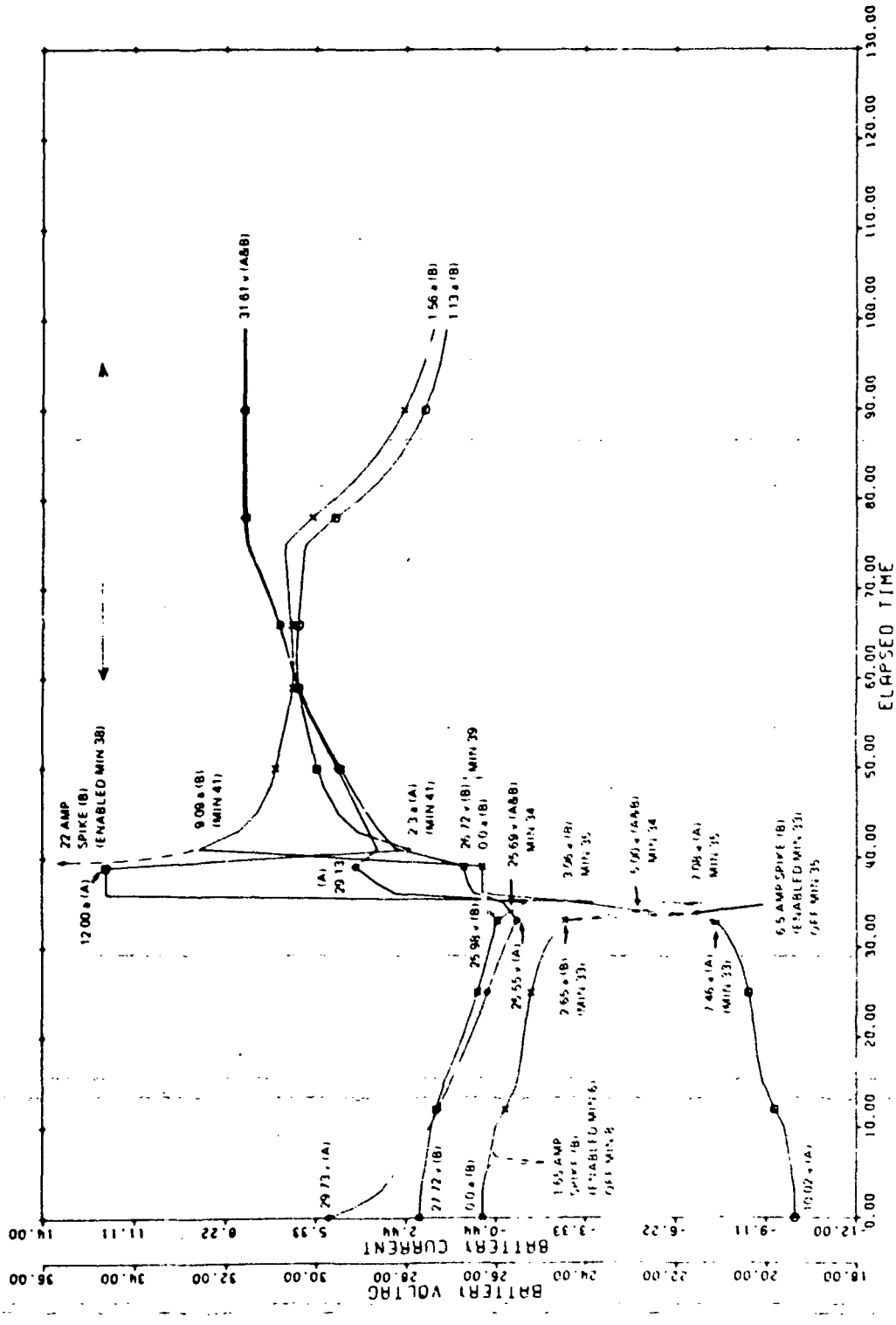

Figure 33. Enable/Disable Test, SOD, EOD, SOC with 77 Milliohm Cable

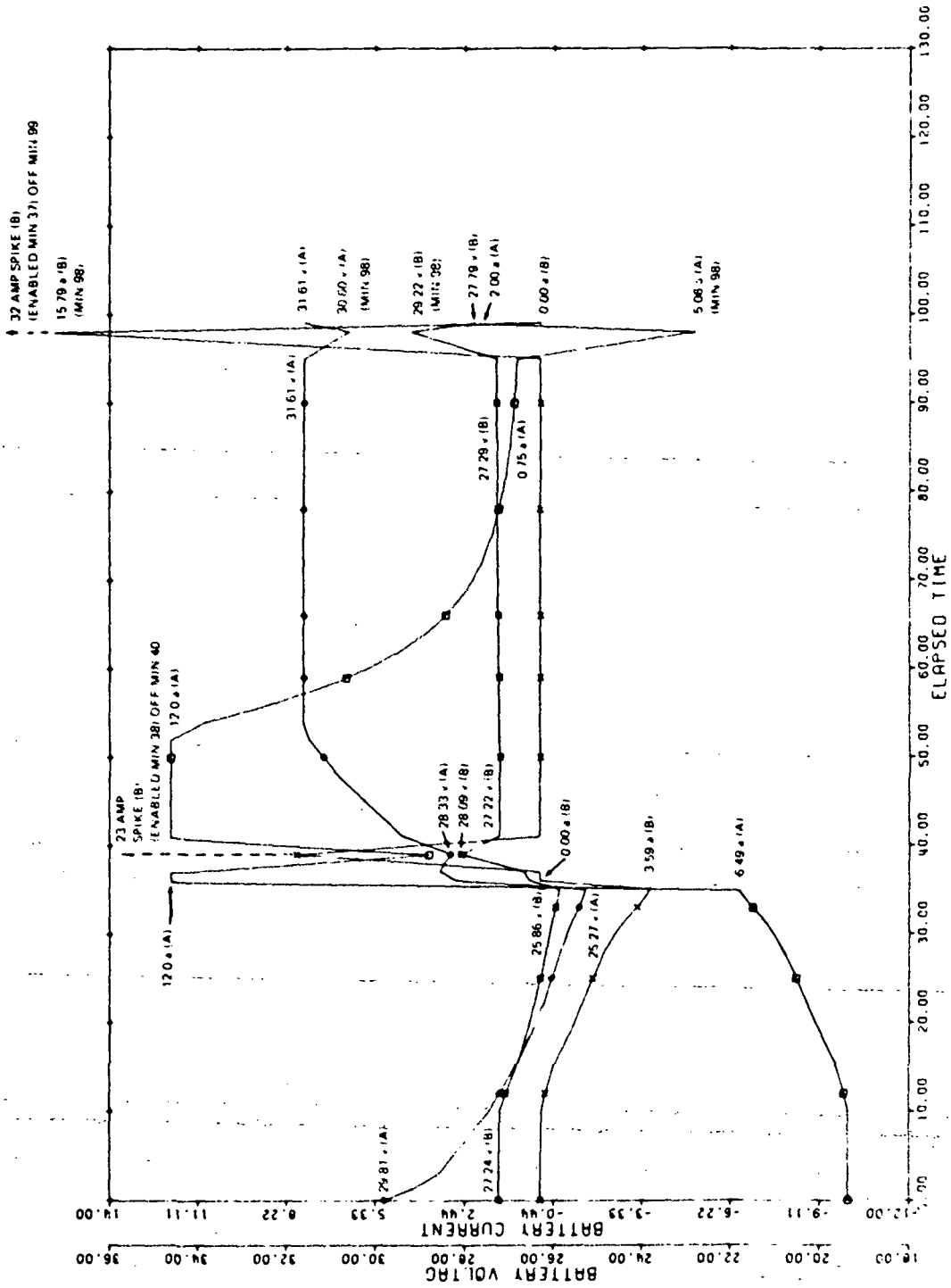

Figure 34. Enable/Disable Test, SOC, EOC with 77 Milliohm Cable

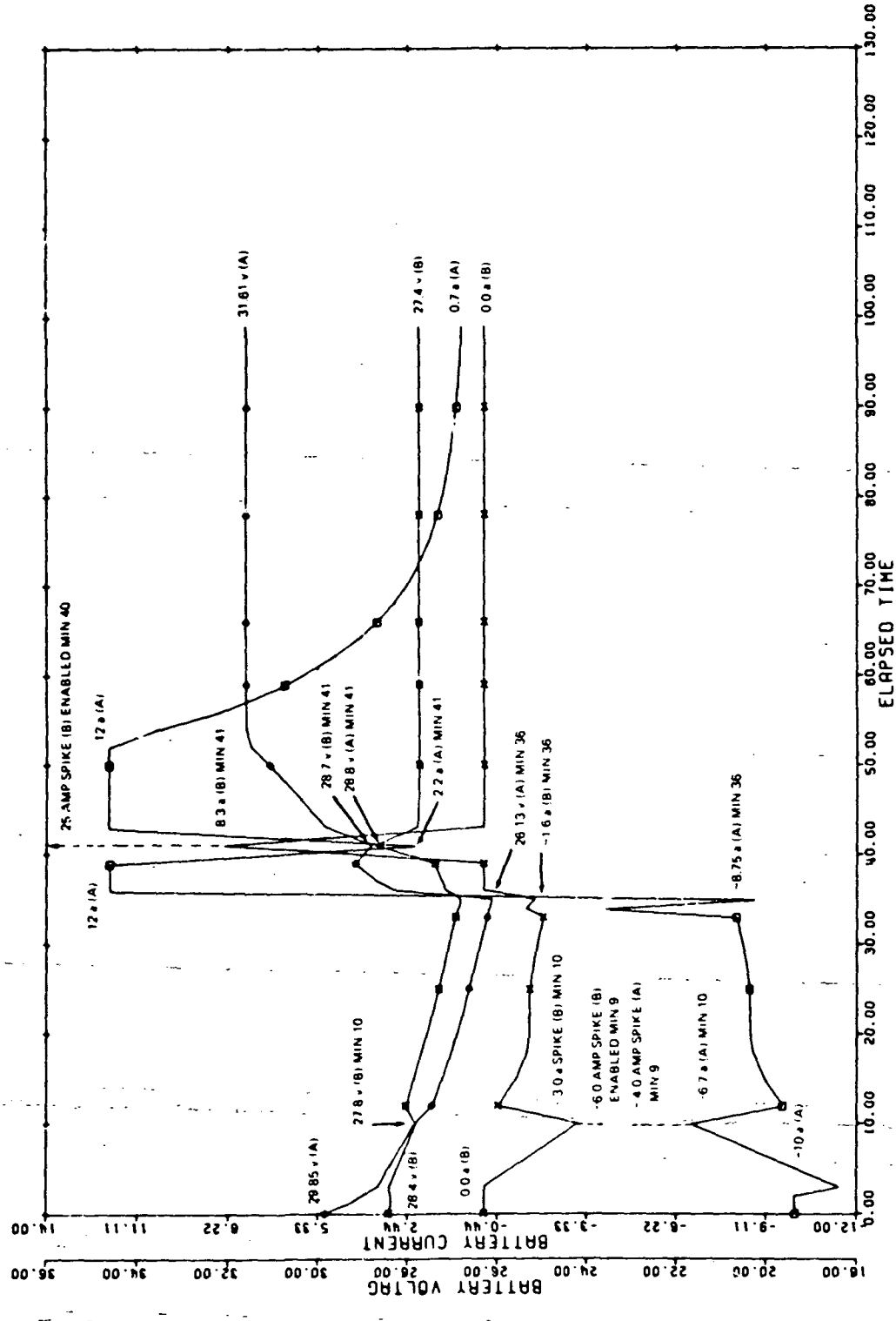

Figure 35. Enable/Disable Test, SOD, EOC, SOC with 10 Milliohm Cables

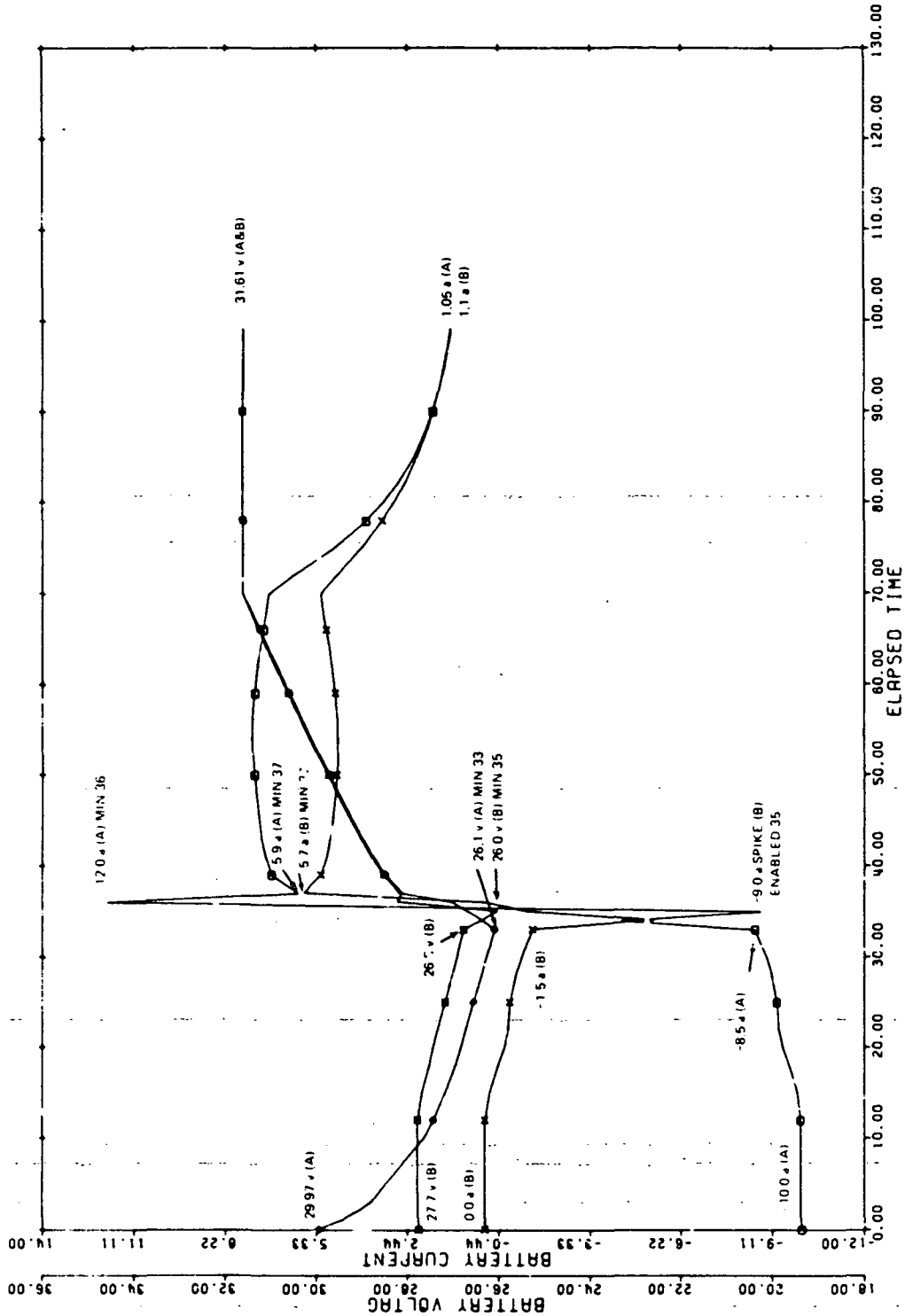

Figure 36. Enable/Disable Test, EOD with 10 Milliohm Cables

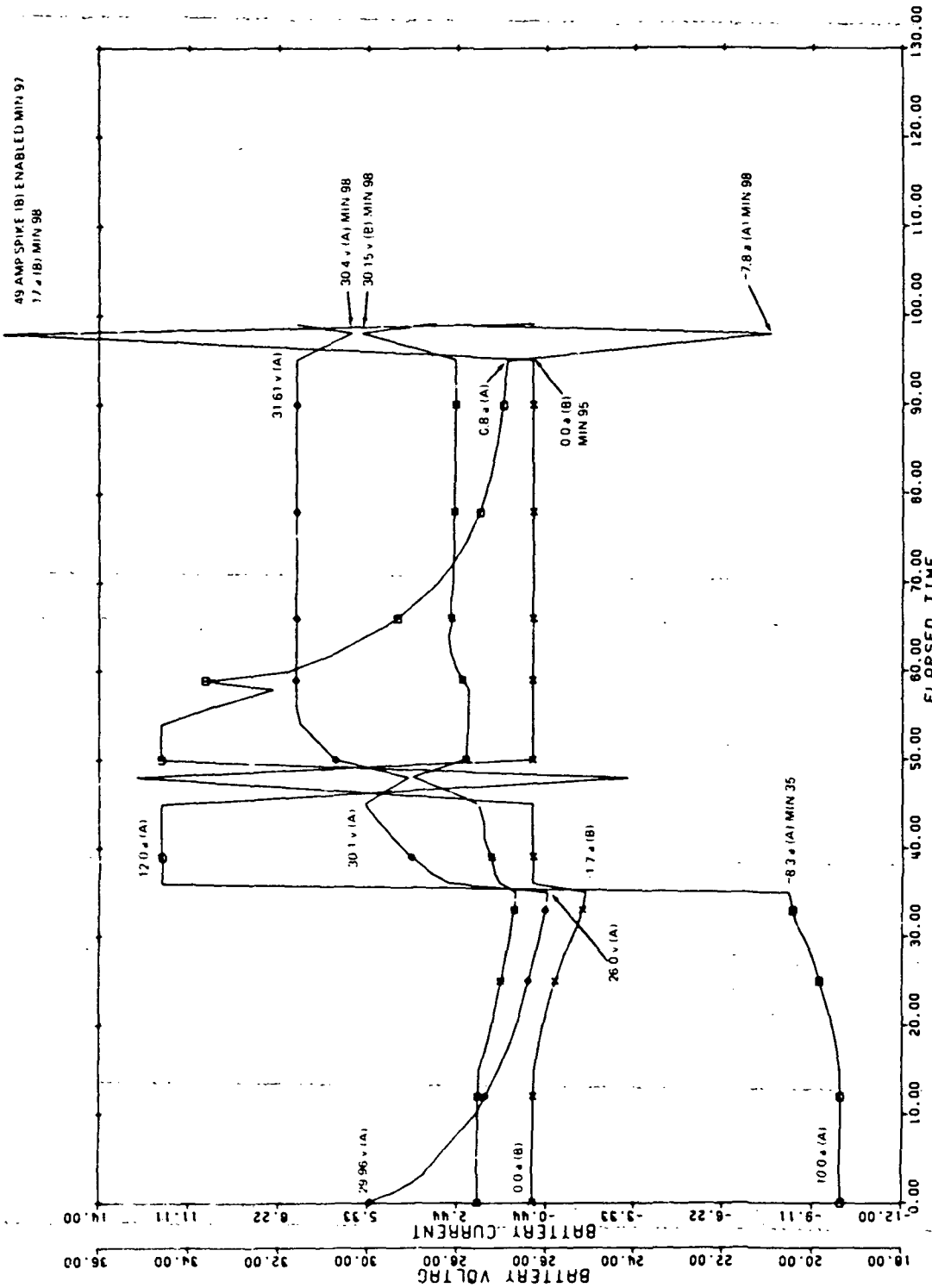

Figure 37. Enable/Disable Test, EOC with 10 Milliohm Cables

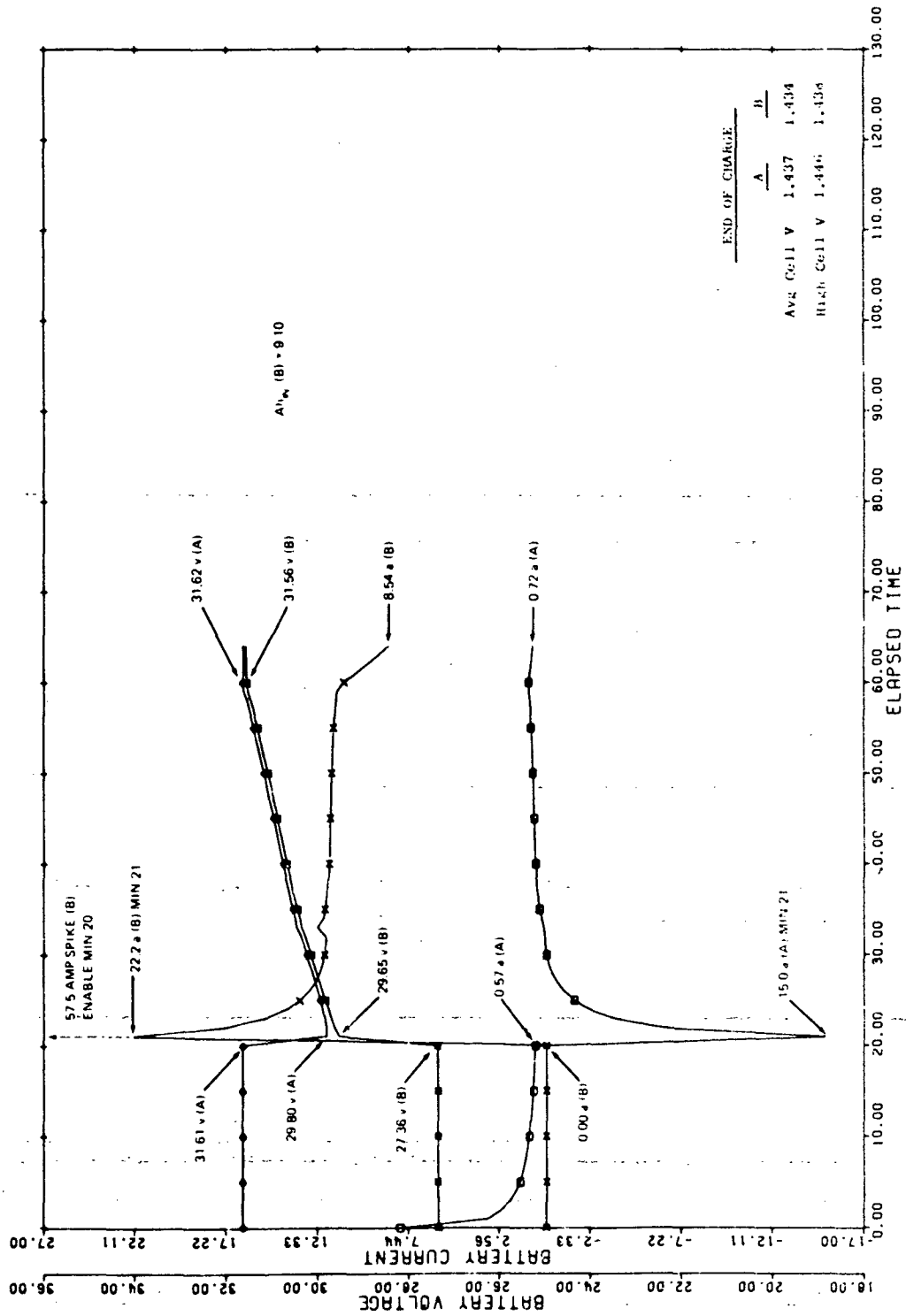

Figure 38. Enable/Disable Test, Complete Capacity Unbalance with 10 Milliohm Cables

Higher current transients were observed when battery B was enabled at either the start or end of change period as compared to the discharge period. This corresponded to the greatest difference in individual battery voltages.

For instance, from Table 9, prior to enabling battery B at the end of charge, battery A had completed a full recharge while battery B experienced a cummulative discharge lose of 5.34 Ahr when removed from the charger bus three previous orbits. The difference in the battery voltage was 4.3 volts prior to enabling battery B. The current transient into battery B was 32.0 amperes. This is in contrast to enabling battery B at either start or end of discharge where battery voltages are very similar and the resulting current peaks are less than 7.0 amperes.

The trend toward higher peaks also occurs as the cable resistance was lower as seen from a comparsion of Table 9 and 10. Citing the previous example, current spikes of approximately 49.0 amperes was observed when the test was repeated with approximately 10 milliohm cable resistance.

The highest current transient occurred with a complete capacity imbalance between batteries. Battery B was removed from the bus and discharged to 100% DOD based on rated capacity. Battery A remained on the charger bus with an end of charge current of 0.57 amperes. When battery B was enabled to the charger bus, a current peak of 57.5 amperes was measured.

1.6 Effect of life cycling and battery characteristics

1.6.1 Battery charge response at voltage level 5 and within the temperature range 0°C to 20°C

This test was performed after approximately 11,500 orbits. The final test results which are compared to the previous test results obtained within the first 1000 orbits are given in Table 11. While there is no significant change in battery C/D ratio and load sharing, a comparison of battery characteristics from Figures 5 thru 7 and Figures 39 thru 41 indicated that cell pressures have increased typically from 13 psia to 28 psia.

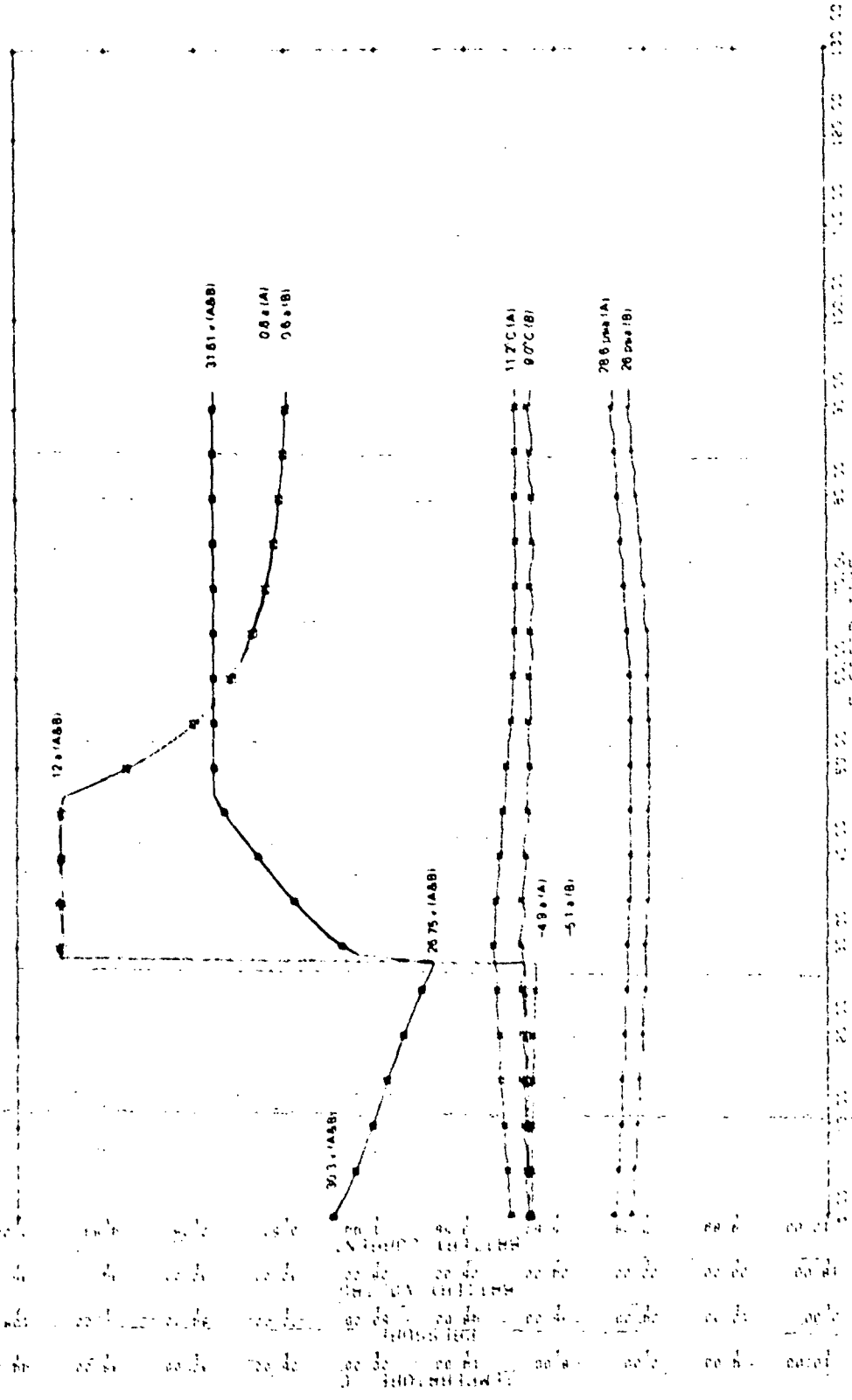

Figure 39. Battery Charge Response at Level 5 and 10°C

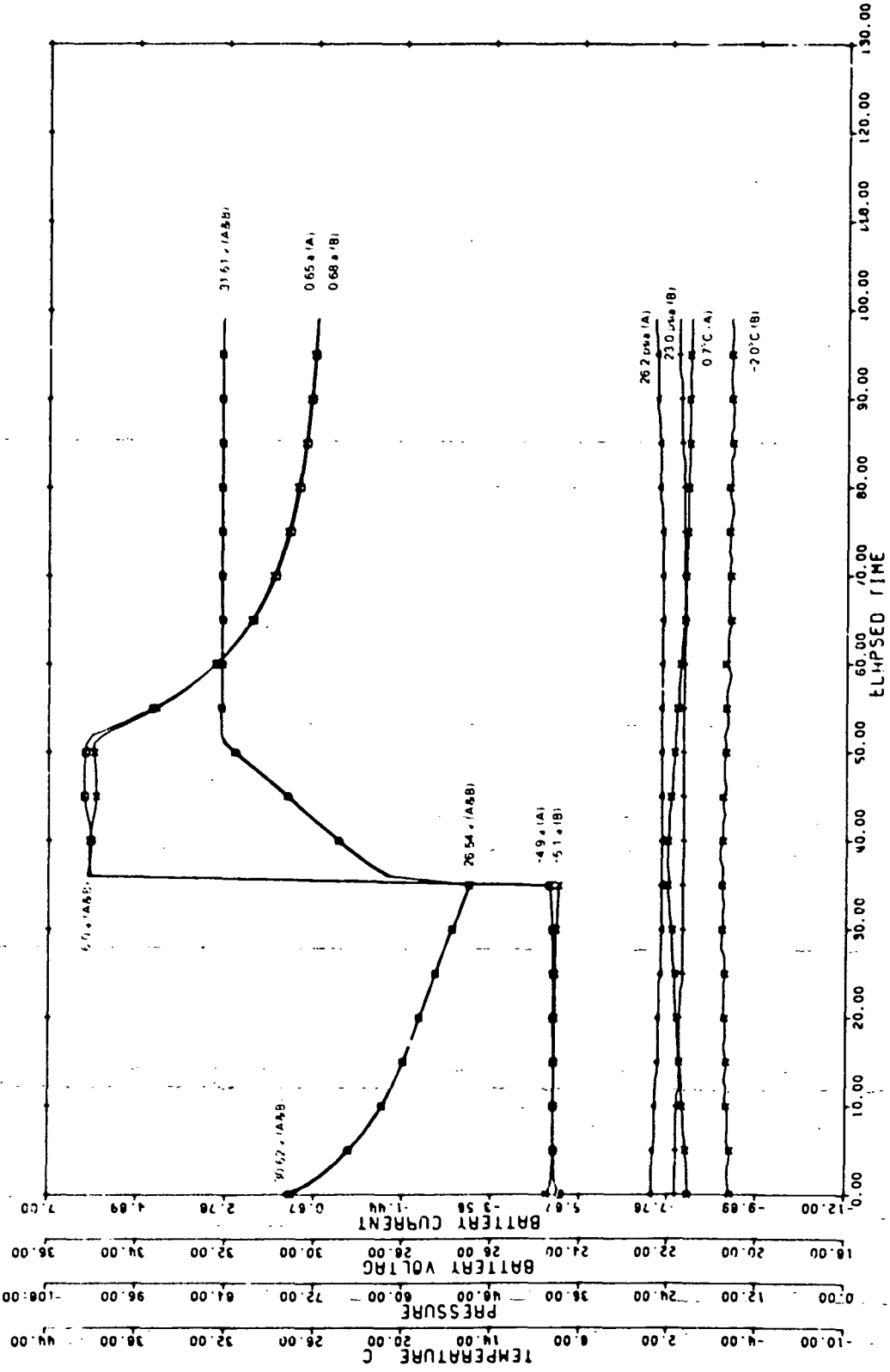

Figure 40. Battery Charge Response at Level 5 and 0°C

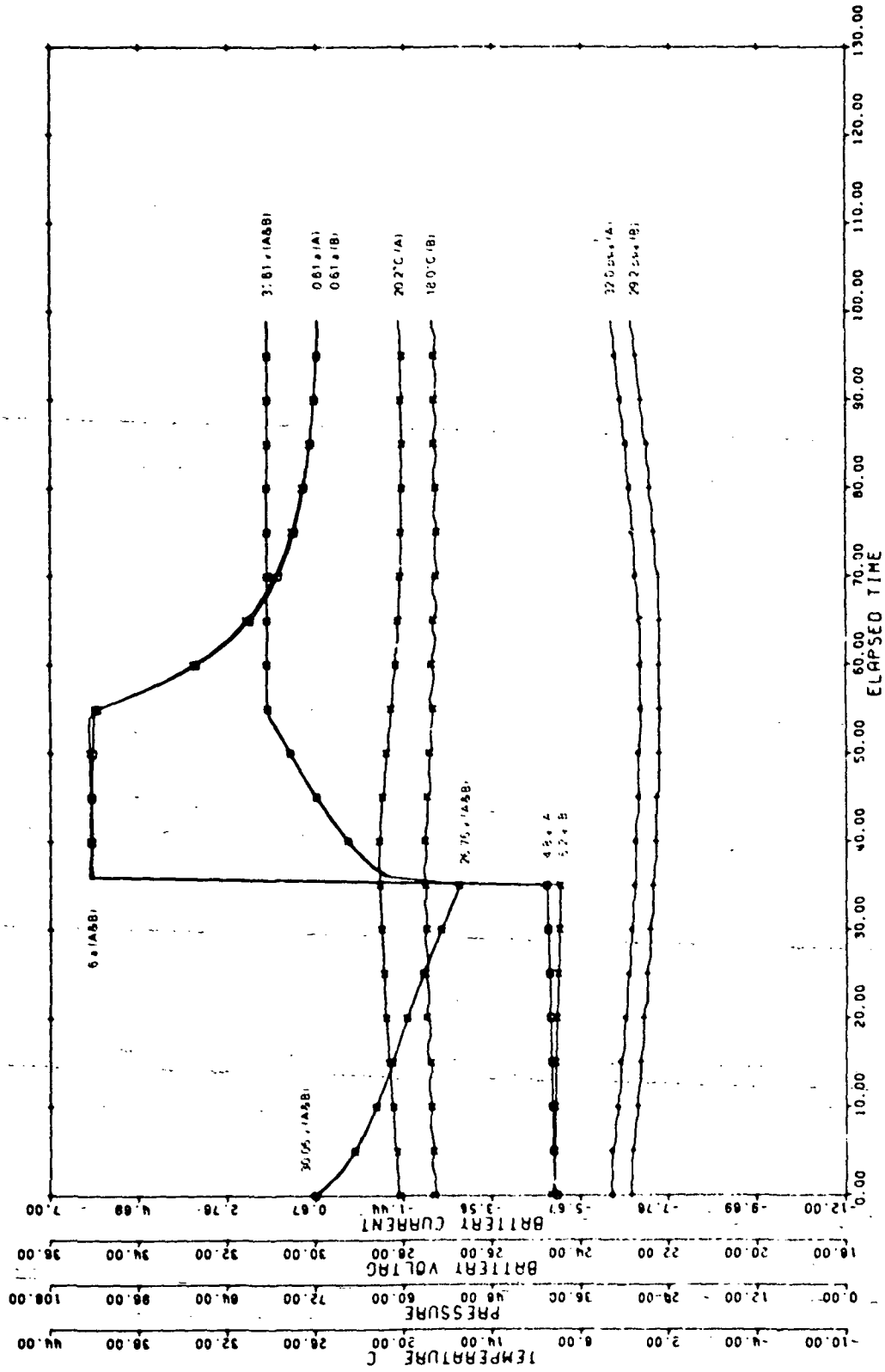

Figure 41. Battery Charge Response at Level 5 and 20°C

Table 11
Comparsion of Battery Charge Response at Level 5 and 0° 10° and 20°C

ORBIT	TEMP (°C)	EOD VOLTAGE	EOD PRESSURE (PSIA)	EOC PRESSURE (PSIA)	EOC CURRENT (AMP)	C/D
	0	26.84	12.7	13.2	0.56	1.02
<1000	10	27.06	13.6	14.5	0.52	1.03
	20	27.23	11.1	11.6	0.51	1.05
	0	26.53	25.0	26.2	0.66	1.01
~11500	10	26.66	27.5	29.8	0.62	1.03
	20	27.77	28.7	31.9	0.61	1.05

1.6.2 Battery discharge voltages trend

Figure 42 depicts battery end-of-discharge voltage profile at 25% DOD and 10°C. Although the life cycle program continued for over 14,000 cycles, no useful data was available at these operating parameters due to extended cycling at other test conditions.

1.6.3 Effect of one shorted cell on parallel battery performance

This test originally performed at orbit 2000 and discussed earlier was repeated after 11,800 orbits following procedures outlined previously.

These results which appear in Tables 12 thru 14 and Figures 43 thru 45 depict shorted cell and battery characteristics highlighted during similar test periods in the first evaluation. See Tables 6 thru 8 and Figures 29 thru 31.

A comparsion of partially shorted cell characteristics indicated that the same cell decayed more rapidly, cycle for cycle, during the second evaluation as indicated by the lower voltages on charge and discharge. Further analysis indicated that the battery discharge voltage was lower prior to the

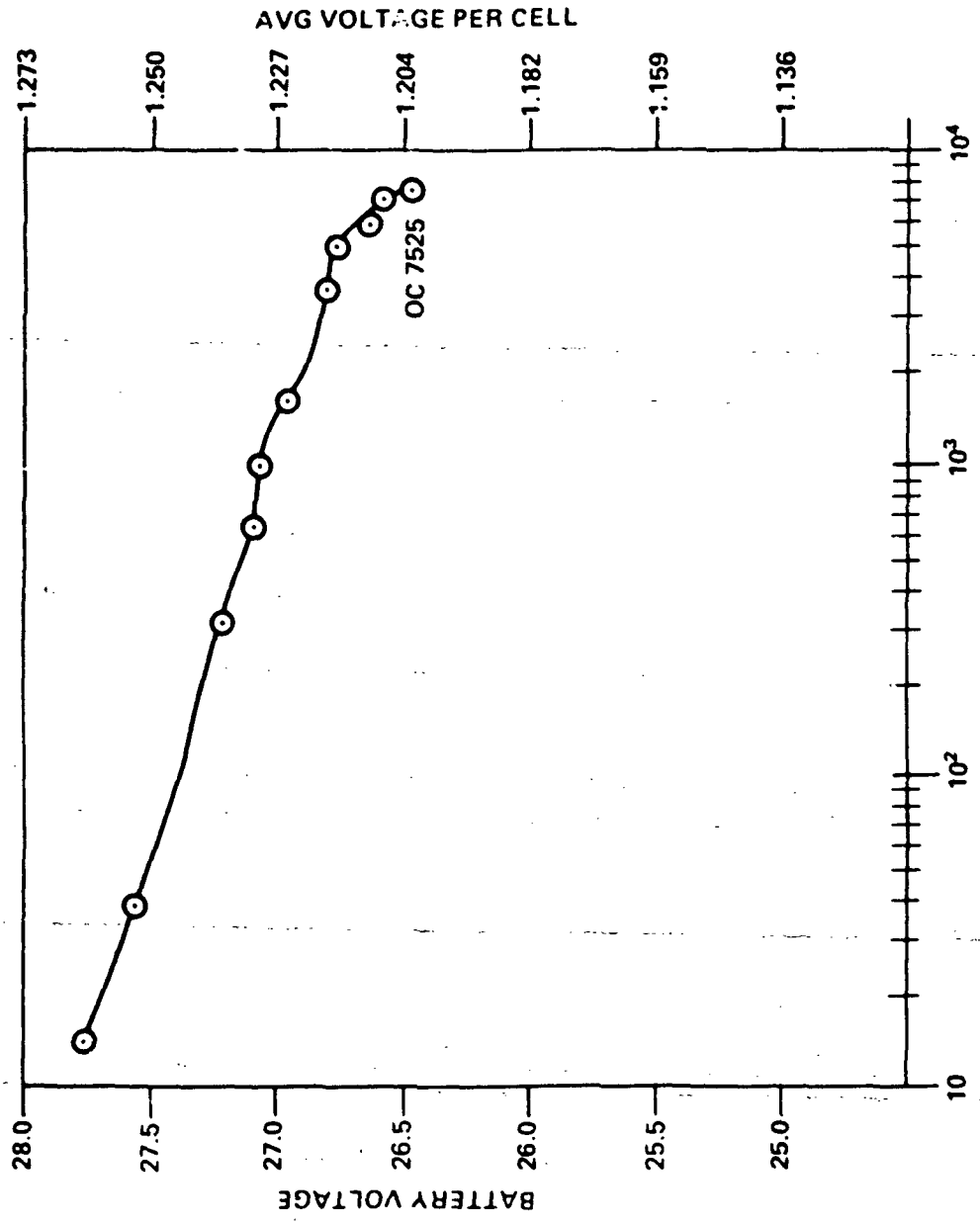

Figure 42. Battery Discharge Voltage, Level 5, 25% DOD, 10°C

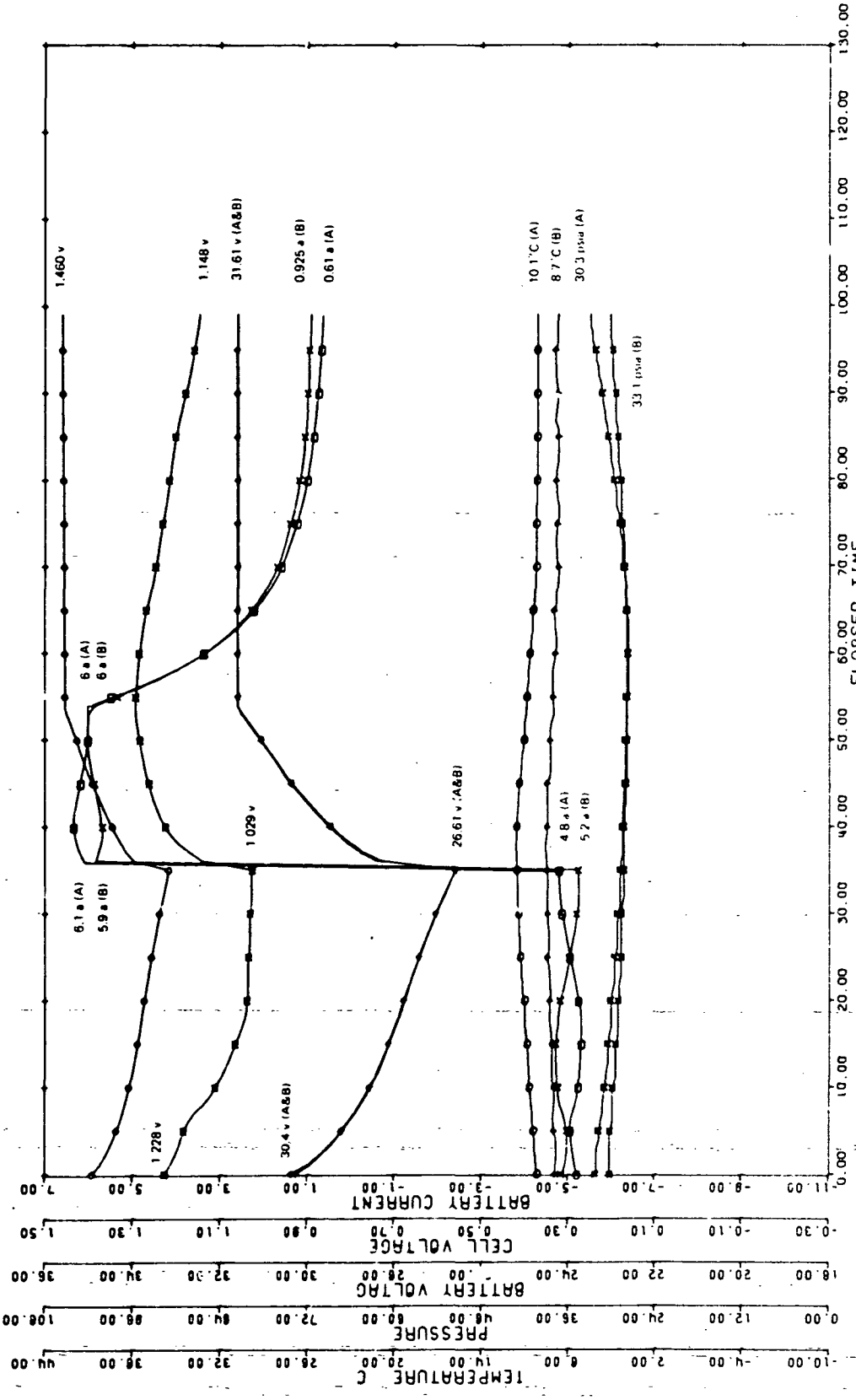

Figure 43. Battery Characteristics During Partially Shorted Cell Period at VL5

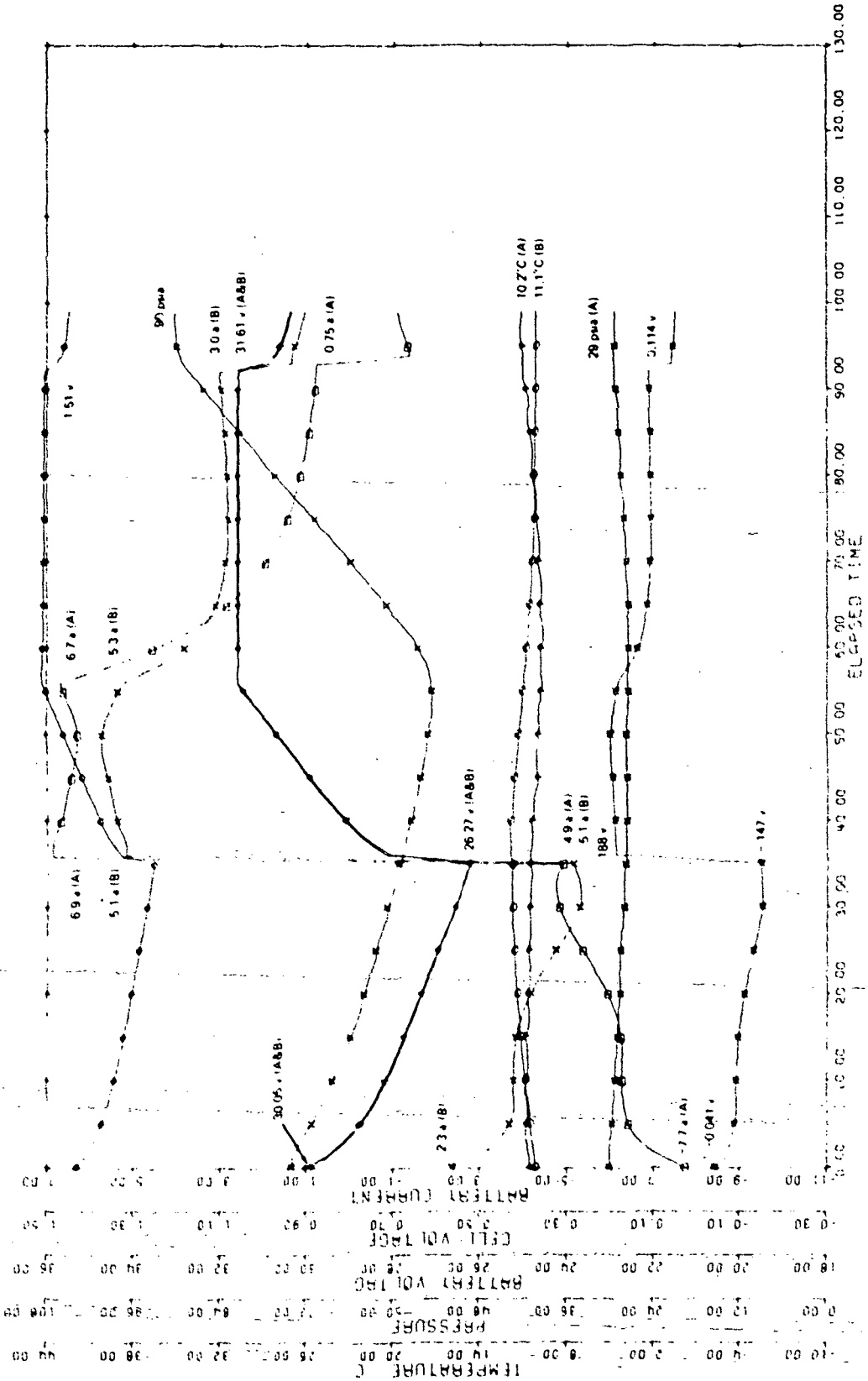

Figure 44. Battery Characteristics During Hard Cell Short at VL5

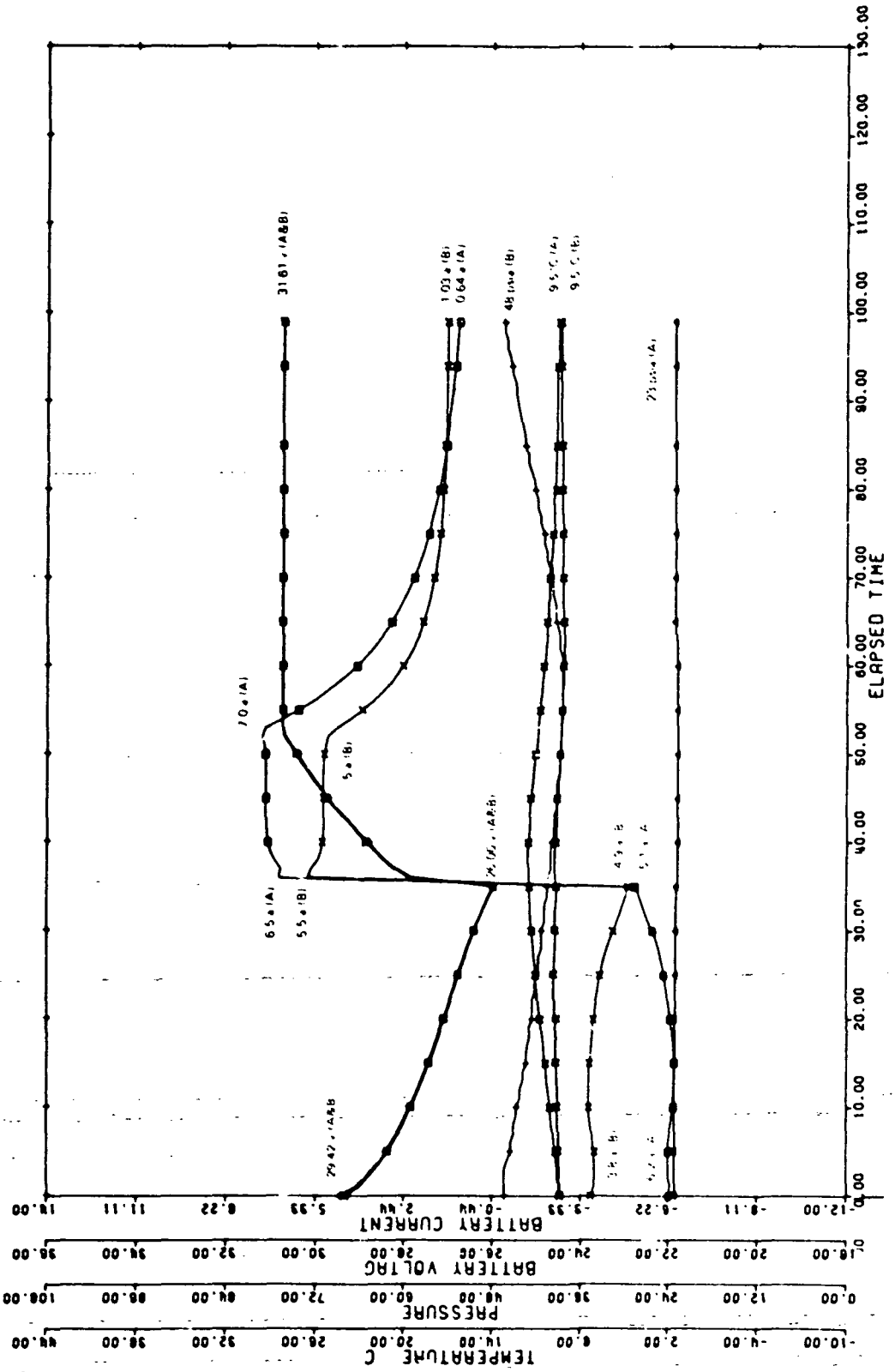

Figure 45. Battery Characteristics During Hard Cell Short at VL3

Table 12
Partially Shorted Cell Characteristics During Decay Period at V.L. 5

CYCLE	END OF DISCHARGE VOLTAGE	END OF CHARGE VOLTAGE
1	1.190	1.315
2	1.126	1.272
3	1.045	1.260
4	1.029	1.150
5	0.27	--

NOTE: At the beginning of charge period on cycle 4, the 1.0 ohm resistor was replaced with a 0.5 ohm resistor

start of the test. This is further emphasized by comparing battery characteristics during the cell decay period. While battery voltages are lower, the overall behavior of the partially shorted battery is similar to the previous results.

The most dramatic change occured when the cell load resistor was replaced with a hard short as the batteries were allowed to continue to cycle at level 5. Within the first charge period after the hard short was applied, the C/D ratio of battery B increased substantially from 1.04 to 1.70 as cell pressures rose from 30 psia to 75 psia. During the next cycle, the C/D ratio decreased slightly to 1.60 while the end of charge current peaked at 3.0 amperes and cell pressures exceeded 90 psia. Cell temperatures measured at various cell tops were generally 1.5°C higher than the ambient while temperatures at the broad face of interior cells were typically 3°C higher than the ambient. In contrast battery A was experiencing a more typical 101% recharge as cell pressures and temperatures remained nominal. An overall comparsion of battery characteristics during the hard cell short period at level 5 are summarized in Table 14. Cell pressures in battery B increased rapidly probably due to the higher initial pressures. The C/D ratio, charge currents, and cell temperatures

Table 13
Battery Comparsion Characteristics During Cell Decay Period

CYCLE	BATTERY A				BATTERY B			
	END OF DISCH VOLTAGE	END OF DISCH CURRENT	C/D	END OF CHARGE CURRENT	END OF DISCH VOLTAGE	END OF DISCH CURRENT	C/D	END OF CHARGE CURRENT
1	26.66	−4.9	1.03	0.61	26.65	−5.1	1.05	0.77
2	26.67	−4.9	1.03	0.61	26.66	−5.1	1.04	0.79
3	26.63	−4.8	1.03	0.61	26.62	−5.2	1.05	0.80
4	26.61	−4.8	1.03	0.61	26.60	−5.2	1.06	0.92
5	26.27	−7.6	–	–	26.28	−2.8	–	–

NOTE: At the beginning of charge period on cycle 4, the 1.0 ohm load resistor was replaced with a 0.5 ohm resistor

Table 14
Battery Comparsion Characteristics During Hard Cell Short Period at V.L. 5

CYCLE	BATTERY A					BATTERY B				
	END OF DISCH CURRENT (AMP)	Ahr OUT	C/D	END OF CHARGE CURRENT (AMP)	END OF CHARGE PRESSURE (PSIA)	END OF DISCH CURRENT (AMP)	Ahr OUT	C/D	END OF CHARGE CURRENT (AMP)	END OF CHARGE PRESSURE (PSIA)
1	−7.6	3.3	1.02	0.66	30	2.4	2.5	1.7	2.9	75
2	−4.9	3.5	1.00	0.75	30	−5.1	2.5	1.6	3.0	90

NOTE: At the end of the discharge period on cycle 1, the 0.5 ohm load resistor was replaced with a hard short.

of the shorted cell battery were distinctly lower prior to terminating the test at the 90 psia safety limit in comparison to the first evaluation.

Because of the unstable condition of battery B, the charger level was reduced to level 3. This resulted in lowering the C/D ratio of battery B from 1.60 to 1.15 as cell pressures stablized to less than 50 psia. However, battery A now experienced a 99% recharge as this battery continued to support approximately 60% of the load.

The batteries were cycled at level 3 for a total of 440 orbits. During this period several trends illustrated in Figures 46 and 47 became apparent. The C/D ratio of battery B steadily increased rising from 1.15 to 1.48 with cell pressures increasing from 50 psia to slightly over 100 psia. Measured cell temperatures also increased and were similar to those experienced during the hard cell short condition at level 5. The end of charge delta between high and low cells in battery B increased from 40 millivolts which was typical prior to the short cell evaluation to over 130 millivolts. In contrast, battery A experienced a 99% recharge while supporting between 56 and 62% of the load as batteries experienced divergent discharge currents. The end of charge delta between cells was typically 15 millivolts.

In response to the high cell pressures in battery B, the charger level was lowered to level 2 as the batteries continued to operate for an additional 250 orbits. In contrast to the previous level, battery B gradually supported a greater portion of the load as its depth-of-discharge increased from 25% to 28% while its C/D ratio dropped from 1.22 to 1.08 as cell pressures stablized between 60 to 80 psia. At this lower level battery A now experienced a slightly lower percent recharge, 97.5% with a gradually decreasing depth-of-discharge. The end-of-charge delta between high and low cells in battery B was reduced to 120 millivolts while the delta for battery A cells was approximately 10 millivolts.

After a total of 700 orbits, this evaluation was terminated by simulating an extended eclipse season and allowed the batteries to discharge at 10.0 ampere total to 100% DOD. The final battery and

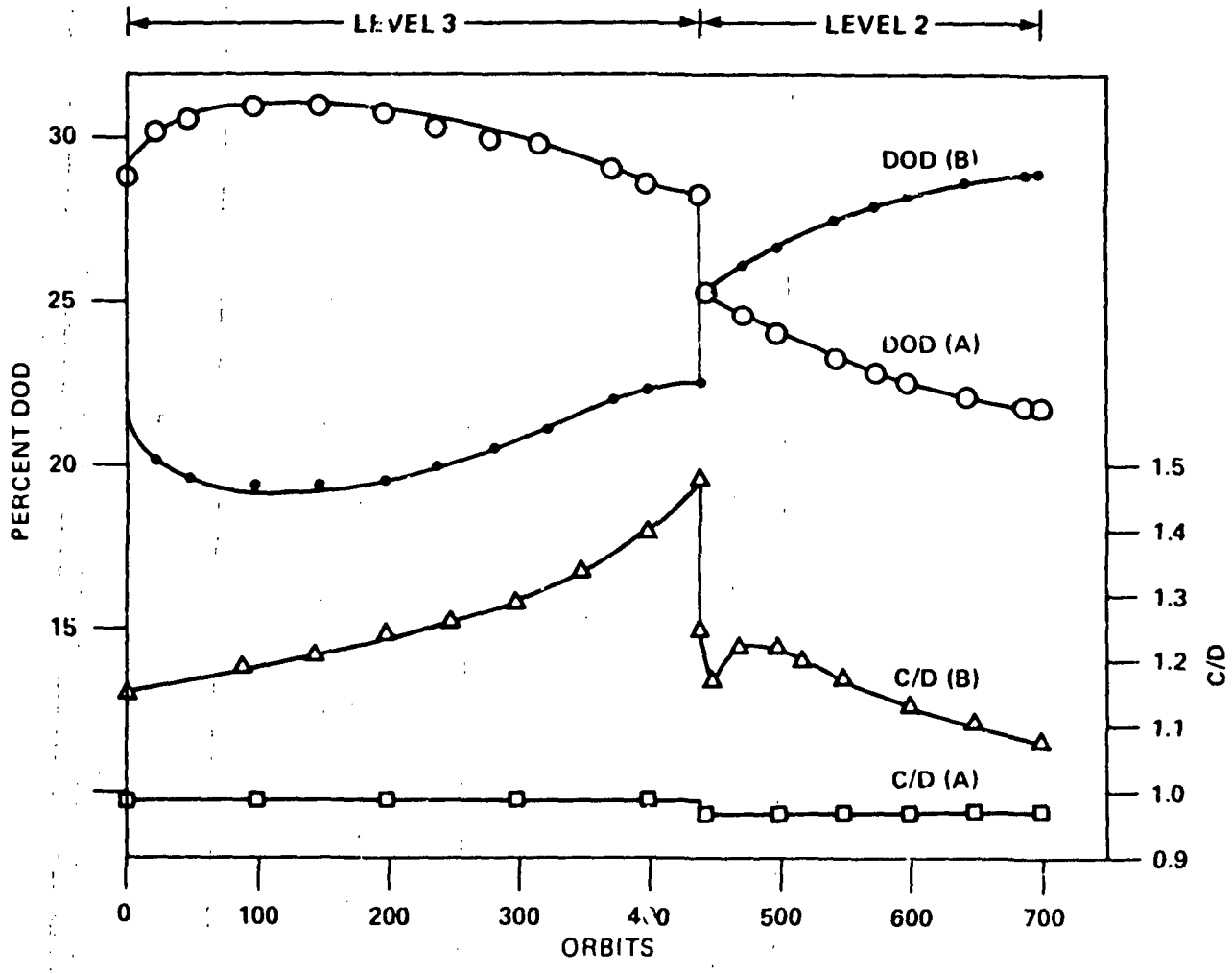

Figure 46. Battery DOD and C/D Trend During Hard Cell Short Period at Level 3 and 2

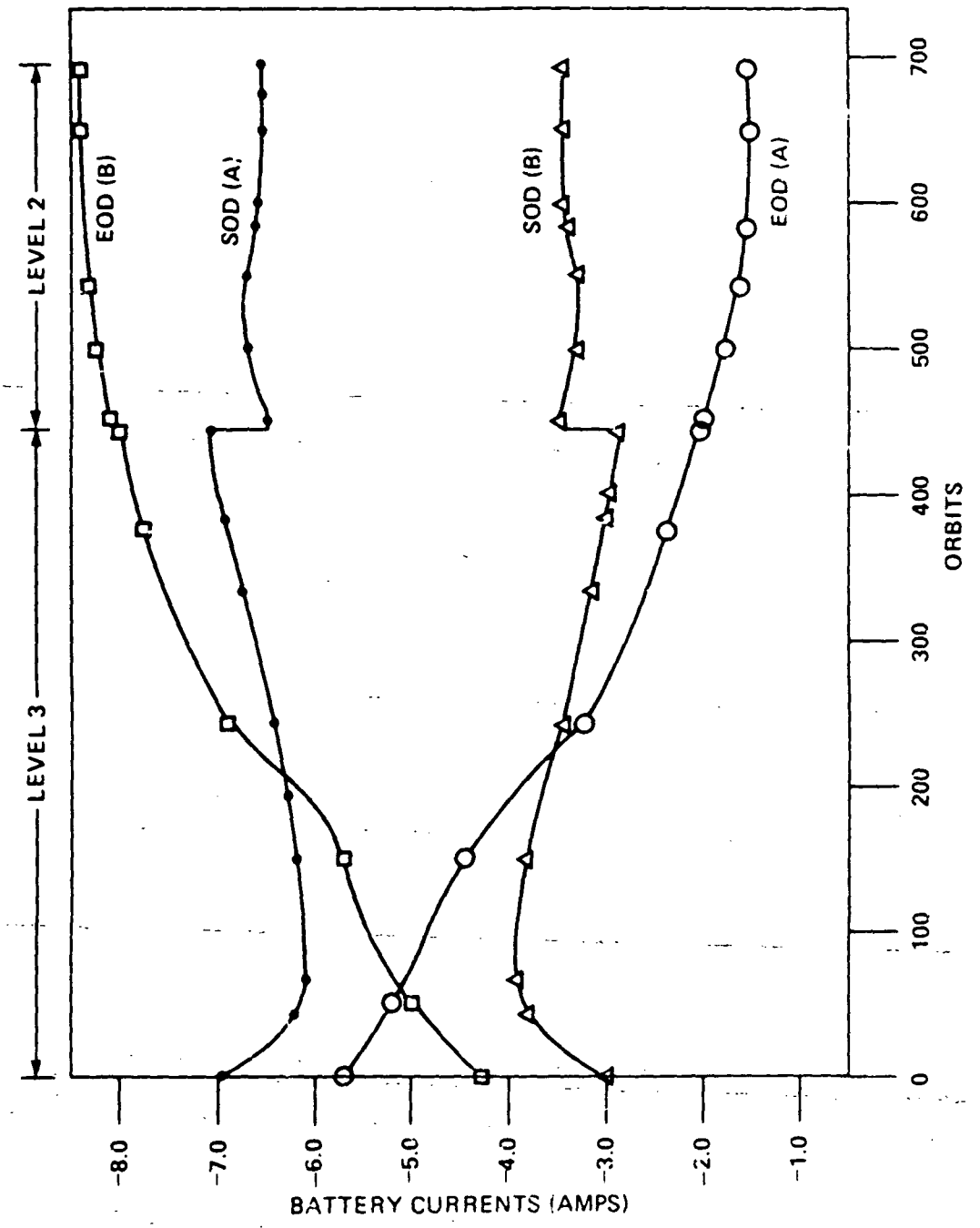

Figure 47. Battery EOD and SOD Trends During Hard Cell Short at Level 3 and 2

cell characteristics appear in Figures 48, 49, and 50. Battery A at the lower state of charge delivered 8.50 Ahrs as its lowest cell dropped below 0.5 volts. Battery B delivered 9.40 Ahrs up to this point. After disconnecting battery A from the load, battery B was discharged further and delivered a total capacity of 11.1 Ahrs.

A highlight in the shorted cell evaluation was determining battery state-of-charge (SOC) for cycling below 100% recharge for extended periods. The procedure, which was accomplished on three separate occasions, required measuring the difference between charge and discharge ampere-hours every cycle. The discharge cycle was then extended to permit batteries to discharge to 100% DOD. These results appear in Figure 51. By substracting the name plate capacity from the actual capacity obtained from the discharge, it is possible to approximate the actual loss in battery capacity anytime during an extended period. This is represented by the dotted curve in the above referenced figure.

Baseline level cycling at level 5 and 25% DOD was re-established after removing the hard cell short from battery B and fully re-charging the shorted cell using a separate power supply. Immediately, the batteries experienced slightly unequal load sharing with battery A at 27.5% DOD in contrast to 23.3% for battery B. While battery A was experiencing a normal 103% recharge as cell pressures stablized below 30 psia the percent recharge of battery B increased steadily from 107 to 118°C within 175 orbits as cell pressures remained stabled between 60 to 85 psia. Cycling was terminated when several cells exceeded the software safety limit of 1.50 volts per cell on charge. At this time both batteries were electrically separated and connected to individual power supply exercisers and charged at C/30 for 66 hours. Following this trickle charge, the batteries were disconnected and allowed to remain open-circuit for 72 hours. The final results are illustrated in Figures 52 thru 56. While the cells in battery A exhibited closely matched charge and self-discharge profiles, battery B cells possessed widely different profiles but generally in two distinct groupings.

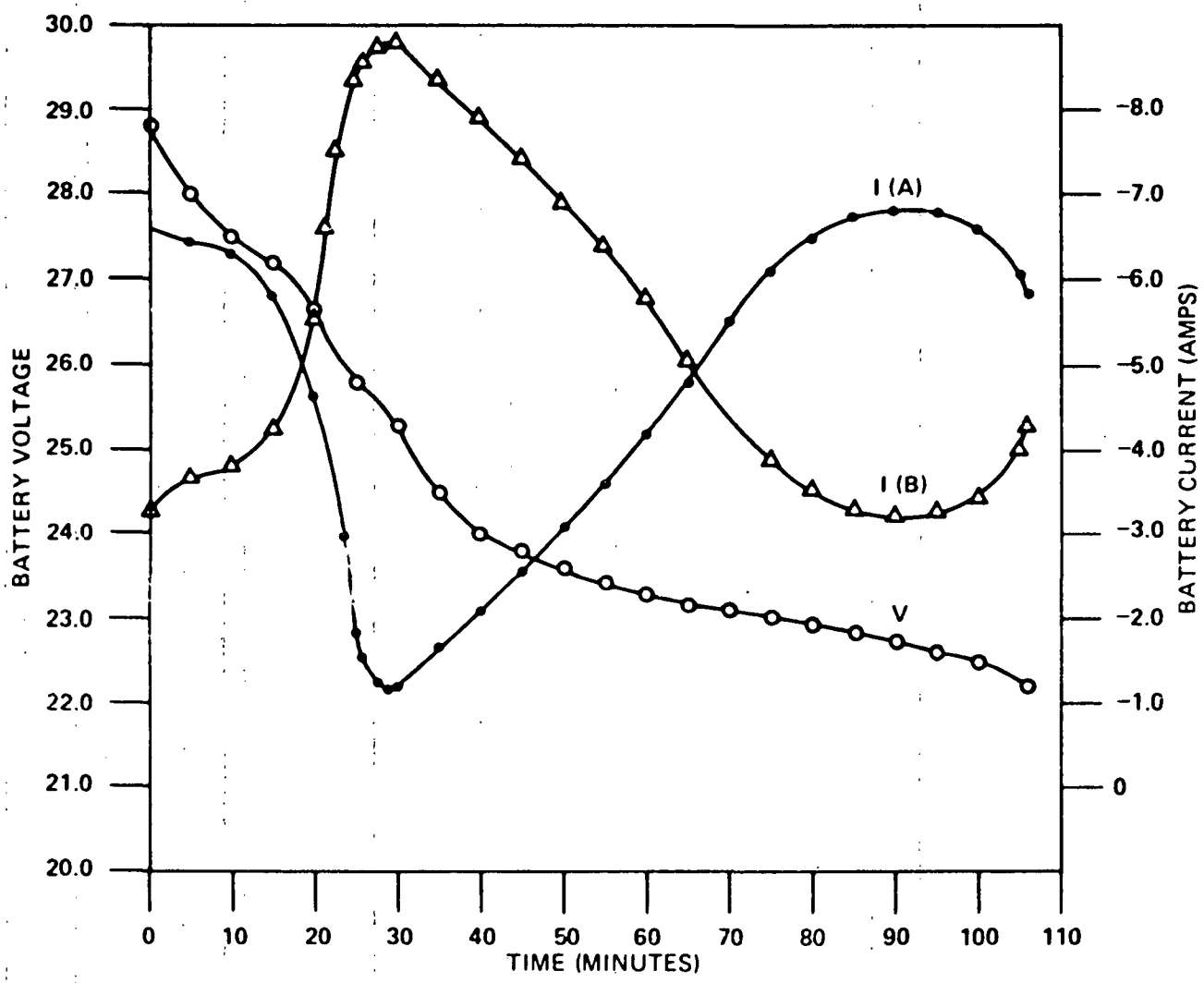

Figure 48. Battery Discharge Characteristics During Final Capacity Test, Shorted Cell Evaluation

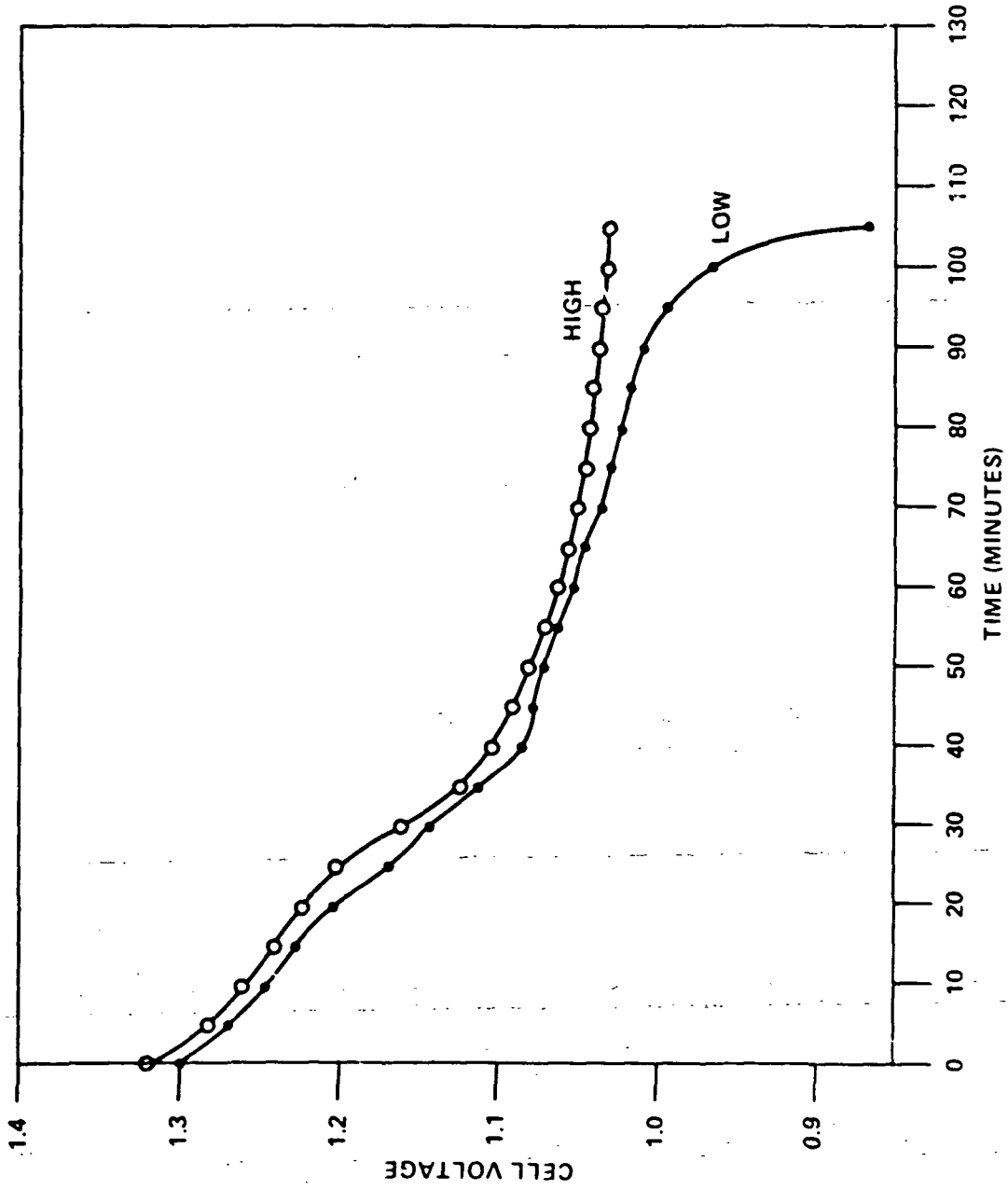

Figure 49. Battery A Cell Discharge Profile, Shorted Cell Evaluation

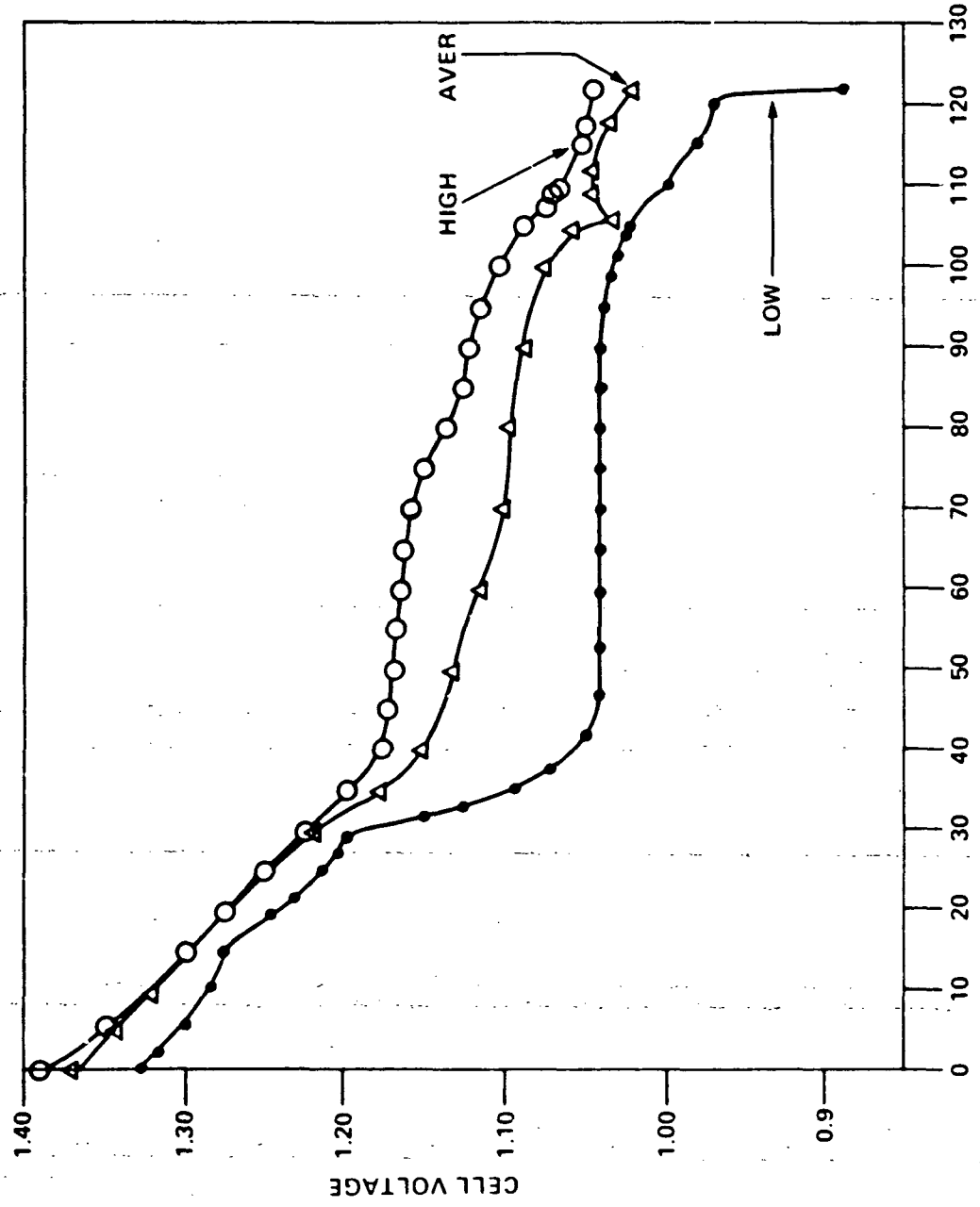

Figure 50. Battery B Cell Discharge, Profile, Shorted Cell Evaluation

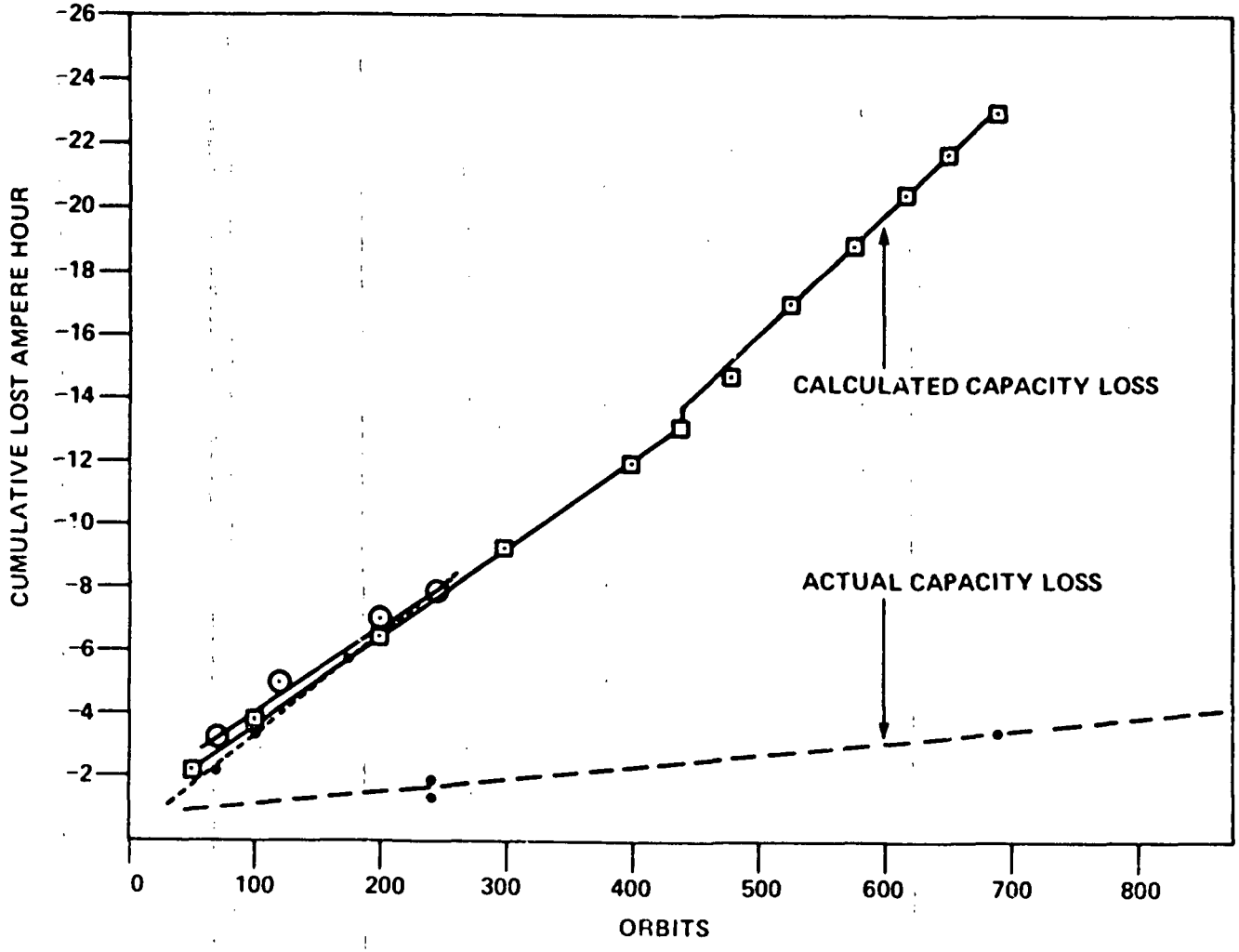

Figure 51. Battery State of Charge Profile

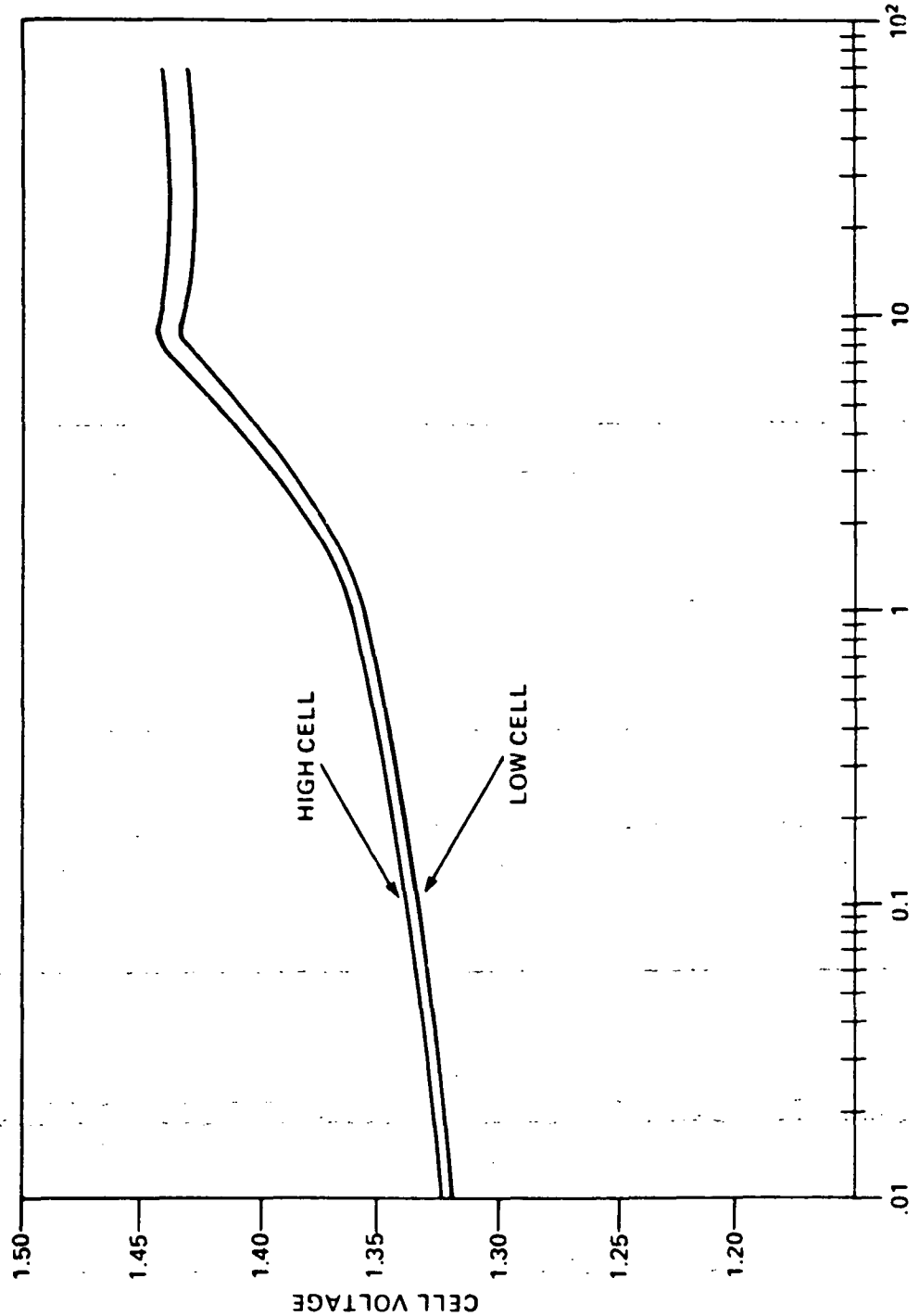

Figure 52. Cell Charge Profile, Battery A, C/30 for 66 hrs at 10°C

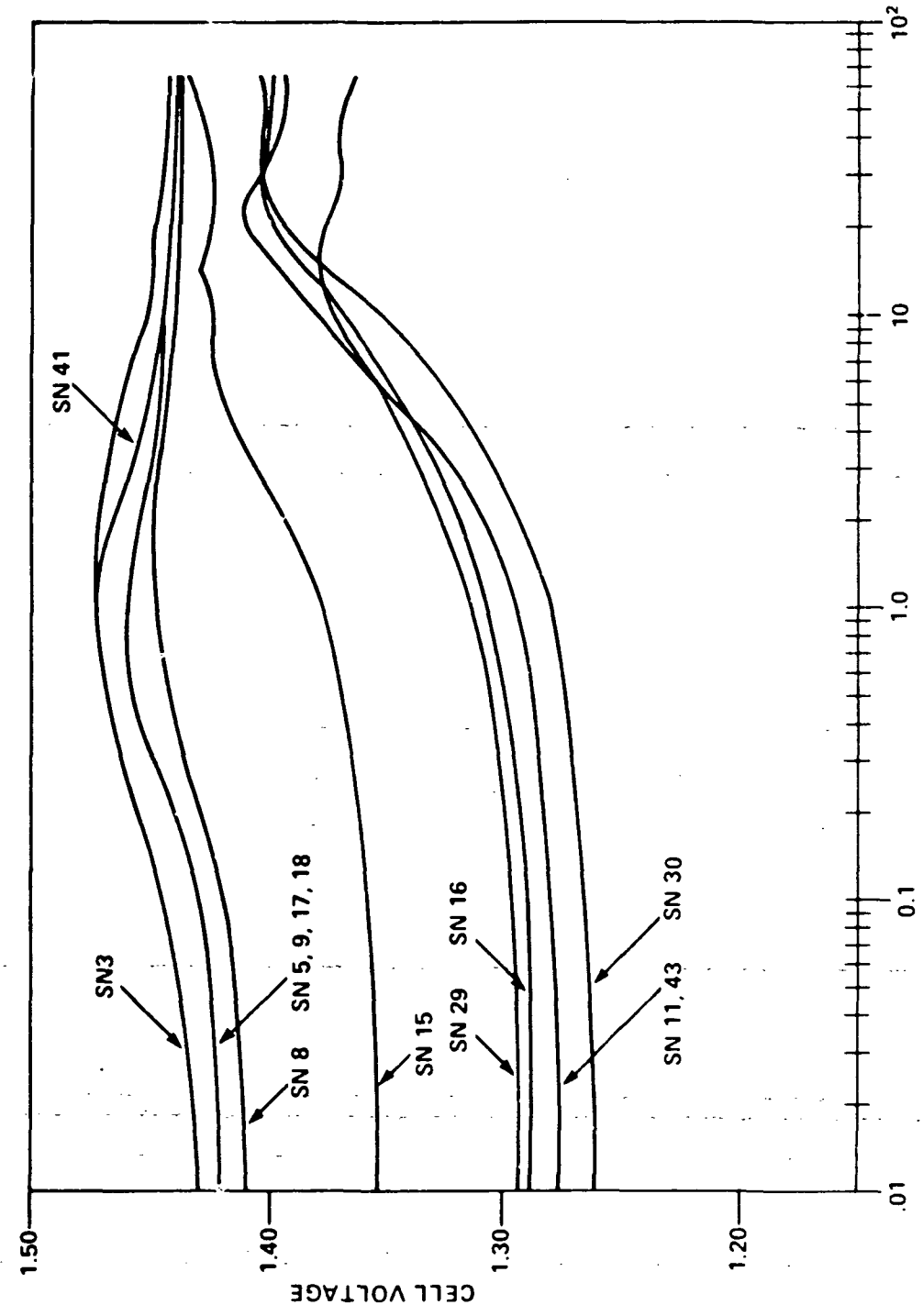

Figure 53. Cell Charge Profile, Battery B, C/30 for 66 hrs at 10°C

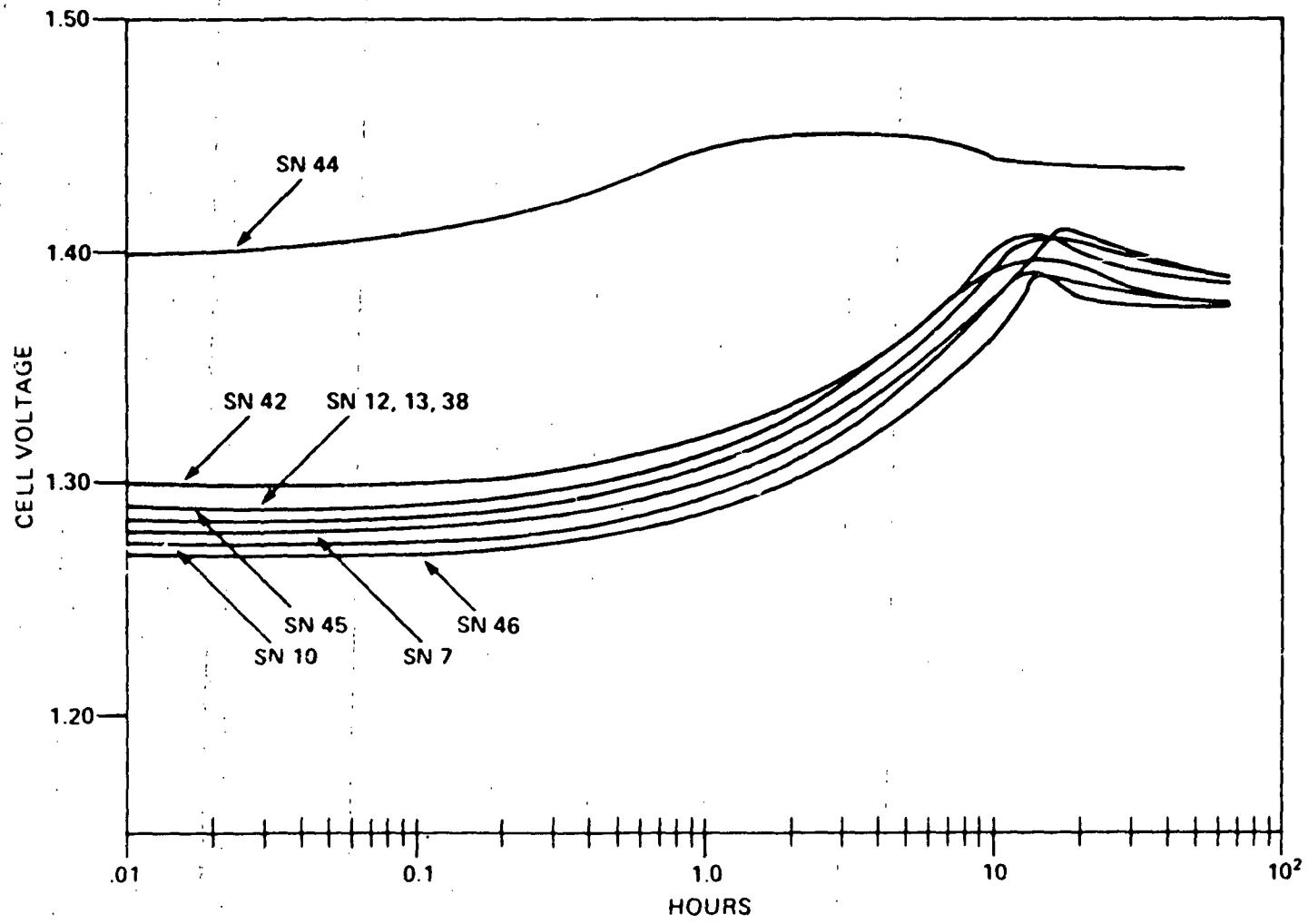

Figure 54. Cell Charge Profile, Battery B, C/30 for 66 hrs at 10°C

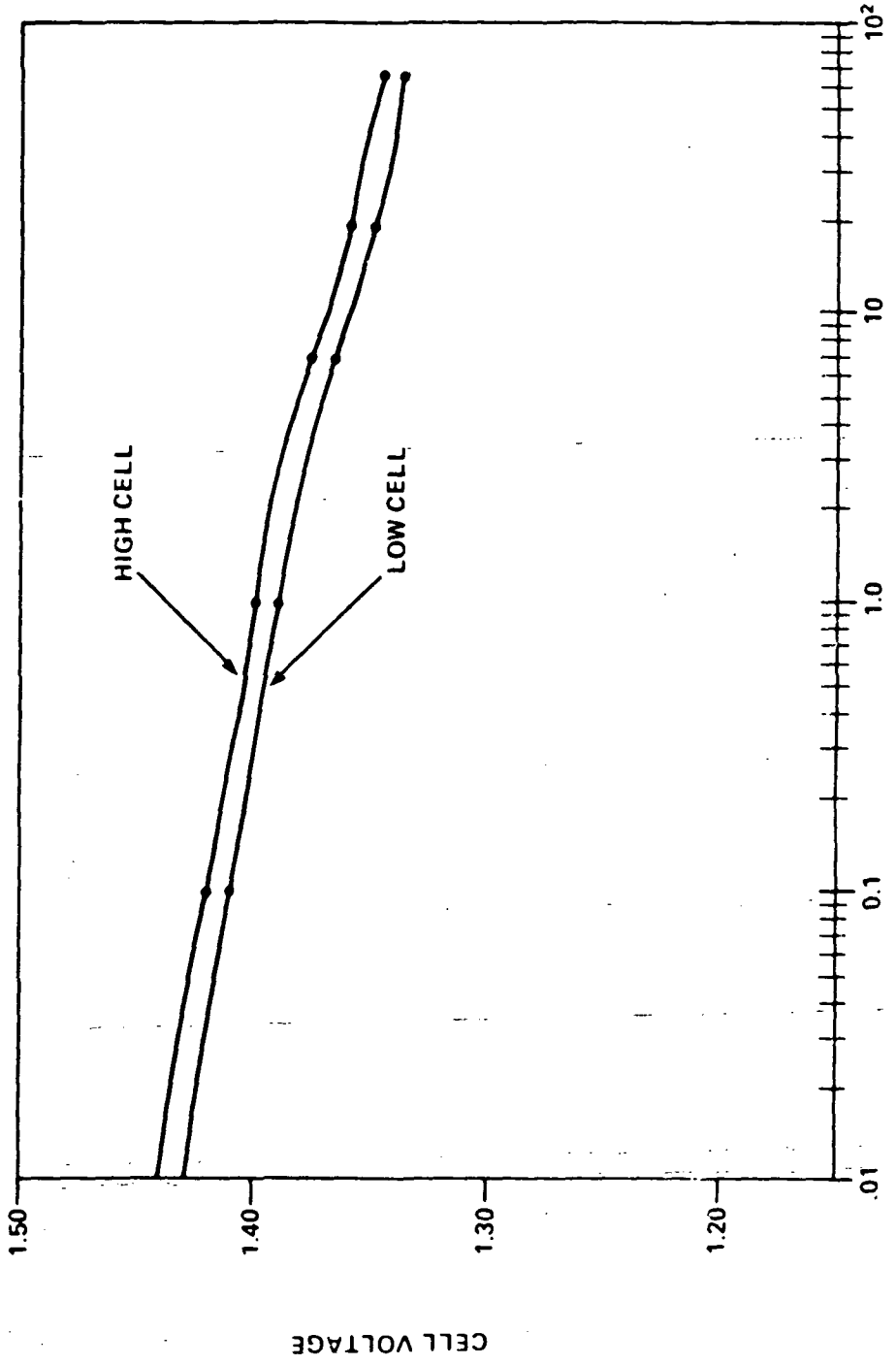

Figure 55. Self Discharge Cell Profile, Battery A

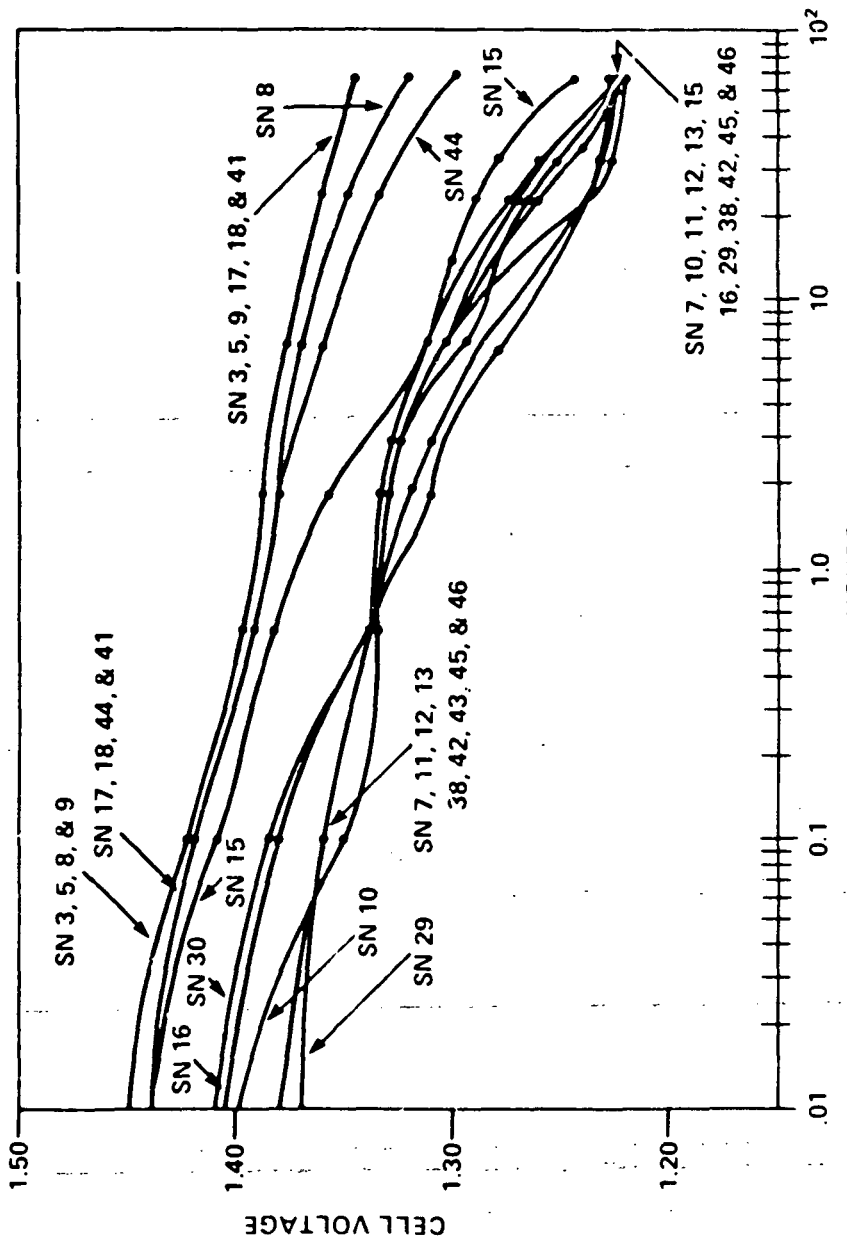

Figure 56. Self Discharge Voltage Profile, Battery B

Parallel battery operations were resumed by lowering the charger level from five to three. This resulted in lowering the C/D ratio of both batteries to 0.99 with battery A and B experiencing a 26% and 24.6% DOD respectively.

Further battery tests and cell analysis are anticipated and will be subject of a future report.

Conclusions

The voltage vs temperature levels of the Modular Power System has sufficient versatility to accommodate a wide range of battery design parameters, applications and abnormal flight conditions.

For a normal 25% depth of discharge on each battery, charger level 5 provided for optimum battery recharge between 101% and 104% over the design temperature range of the MPS.

The effect of battery temperature inbalance of plus and minus 10 degrees Celsius with one battery maintained at 10 degrees Celsius resulted in divergence in both the depth of discharge and ampere-hour percent recharge. Charger level 5 offered the best short term stable operation where the imbalance in percent recharge was less than 4% at the maximum temperature imbalance. At this level both batteries experienced between 100 to 104% recharge while the battery maintained at the higher ambient temperature experienced a DOD typically less than 27% while the other battery at slightly greater than 23% DOD. At higher levels the recharge ratio ranged from typically 1.05 to 1.30 depending on the charger voltage level while the imbalance in the depth of discharge became less significant.

The effect of battery cable mismatch on load sharing resulted in divergence of battery depth of discharge while the ampere-hour recharge ratio remained essentially independent of the cable mismatch. Increasing the resistance of one parallel path from .077 to 0.177 ohms resulted in a decrease in depth-of-discharge from 25 percent to 22 percent. The other battery with cable resistance of .077 ohms experienced a increase from 25 percent depth of discharge to 28 percent. The divergence in percent depth-of-discharge was negligible regardless of the mismatch when the cable resistance was

.010 ohms. With the lower cable resistance, the internal battery impedance has a greater influence on load sharing between parallel batteries. No deleterious effects are anticipated if harness and associated circuitry impedances are matched within 10%.

The simulation of a partially shorted cell in one battery at level 5 resulted in a slight difference between battery operating characteristics. However, within one orbit of simulating a hard cell short condition, the battery with the shorted cell experienced a drastic increase in the recharge ratio from a normal 1.06 to over 1.60 accompanied by high cell pressures and increasing end of charge currents exceeding 3.0 amperes. Because of this unstable condition the charger level was lowered from five to three resulting in a satisfactory short term operation with the recharge ratio of 1.2 for the battery with the shorted cell and 0.99 for the 22 cell battery. With the added flexibility of lower charger levels, it was demonstrated that this battery imbalance was stable and prolonged for several hundred orbits.

As a result of this simulation, the ability to monitor the voltage across each group of eleven cells was an aid in detecting a hard cell short within the battery.

Disabling and enabling one battery from the charger bus resulted in peak current transients typically 5 milliseconds in duration. The current peaks were dependent on the difference in battery voltage which was the greatest when a partially discharged battery is re-enabled at the start of charge or at the end of charge period in the orbit. The trend toward higher peaks was also demonstrated to be a function of harness impedance in each parallel battery circuit. Current transients of 32.0 and 49.0 amperes were measured during enabling at the end of charge period with .077 and .010 ohm battery cables respectively. The highest current peak of 57.0 amperes was measured when one battery was fully charged and the other battery was discharged to 100% of rated capacity.

The results demonstrate that the eight commandable voltage versus temperature levels designed into the MPS provide a very flexible power system that not only can accommodate a wide range of normal power system operation, but also provides a high degree of flexibility in responding to abnormal operating conditions.

References

1. "OAO-2 Battery Data Analysis", NASA/GSFC Contract NAS 5 11465, Feb 1973

2. "Characterization of 20 AH nickel-cadmium cell used for Energy Storage on OAO Spacecraft", F. Ford, GSFC Report X 761-72-330. Sept 72

3. "Orbiting Solar Observator Battery and Power Design", F. Ford, 1977 Battery Workshop

4. "Summary of the Manufacturing and Testing of 12AH nickel-cadmium cells for the IUE spacecraft", D. Baer, GSFC Report X 711-76-18

APPENDIX A

Cell and Battery Design

The 12 Ahr nickel cadmium cells for the program were procured from General Electric Company in October 1975 under NASA contract # NAS 5-19952 to the Goddard Specification for Aerospace Nickel Cadmium Storage-Cell, S-716-P-6. These cells were manufactured according to GE MCD 232A2222AA54 Revision 18. The cell design is the standard GE design and configuration. The design contains 11 positive plates, 12 negative plates, Pelion 2505 as the separator with other special design features as follows:

1. Nickel-braze, ceramic-to-metal seal both terminals
2. Cell case wall 0.43 mm
3. Teflonation of negative plates (level 1)
4. Plates treated with carbonate reduction process.
5. The average positive and negative plate loading was 12.5 gm/dm^2 and 15.7 gm/dm^2, respectively
6. Potassium hydroxide (KOH) quantity was 46 cc

Additional information concerning these cells may be found in GSFC report #711-76-18.[4]

Each cell was subjected to a series of acceptance tests performed at General Electric in accordance with test procedure P24A-PG-211 given in Appendix C. Cell selection for each battery was predicated on these tests and based on capacity matching at 10°C given in Appendix D.

The overall battery design represented a standard electrical approach and an extension of the IUE thermal and mechanical design.

The electrical battery design included twenty-two cells in series with the most negative cell containing the signal electrode and under voltage sensing accomplished in groups of eleven cells. Two cells in each battery are instrumented with electronic pressure transducers which act as a safety device to terminate the test should pressures exceed 100 psia.

The battery assembly which is an extension of the 17 cell battery design developed for the IUE spacecraft consists of two rows of eleven cells enclosed in a five sided magnesium box. Cell are electrically isolated from each other and the sides of the battery frame by laminated silicone glass insulators. The most unique design feature is that there is no intercell fins for heat removal. The depression in each cell bottom was encapsulated with a polyurethane resin composed of 80% aluminum oxide by weight. The batteries which were instrumented with copper-constantan thermocouples were secured to copper cooling plate and placed in individual forced air temperature chambers. The final battery assembly is shown in Figure 2.

A histogram illustrating the capacity distribution of 10°C for battery A (−2%, + 2.6%) and battery B (−2%, + 3.3%) is presented in Appendix C and D. Note that the average capacity of battery A and B are closely matched at 15.1 and 15.3 ampere-hours respectively.

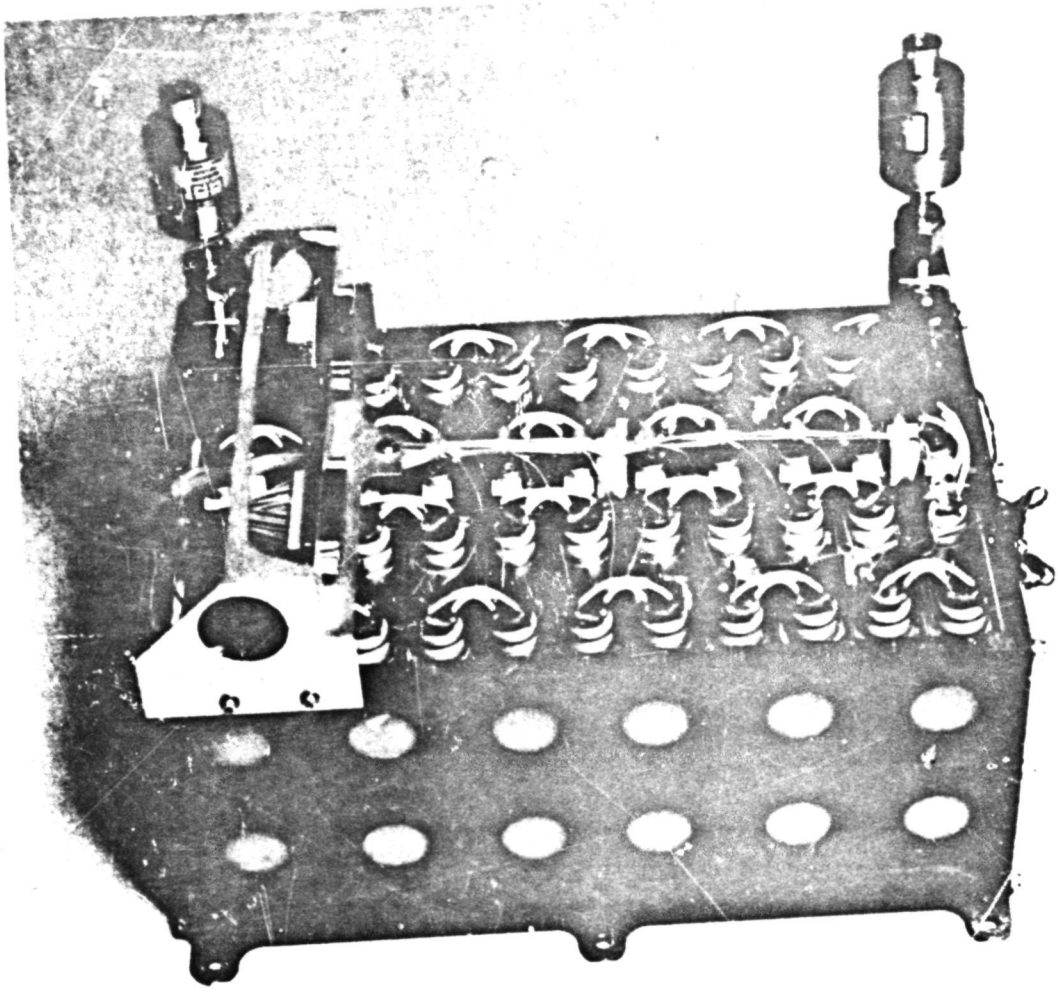

PARALLEL BATTERY TEST

CAPACITY: 12Ah

WEIGHT: 13.47KG.

DIMENSION: 26.52Cm X 21.18Cm X 15.72Cm

NASA 76-012062

Figure 2.

APPENDIX B

Test System Console

The entire test system consists of a data acquisition system, power system exerciser and a system under test.

The data acquisition system with the capability of scanning 75 channels per minute included an H/P tape drive channel scanner and computer buffer. Signal data collected included 44 cell voltages, 2 battery currents and voltages, 4 half battery and 2 third electrode voltages, and charger currents and voltages. In addition, batteries were instrument with 4 pressure transducers and 14 copper-constantan thermocouples. Software safety limits were established for cell voltages and temperature chambers while hardware limits were set up for half battery voltage and cell pressure limit of 200 psia. Real time data was monitored with the aid of data print out, electronic ampere-hour integrator and multipoint recorder.

The power system exerciser consisted mainly of charge/discharge power supply, battery cycler and orbital timer. This entire power console possessed the capability of programming and monitoring charge/discharge parameters and orbital time.

The battery assembly, cooling plate, thermal chamber and cable interface module constituted the system under test. Signal and power cables from the battery were first terminated at the interface module before routed to the DAS and PSE consoles.

APPENDIX C

Acceptance Test Sequence, G.E. P24A-PB-211

Para. #

4.0 Burn in Cycling, 10 cycles @ ± 3.3°C:

1. Charge at 6.0 amps for 125 minutes
2. Discharge at 6.0 amps to 1.0 volt/cell

5.0 Overcharge @ 22 ± 3.3°C:

1. Charge at 1.2 amps for 48 hours
2. Discharge at 6.0 amps to 1.0 volt/cell

6.0 Electrolyte adjustment omitted.

7.0 Overcharge - omitted.

8.0 Room Temperature Capacity at 22 ± 3.3°C:

1. Charge at 1.20 amps for 16 hours
2. Discharge at 6.0 amps to 1.0 volt/cell

9.0 35 ± 1.7°C Capacity:

1. Charge 1.2 amp for 24 hours
2. Discharge at 6.0 amps to 1.0 volt/cell

10.0 0 ± 1.7°C Capacity:

1. Charge 0.60 amp for 72 hours
2. Discharge at 6.0 amps to 1.0 volt/cell

11.0 Capacity Matching at 10 ± 1.7°C:

1. Charge at .60 amp for 48 hours
2. Discharge at 6.0 amps to 1.0 volt cell

Para. #

12.0 Charge Retention:

1. 0.5 Ω resistor short for 16 hours
2. Dead short for 1 hour
3. Open circuit for 24 hours

13.0 Internal Resistance:

1. Charge at 6.0 amps for 2 hours
2. Discharge at 6.0 amps for 60 min.
3. Open circuit for 5 minutes
4. Pulse discharge each cell at 60 amps for 10 seconds
5. Discharge at 6.0 amps to 1.0 volt/cell

14.0 Cell Impedance:

Measure cell and third electrode impedance with a Hewlett Packard 4328A Milliohm Meter.

15.0 Auxiliary Electrode Pressure Voltage Test (200 Ω Load)

1. Charge at 6.0 amps and open circuit each cell as it reaches 10 psig.
2. Open circuit stand for 60 minutes.
3. Discharge at 6.0 amps to 1.0 volt/cell.

Note: 1.0 ohm resistors were placed across each cell during the temperature soak periods. Temperature soak periods were for 4 hours minimum.

Unless otherwise specified the test temperature was 22°C.

APPENDIX D

CELL CAPACITY DISTRIBUTION AT 10°C
PER GE P24A-PB-211 PARA 11.0

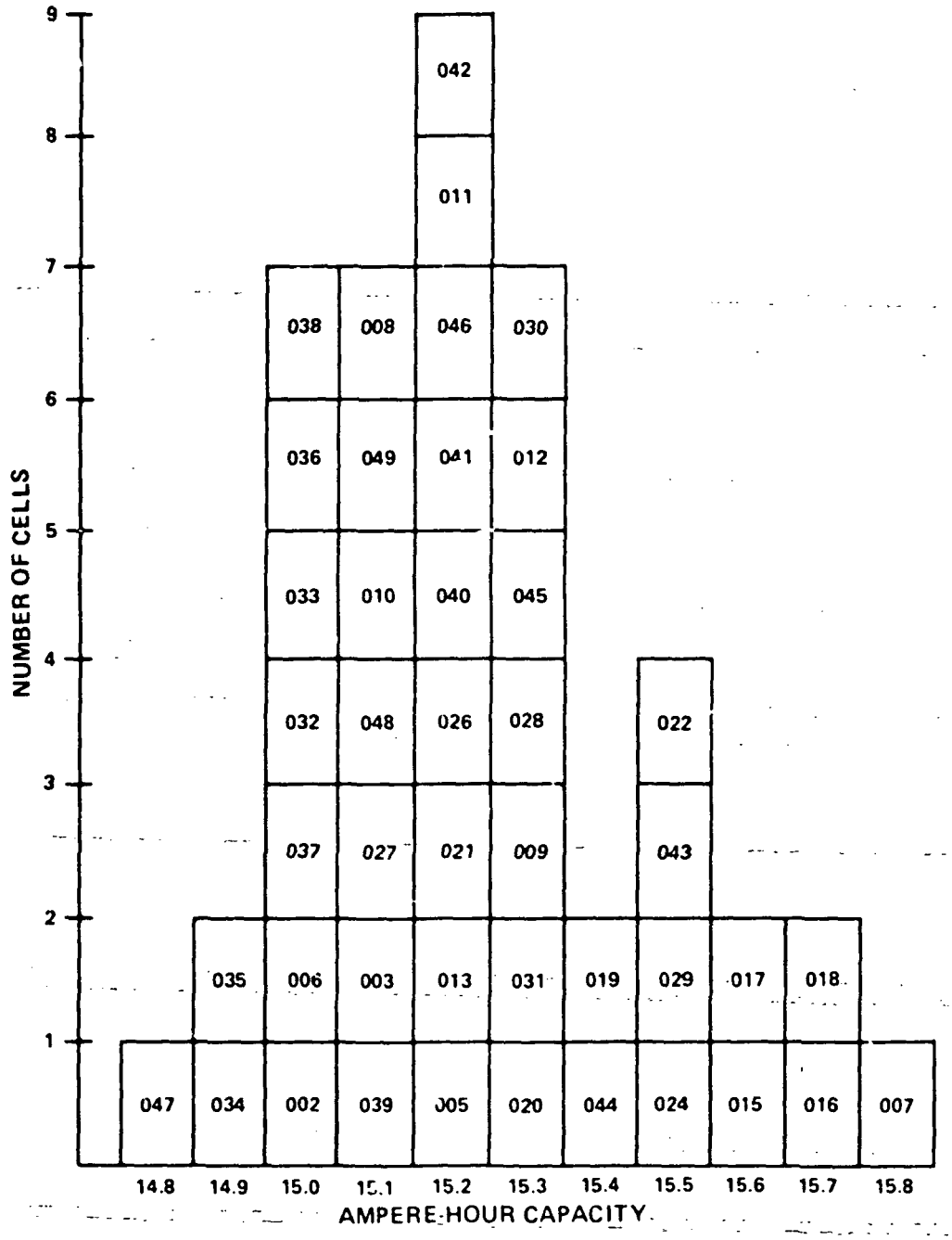

APPENDIX E

BATTERY A CELL CAPACITY DISTRIBUTION AT 10°C
PER GE P24A-PB-211 PARA 11.0

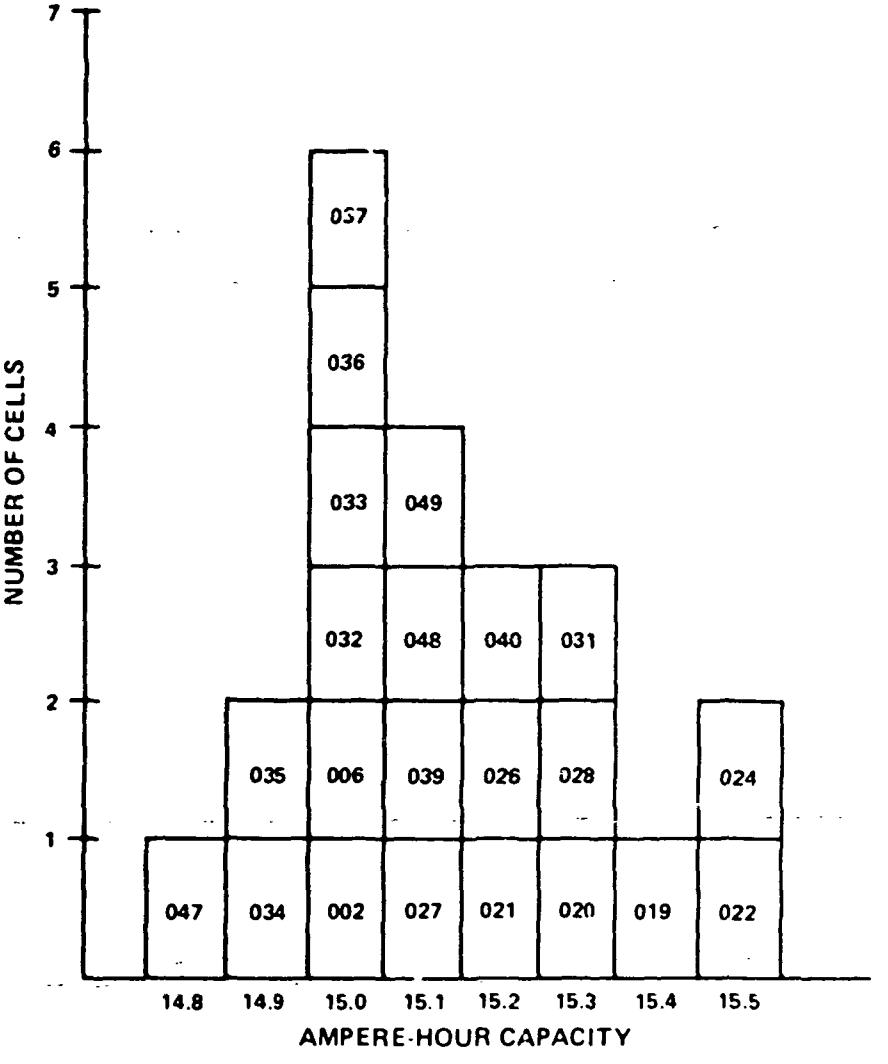

APPENDIX F

BATTERY B CELL CAPACITY DISTRIBUTION AT 10°C
PER GE P24A-PB-211 PARA 11.0

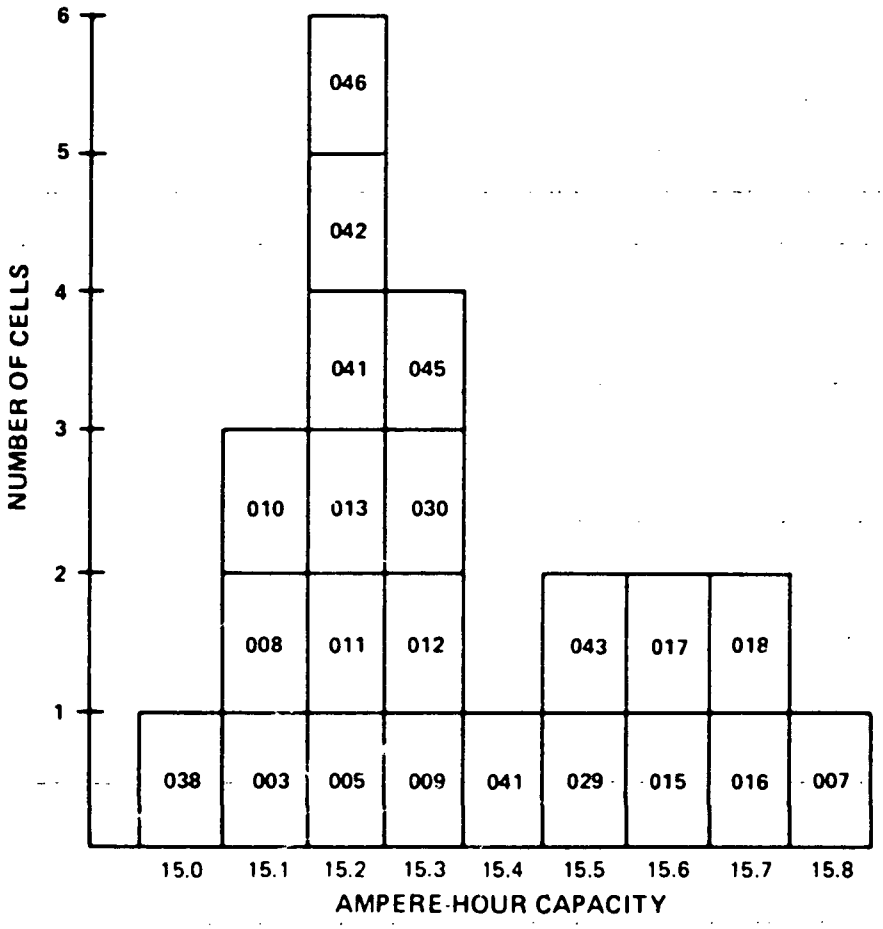

END

DATE

FILMED

MAR 23 1981